Simulating EEG in Schizophrenia Through Targeted Structural Connectivity Manipulation in 'The Virtual Brain'

DIPLOMARBEIT

zur Erlangung des akademischen Grades

Diplom-Ingenieur

im Rahmen des Studiums

Biomedical Engineering

eingereicht von

Simon Beyer, BSc.
Matrikelnummer 1125143

an der Fakultät für Mathematik und Geoinformation

der Technischen Universität Wien

Betreuung: Univ.-Prof. DDDr. Frank Rattay
Mitwirkung: Prof. Alexandre Andrade, Universidade de Lisboa, Lx, Portugal
Sofia R. Fernandes Ph.D., Universidade de Lisboa, Lx, Portugal

Wien, 03.10.2024

Simon Beyer   Frank Rattay

Acknowledgements

Writing this thesis has been an overall great experience. I am thankful to my academic advisor Univ.-Prof. DDDr. Frank Rattay who, by taking on the role of academic advisor at my home university, made it possible for me to write this thesis abroad in the first place.

I am also extremely grateful to Prof. Alexandre Andrade and Sofia R. Fernandes Ph.D. for welcoming me at the Institute for Biomedical Engineering and Biophysics at Universidade de Lisboa, for guiding me through the processes of developing the concept for this thesis and always being ready to give helpful advice or a word of encouragement.

Last but not least I want to thank my family and friends for their unending support throughout this journey.

Kurzfassung

Diese Arbeit untersucht die Simulation von Elektroenzephalographie (EEG)-Signalen bei Schizophrenie durch die Manipulation der strukturellen Hirnkonnektivität mittels der Plattform The Virtual Brain (TVB). Schizophrenie, eine komplexe psychische Erkrankung, ist durch Störungen der Hirnfunktion gekennzeichnet, doch ihre neurobiologischen Grundlagen sind nach wie vor unklar. Die Studie zielt darauf ab, zu erforschen, wie sich Veränderungen der strukturellen Konnektivität, insbesondere der weißen Substanz, auf die EEG-Muster bei Schizophrenie auswirken. Mithilfe von diffusion tensor imaging (DTI) und graphtheoretischen Analysen wurden Bahnen der weißen Substanz modelliert, um realistische Hirnkonnektivitätsmatrizen zu erstellen. Diese Matrizen wurden verwendet, um EEG-Signale zu simulieren und zu bewerten, wie Veränderungen der Konnektivität bekannte Veränderungen des EEG Spektrums bei Schizophrenie widerspiegeln. Obwohl die EEG-Simulationen die erwarteten makroskopischen Störungen teilweise erfassten, deuten Einschränkungen hinsichtlich der Vereinfachungen der weißen Substanz und der Modellannahmen darauf hin, dass weitere Verfeinerungen erforderlich sind.

Abstract

This thesis investigates the simulation of electroencephalography (EEG) signals in schizophrenia by manipulating structural brain connectivity using the Virtual Brain (TVB) platform. Schizophrenia, a complex mental disorder, is characterized by disruptions in brain function, yet its neurobiological underpinnings remain unclear. The study aims to explore how changes in structural connectivity, particularly in white matter, affect EEG patterns in schizophrenia. Using diffusion tensor imaging (DTI) and graph-theoretical analysis, white matter tracts were modeled to generate realistic brain connectivity matrices. These matrices were then used to simulate EEG signals and assess how alterations in connectivity reflect known EEG spectral changes in schizophrenia. While the EEG simulations captured some of the expected macroscopic disruptions, limitations regarding the simplifications of white matter integrity and model assumptions suggest further refinement is needed.

Contents

1 INTRODUCTION 1

2 THEORY 3
- 2.1 Basics of Brain Anatomy . . . 3
- 2.2 Principles of Electroencephalography . . . 6
- 2.3 Schizophrenia . . . 10
  - 2.3.1 Symptomatology of Schizophrenia . . . 10
  - 2.3.2 Risk Factors . . . 11
  - 2.3.3 Hypotheses on the Etiology of Schizophrenia . . . 12
  - 2.3.4 EEG in schizophrenia . . . 14
- 2.4 Graph Theory . . . 16
- 2.5 Diffusion Tensor Imaging and Fractional Anisotropy . . . 21
- 2.6 Brain Connectivity . . . 22
  - 2.6.1 Connectivity in Schizophrenia . . . 24
- 2.7 Computational Neuroscience and Brain Modeling . . . 28
  - 2.7.1 Historical Perspective . . . 28
  - 2.7.2 The Rationale Behind Brain Modeling . . . 30
  - 2.7.3 Modeling Approaches . . . 31
  - 2.7.4 Neural Mass and neural field Models . . . 32
- 2.8 The Virtual Brain . . . 34
  - 2.8.1 Motivation . . . 34
  - 2.8.2 The Modeling Principle of TVB . . . 35
  - 2.8.3 Data Requirements . . . 39
  - 2.8.4 Local Dynamics Model . . . 40

3 MATERIALS AND METHODS 47
- 3.1 Data and Data Processing . . . 47
  - 3.1.1 Structural Connectivity Matrices . . . 47
  - 3.1.2 Surface Data . . . 49
  - 3.1.3 Graph-Theoretical Analysis . . . 52
- 3.2 Model Setup . . . 54
  - 3.2.1 Configuring the Simulation . . . 54
  - 3.2.2 First Simulation Run . . . 56
  - 3.2.3 Full Length Simulations . . . 56

3.2.4 Data Processing and Analysis 56

4 RESULTS **59**
4.1 TVB Ready Dataset 59
4.2 White Matter Matrices 63
4.3 Graph-Analysis 71
4.3.1 Global Metrics 72
4.3.2 Local Metrics 78
4.4 Simulation Results 82

5 DISCUSSION **93**

Bibliography **iii**

1 INTRODUCTION

The human brain, often described as the most complex organ in the body, is the central focus of neuroscience research due to its intricate structure and varied functions. Representing only about two percent of body weight but accounting for approximately twenty percent of its energy consumption, the brain is the seat of consciousness, responsible for interpreting sensory information, generating emotions, and controlling behavior. Despite significant advancements in neuroscience, the detailed mechanisms underlying brain function and dysfunction remain elusive, particularly in the context of mental health disorders such as schizophrenia.

Schizophrenia is a debilitating mental disorder characterized by profound disruptions in cognition, emotion, and behavior. Despite the profound impact it has on affected individuals and society as a whole, the precise neurobiological underpinnings of schizophrenia are not fully understood. Traditional methods of studying the brain, such as histology and in vivo imaging, provide valuable insights but are limited by their scope and resolution. Consequently, there is a critical need for integrative approaches that can bridge the gap between molecular-level interactions and large-scale brain dynamics to better understand the pathophysiology of schizophrenia.

This thesis aims to develop a systematic approach to investigate alterations in brain structural connectivity associated with schizophrenia using computational modeling in *The Virtual Brain* (TVB). The primary objective is to create a model that produces EEG signals based on realistic structural connectivity resembling that of a human brain. By manipulating specific aspects of this structural connectivity, the study seeks to observe the resultant changes in EEG signals and determine if these changes align with expectations based on current scientific understanding of the disorder.

The implementation of the model employs a multi-faceted approach, combining theoretical knowledge, datasets created with advanced neuroimaging techniques, and computational neuroscience. Key methodologies include:

- **Structural Connectivity Analysis:** Utilizing data recorded with diffusion tensor imaging (DTI) to map the white matter tracts and generate structural connectivity matrices.

- **Graph-Theoretical Analysis:** Applying graph theory to analyze the connectivity patterns and identify relevant network properties such as clustering coefficient, path length, and modularity.
- **Neural Mass Modeling:** Implementing neural mass models to create a whole brain model and simulate the average activity of neuronal populations and their interactions in TVB.
- **EEG Simulation:** Using the TVB platform to simulate EEG signals based on the derived structural connectivity and observing how manipulations of this connectivity affect the simulated signals.

Understanding the connectivity alterations in schizophrenia has profound implications for both basic neuroscience and clinical practice. By elucidating the network dynamics that underlie the disorder, the development of more targeted therapeutic interventions and improved diagnostic accuracy could be supported. Additionally, the use of computational models provides a powerful tool for hypothesis testing and the exploration of complex brain - behavior relationships in a controlled virtual environment.

The thesis is organized as follows:

- **Chapter 1 - Introduction**
- **Chapter 2 - Theory:** Provides an overview of brain anatomy, principles of electroencephalography, and the current understanding of schizophrenia, including symptomatology, risk factors, and hypotheses on its etiology as well as an introduction to brain modeling and its different approaches with a focus on TVB.
- **Chapter 3 - Materials and Methods:** Describes the data collection, processing techniques, and the setup of the computational model used in the study.
- **Chapter 4 - Results:** Presents the findings from the simulations and analyses, highlighting key changes in connectivity and EEG signals associated with schizophrenia.
- **Chapter 5 - Discussion:** Interprets the results in the context of existing literature, discusses their implications, and suggests potential directions for future research.

2 THEORY

2.1 Basics of Brain Anatomy

The brain is often described as the most complex organ in the human body. Despite comprising only about two percent of body weight, it accounts for approximately twenty percent of its total energy requirements. It is the seat of consciousness, interprets sensory information it receives from widespread parts of the nervous system and creates emotions in an intricate interplay with the other parts of the body. Together with the spinal chord, it forms the central nervous system serving as the control center for the entire body. The functions of the brain are manifold, but a concise way of describing its primary purpose is: "The brain is an anticipating memory system that learns to represent expectations of the world, which can be used to generate goal-directed behaviour" (Trappenberg 2023). How it accomplishes this feat is still not fully understood.

Looking at the brain on the micro scale, its two main constituents are neurons and glial cells (Fan and Markram 2019). Glial cells were believed to serve mainly structural and metabolic functions; however, ongoing research suggests their active involvement in various brain functions such as modulation of synaptic connections and protection against disease (Jäkel and Dimou 2017). The neuron is considered to be the primary computational unit of the brain in particular, and the nervous system in general (much like a transistor on a computer chip, but more complex in its functionality), and due to its electrical excitability, which correlates with higher brain functions, has been in the spotlight of neuroscience for a long time (Fan and Markram 2019).

Neurons are composed of three primary parts (see figure: 2.1): the cell body (or soma), dendrites, and axons. The cell body contains the nucleus and other essential organelles for the neuron's metabolic activities and is surrounded by a lipid bilayer known as the cell membrane (Ackerman 1992). This membrane functions similarly to a capacitor, regulating the neuron's electrical potential. Ions move across this membrane through specialized channels that regulate ion diffusion via various gating mechanisms. When certain conditions are met, such as a specific threshold membrane potential, an action potential is triggered (Ackerman 1992;

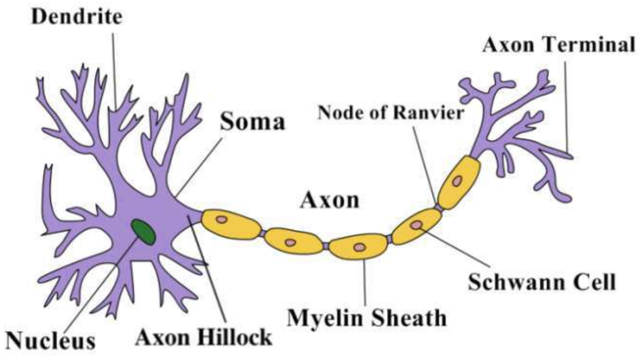

Figure 2.1: Schematic illustration of a neuron (Wikipedia contributors 2024).

J. Zhang 2019a).

The axon, an extension of the neuron, conducts action potentials away from the cell body. Often axons are insulated by a myelin sheath, which significantly increases the speed of electrical signal transmission along the axon. This myelination is crucial for efficient signal conduction, especially over longer distances within the nervous system. These myelinated axons are referred to as fibers (Axer and Amunts 2022). The axon typically terminates in connections with other neurons at structures called synapses. Here, the axon releases neurotransmitters stored in vesicles into the synaptic cleft, the small gap between the axon of one neuron and the dendrite of another. These neurotransmitters then bind to the receptors of a receiving neuron's dendrite, thereby passing on the signal (Ackerman 1992; J. Zhang 2019a).

Dendrites, which are branching from the cell body, are structures that receive these chemical signals. The chemical signal is converted back into an electrical signal, which can then trigger a new action potential in the receiving neuron, continuing the process of neural communication (Ackerman 1992; J. Zhang 2019a).

Neurons that are in close proximity to each other are also able to exchange signals directly via electrical Synapses.

These individual connections form the basis of local neuronal circuits, small networks of neurons that work in concert, forming specific emergent functional properties and states (Yuste 2015). Local circuits interact and further connect with each other, to form ever larger neuronal network structures that increase in their complexity to form what we know as the brain. The study of neuronal networks, as opposed to single neurons, provides insights into higher cognitive processes that could not be gleamed by examining a single, isolated neuron. This marks a shift from the neuron doctrine, which sees neurons as discrete information processing units, to network models, that consider emerging properties to be a result of widespread neuronal interactions (Yuste 2015).

Zooming out to look at the macroscopic structures of the brain provides another perspective. At a macroscopic level, different regions composing the brain can be classified and categorized using distinctions of neural structure, connectivity, functionality and chemistry, all resulting in different ”atlases” (J. Zhang 2019b).

In one such approach, the brain is roughly divided into three main regions that are present from the onset of development: the forebrain, hindbrain and midbrain.

The hindbrain consists of the medulla oblongata, the pons, and the cerebellum. The brainstem, which includes the midbrain, pons, and medulla oblongata, sits beneath the forebrain. The forebrain makes up the largest part of the brain. It consists of the cerebrum on the outside and the diencephalon, which houses the thalamus and hypothalamus, buried deeper inside the structure. The cerebrum is divided into two hemispheres, connected by a thick fiber tract called the corpus callosum, and a smaller fiber bundle called the anterior commissure. The cerebrum contains the basal ganglia and the limbic system. The outer surface of the cerebrum and cerebellum consists of a layer of tissue, only a few millimeters thick, called the cortex. The cerebral cortex, is where most information processing occurs. (L. Luo 2021; J. Zhang 2019b).

The cerebral cortex is anatomically organized into distinct lobes. These lobes are delineated by notable grooves or sulci, that can be used as landmarks in the topography of the brains surface. The most prominent of these, called the longitudinal fissure, bisects the brain into its left and right hemispheres. Each hemisphere is further partitioned into four primary lobes. The frontal and parietal lobes are separated by the central sulcus, while the lateral sulcus (also known as the Sylvian fissure) distinguishes the temporal lobe from both the frontal and parietal lobes. Additionally, the parieto-occipital sulcus demarcates the boundary between the parietal and occipital lobes. A fifth lobe, the insula, is partly covered by parts of the other lobes (L. Luo 2021; J. Zhang 2019b; Kandel 2013). The structures of the cortex can be classified according to different criteria and methods, often tailored to specific purposes. This results in a diverse array of brain atlases, each offering different levels of granularity.

The cortex exhibits a hierarchical, laminar structure, the six layers of which can be differentiated on the basis of their unique cytoarchitecture and layer specific termination patterns for feed forward and feedback pathways (Larkum et al. 2018). Starting from the outermost layer, these include the molecular layer, primarily consisting of signal exchange junctures, apical dendrites of pyramidal cells and horizontal axons, the external granular layer mainly containing interneurons, the external pyramidal layer containing large principal cells, the internal granular layer where the thalamic fibers terminate, the internal pyramidal layer with axons extending to subcortical areas, and the multiform layer with axons projecting to the thalamus and other cortical areas. The thickness of these layers varies across different cortical areas and can indicate functional relationships (Ackerman 1992).

The cerebral cortex's neural network includes both short and long-range axonal connections. Short-range connections form circuits within local areas, such as the fibers linking adjacent gyri, while long-range connections integrate different distant brain regions, either within the same hemisphere or across hemispheres. In addition, the cortex is connected to subcortical areas and the spinal cord through ascending and descending axonal projection fibers. Fibers that form connections within a hemisphere are called association fibers, those that form interhemispheric connections between corresponding areas are called commissural fibers and those that link the cortex to subcortical nuclei are called projection fibers. The long-range connections are grouped into large bundles that constitute the brain's white matter, whereas the tissue of the cortex is called gray matter (Axer and Amunts 2022).

These connections, along with the intricate networks they form and the complex interactions between neurons and neuronal circuits they facilitate, are not only essential for communication between different brain regions, but are also believed to be the substrate from which higher cognitive states and the human mind emerge. The macroscopic arrangement of neurons and their synchronized activity form the basis for signals that are measurable via electroencephalography, and the white matter structures formed by bundles of axons will provide the foundation for creating structural connectivity matrices that are essential for the model used in this work.

2.2 Principles of Electroencephalography

Electroencephalography (EEG) is a non-invasive imaging procedure to record the electrical activity of the brain with anywhere from 20 to 256 electrodes, which are placed systematically on the scalp (Nunez and Srinivasan 2007). The EEG signal primarily reflects the summed activity of predominantly cortical pyramidal neurons, with minimal contributions of glial cells. EEG offers a high temporal resolution, making it an excellent tool for studying the dynamic processes of brain activity over time. However, it has poor spatial resolution compared to imaging modalities like functional magnetic resonance imaging (fMRI) or positron emission tomography (Silva 2009; E. K. Louis et al. 2016). Additionally, EEG is highly susceptible to noise interference, resulting in a relatively low signal-to-noise ratio which can be partly mitigated by various filtering processes (Chaddad et al. 2023).

Active neurons produce electrical activity in two main ways. Firstly, there is the rapid depolarization of the cell membrane that results in action potentials (lasting 1-2 ms) that propagate along the axons. Secondly, there are slower changes in membrane potential called postsynaptic potentials, which are initiated by synaptic activation of one neuron by another, through specific neurotransmitters. Unlike action potentials, these postsynaptic potentials do not propagate along the neuron but instead modulate the neuron's membrane potential locally. Depending on the neurotransmitter, theses postsynaptic potentials can be either excitatory or inhibitory. An excitatory postsynaptic potential causes a movement of ions across the cell membrane that positively charges the intracellular space, whereas an inhibitory post synaptic potential results in a movement of ions that leaves the intracellular space negatively charged. At the site of an excitatory synapse, the positive charge inside the neuron creates an active sink in the extracellular space on the other side of the cell membrane. Conversely, at an inhibitory synapse, the negative charge inside the neuron results in an active source in the extracellular space. As a consequence of this redistribution of charges and the generation of active sources and sinks in the extracellular space, passive sinks and sources spring into existence along the cell membrane. These movements of charges create an electrical field that can be detected as variations in potential difference by EEG electrodes. The interplay between these sinks and sources, governed by neuronal and synaptic activity, shapes the electrical patterns recorded by EEG and reflects the brain's functional state (Silva 2009; E. K. S. Louis, Frey, and Britton 2016).

Cell geometry and cortical structure are crucial for what is measured in EEG. Neurons in the cortex form vertically and laterally integrated units. The vertical aspect of this organisation can be described as columns of neurons that span several cortical layers with the main axis of their dendritic trees perpendicular to the pial surface and parallel to each other (E. K. S. Louis, Frey, and Britton 2016). The smallest unit of this columnar organization is the so-called mini-column. These mini-columns form functional units called macro-columns, which fire in a synchronized manner (Mountcastle 1997). Synchronization can also occur across several macro columns, due to the lateral integration of different units. The sink/source configurations that form along the cell membranes are confined within this columnar structure and may be interpreted as dipoles that are oriented perpendicular to the pial surface. A single dipole is too weak to be measured by EEG, but when neurons fire in synchronicity, the electric dipole moments with the dipole vector

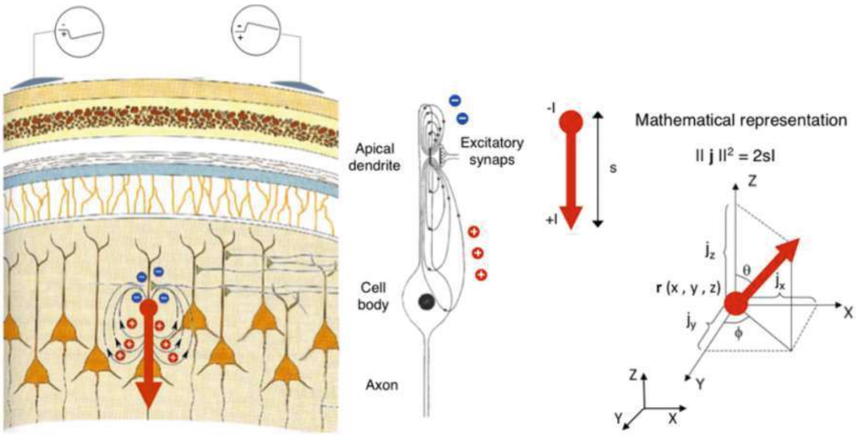

Figure 2.2: Schematic representation of the generation of an electrical neuronal signal, as measured by EEG (Strobbe 2015).

parallel to the orientation of the pyramidal cells add up (E. K. S. Louis, Frey, and Britton 2016). The electric fields generated by these dipoles extend beyond the immediate vicinity of their source, and the summed activity becomes strong enough to be detected by the EEG electrodes placed on the skull (Nunez and Srinivasan 2007).

A consequence of the folded structure of the cortical surface is that the orientation of cortical neurons varies. Neurons located in the gyri are generally perpendicular to the skull and thus contribute significantly to the EEG signal. In contrast, neurons located in the sulci are oriented parallel to the skull, and their electrical activity tends to cancel out, significantly reducing their contribution to the EEG signal (Silva 2009).

In summary, the synchronized activity of many neurons across multiple cortical columns can generate electrical signals strong enough to be measured by EEG, providing a window into the brain's electrical activity.

To perform an EEG measurement, electrodes are placed methodically on the scalp, often utilizing the 10-20 system or its adaptations for standardized placement. These electrodes are secured in place with special pastes, caps, or nets to ensure stable contact. Given the EEG signal's low voltage levels, a differential amplifier is used to record the signals and enhance signal-to-noise ratio (Nunez and Srinivasan 2007).

EEG signals can be recorded using several methods. In referential recordings, the potential differences between individual electrodes and a common reference electrode are captured. Bipolar recordings measure the potential difference between pairs of adjacent electrodes. For setups employing more than 64 electrodes, the common average reference method can be used, where the potential at each electrode is calculated relative to the average potential of all electrodes. The electrode placement and the different ways of combining the measured signals, form the electrode montage (Nunez and Srinivasan 2007).

The estimation of the location of the neuronal sources generating the EEG signals measured on the scalp poses a challenging problem. As electric fields generated by brain activity must traverse several layers of conductive tissues (cerebrospinal fluid, skull, scalp), that are arranged in the complex geometry of the head, they undergo attenuation and distortion (Lopes da Silva 2013). This estimation process is known as the inverse problem, which is mathematically ill-posed due to the non-uniqueness of its solutions. In essence, multiple different source configurations can produce the same electrical patterns on the scalp. To constrain the infinite solution space of the inverse problem and achieve plausible source estimations, several assumptions about the nature of the sources and the conductive properties of the head are necessary (Silva 2009).

In conjunction with the inverse problem, forward modelling plays a crucial role in EEG analysis. Forward modeling involves predicting the electrical fields on the scalp that would result from known sources within the brain, based on a model of the head's conductive properties (Lopes da Silva 2013). By understanding how electrical signals propagate through the head's various tissues, forward modelling provides a necessary framework for interpreting scalp EEG data in terms of underlying brain activity. The forward-inverse relationship is reciprocal: Forward modeling validates the assumptions of the inverse problem, confirming that estimated sources can create the observed EEG signals. These methods are vital for accurately connecting EEG data to neuronal activity, thereby improving our understanding of brain function (Silva 2009; Nunez and Srinivasan 2007).

The EEG signal is measured as voltage fluctuations over time. To ensure clarity and precision in these measurements, the raw EEG signal undergoes extensive processing. This processing includes amplifying the signal to make it more discernible, reducing noise and artifacts to enhance signal quality, and extracting features such as amplitude, power, coherence, and phase. Additionally, the signals are filtered into specific frequency bands for analysis. The traditional frequency bands are Delta (1-4 Hz), Theta (4-8 Hz), Alpha (8-12 Hz), Beta (12-30 Hz), and Gamma (30 Hz and above), each often associated with distinct brain states (Nunez and Srinivasan 2007; Silva 2009).

2.3 Schizophrenia

Schizophrenia is a debilitating psychological disorder that deeply affects the life of individuals who suffer from the condition, often leading to social and occupational decline. Unemployment rates among those affected ranges between 70 and 90% (Marwaha, Johnson, et al. 2007), and the disorder is associated with a reduced life expectancy of 3 to 15 years (Marwaha and Johnson 2004). Characterized by a profound disruption in cognition and emotion, schizophrenia affects fundamental human attributes such as perception, thought, and speech, manifesting through a wide range of symptoms. Its onset typically occurs in late adolescence or early adulthood, resulting in significant implications for the individual's functioning and quality of life. Approximately 1% of the population are at risk of developing schizophrenia at one point in their lifetime (McGrath et al. 2008; Jongsma et al. 2019). The etiology of schizophrenia is multifactorial, involving genetic, environmental, and neurobiological influences. This chapter aims to explore the current understanding of schizophrenia, delving into its symptomatology, risk factors, and theoretical etiological models.

2.3.1 Symptomatology of Schizophrenia

The onset of Schizophrenia often occurs in early adulthood and is often preceded by prodormal symptoms that can last anywhere from a week to several years, but these symptoms are heterogeneous in nature and lack precise definition (Jauhar, Johnstone, and McKenna 2022). The condition severely disrupts the individual's thoughts and affect, hampering their ability to navigate social environments and form meaningful connection. Depending on the source, symptoms of schizophrenia are grouped into three categories: positive, negative, and cognitive symptoms. Each category is essential for distinguishing schizophrenia from other psychotic disorders (Patel et al. 2014).

Positive symptoms, described as ”psychotic behaviors not seen in healthy people” (Patel et al. 2014) include behaviours such as delusions (e.g. delusions of persecution, passivity, meaning a feeling external control of one's own thoughts and actions, etc.), hallucinations (perceptions without a stimulus, most commonly auditory) and formal thought disorder, manifesting in distorted or illogical speech (Jauhar, Johnstone, and McKenna 2022; M. M. Picchioni and R. M. Murray 2007; Owen, Sawa, and Mortensen 2016; M. Picchioni and R. Murray 2008).

Negative symptoms are less obvious to the outside observer, but exert a great burden on the afflicted person (Patel et al. 2014). They include social withdrawal, avolition (loss of motivation and initiative), emotional blunting, diminished emotional expression, anhedonia, and paucity of speech (M. Picchioni and R. Murray

2008; Patel et al. 2014). These symptoms are often chronic and can have a long-term negative effect on social function (Owen, Sawa, and Mortensen 2016).

Cognitive symptoms are relatively nonspecific and describe a spectrum of cognitive and intellectual difficulties, ranging from generally impaired intelligence to more specific deficits, e.g. in executive function or working memory (M. Picchioni and R. Murray 2008). These symptoms are generally accompanied by lack of insight (in 97% of patients), that they are the result of an illness (M. M. Picchioni and R. M. Murray 2007).

Another characteristic of schizophrenia is catatonia, which is characterized by abnormal movements and behaviors. It can be observed in approximately 10% of patients suffering from schizophrenia, but has been relegated to the rank of a specifier for several different psychological conditions (Jauhar, Johnstone, and McKenna 2022).

This wide range of symptoms characteristic of schizophrenia can also be observed in other mental health disorders, such as major depressive disorder with psychotic features or schizoaffective disorder. Given this overlap, a comprehensive differential diagnosis is essential to accurately differentiate schizophrenia from these and other conditions that present themselves similarly (Patel et al. 2014).

Today, the notion that schizophrenia represents the extreme end of a continuum of psychotic symptoms is gaining influence, challenging traditional views of the disorder as a stark departure from normal health (Jauhar, Johnstone, and McKenna 2022). Mild symptoms of schizophrenia can manifest in individuals without any associated illness, suggesting that the condition reflects a quantitative deviation from normality, rather than a qualitative one. This perspective underscores a more nuanced understanding of schizophrenia, emphasizing its spectrum nature rather than categorizing it as an isolated or binary condition (M. M. Picchioni and R. M. Murray 2007).

2.3.2 Risk Factors

The risk factors for schizophrenia are heterogeneous and multifactorial, mirroring the complexity of the disease itself. The largest contributor seems to be genetics. While the general population has a lifetime risk of little under 1% to develop schizophrenia, a familial history seems to be the greatest factor for increased risk, with a 6.5% chance for first degree relatives that increases to a 40% risk in mono zygotic twins (Kendler 1993; Cardno et al. 1999). A genome-wide association study found that schizophrenia is a poligenic disorder, originating from the cumulative effects of hundreds to thousands of genes, that are spread across the genome (Psychiatric Genomics Consortium 2014; Jauhar, Johnstone, and McKenna 2022).

In addition to genetic predisposition, a multitude of environmental factors contribute to increasing the risk for developing schizophrenia. Prenatal exposure to infections and malnutrition, neurodevelopmental disruptions, early and heavy cannabis use, showing a dose-response relationship, severe psychosocial stressors, and the challenges faced by people with migrant status, especially in low ethnic density areas, significantly contribute to the risk. These factors underscore the complex interplay between biological and environmental influences in the etiology of schizophrenia (Brown and Lau 2016; Jauhar, Johnstone, and McKenna 2022).

2.3.3 Hypotheses on the Etiology of Schizophrenia

Several hypotheses attempt to explain the origin of schizophrenia. Despite extensive research, the biological underpinnings of schizophrenia remain elusive, suggesting a multi-factorial origin involving genetic predispositions, neurochemical imbalances, and structural abnormalities within the brain. Various pathophysiological mechanisms are being explored as potential contributing factors to the manifestation and progression of the condition, ranging from neurochemical systems to abnormal deviations in brain structure.

Due to the nature of schizophrenia as a disorder involving relapses and remissions, it has long been hypothesized that at least parts of its manifestation emerge from neurochemical imbalances. The two main neurotransmitter systems implicated in schizophrenia are dopamine and glutamate. Dopamine is involved in various functions, including motor function and learning, while glutamate is the brain's primary excitatory neurotransmitter (Jauhar, Johnstone, and McKenna 2022).

The dopamine hypothesis is based on the observation, that anti psychotic drugs work as an inhibitor of dopamine D_2 postsynaptic receptors (Jauhar, Johnstone, and McKenna 2022). A 2018 meta-study supports increased dopamine synthesis capacity in schizophrenia patients as a mechanism (McCutcheon et al. 2017).

The glutamate hypothesis originates from the observation, that healthy subjects, who took the anesthetic drug phencyclidine recreationally often developed prolonged psychotic states. Similar experiments were conducted by administering the drug ketamin to healthy volunteers. Both of these drugs act as inhibitors to the N-methyl-Daspartate or NMDA receptor, which is one of the two main glutamatergic postsynaptic receptor classes (Jauhar, Johnstone, and McKenna 2022).

More evidence for the glutamate hypothesis comes from the symptomatology of an autoimmune disease called anti-NMDA receptor encephalitis. This autoimmune condition leads to the production of Immunoglobulin G (IgG) antibodies that attach to the NMDA receptor leading to its subsequent internalization. The initial symptoms of the disease so closely resemble those observed in schizophrenia, that they pose a severe risk of misdiagnosis (Y. Luo et al. 2022). However, histological post-mortem studies did not find abnormalities in NMDA receptors in schizophrenia patients (Y. Luo et al. 2022).

With the introduction of imaging technologies like positron emission tomography and magnetic resonance imaging (MRI), came the opportunity to non-invasively explore the structural and functional nature of the brain in vivo. These advancements have provided promising insights into many different conditions, including schizophrenia. Imaging studies have uncovered significant structural changes in patients suffering from schizophrenia compared to healthy controls. These changes include enlarged ventricles accompanied by an overall decrease in brain volume, largely attributed to a higher density of pyramidal neurons without affecting the overall number of neurons. This suggests a possible reduction in dendritic spines and axon terminals, which usually fill the space between neurons (Hayempour 2013). This volume loss appears to be progressive, having the largest impact on the frontal and temporal gray matter (Jaaro-Peled et al. 2009).

The development of diffusion tensor MRI (DTI), a specialized form of MRI that measures the diffusion coefficient, which is a proportionality constant that links the diffusive flux to the concentration gradient, has made the noninvasive exploration of the "wiring", represented by the white matter of a patient's brains possible (O'Donnell and Westin 2011). The structure of the white matter, forming ordered pathways along its axon bundles, constrains the movement of water molecules to avenues along these bundles, leading to anisotropic diffusion that can be used to model the orientation and integrity of white matter fibers (O'Donnell and Westin 2011). White matter deficits in schizophrenia patients are commonly reported, with some lines of evidence indicating a connection between white matter abnormalities and psychotic symptoms as well as reduced cognitive function (Erkol et al. 2020). White matter abnormalities have been recorded in first episode schizophrenics and even in high risk patients before they ever developed symptoms (Duchatel, Shannon Weickert, and Tooney 2019). A large study examining 326 schizophrenia patients and comparing them to 197 healthy controls found that widespread reductions in fractional anisotropy (FA) linked to schizophrenia affected over 40% of the cerebral white matter volume, impacting all cerebral lobes (Klauser et al. 2016). Additionally, over 50% of the white matter fiber bundles connecting cortical regions and cortical-subcortical areas in the brain's connectome showed disruption, lending support to the hypothesis of schizophrenia being a condition of neural disconnectivity (Jaaro-Peled et al. 2009; Klauser et al. 2016; Narr and Leaver 2015).

It is however unclear whether theses structural changes occur due to genetic factors, environmental insults or drug therapy, or if they only act to exacerbate these changes (M. Picchioni and R. Murray 2008).

Functional brain changes could be attributed to either of these factors, be it on a level of neurochemical disturbance or on a level of large scale disruptions in brain network connectivity. Ultimately, these changes might be understood as a combination of all these and more factors merging together to create the complex symptomatology seen in schizophrenia.

2.3.4 EEG in schizophrenia

The use of EEG to explore psychological states dates back to the early days of the technology. Schizophrenia in particular has been extensively studied using EEG, leading to a diverse array of publications. Despite variations in methodology and occasional contradictory findings, these studies have identified specific EEG markers closely associated with schizophrenia.

Although EEG has shown potential in revealing the underlying pathology of schizophrenia, it is not established as a standard clinical diagnostic tool (Thilakavathi et al. 2019). Currently, diagnosis primarily depends on clinicians evaluating self-reported experiences and observed abnormal behaviors, following the guidelines of the Diagnostic Statistical Manual for Mental Disorders, with EEG sometimes being used as an adjunct (Thilakavathi et al. 2019). However, no biomarkers have been universally accepted for schizophrenia diagnosis to date (Owen, Sawa, and Mortensen 2016).

A consistent body of research has identified abnormalities in EEG frequency bands among schizophrenia patients. Notably, increased absolute power in the delta and theta bands is a recurring finding. Some studies have pinpointed increases in delta power in specific brain regions such as the frontal, left temporal, central, and parietal areas, while theta power is often observed to be increased across the scalp (Narayanan et al. 2014; Newson and Thiagarajan 2019; Thilakavathi et al. 2019). Frequent observations also include variations in slow and fast alpha band activity. While most studies report decreases in alpha activity there is some discrepancy, with some studies also reporting increases, and other studies reporting a frontal-posterior split with frontal increases and posterior decreases. This inconsistency might be attributable to different methodologies, measuring conditions (like eyes-closed and eyes-open condition) and diagnostic diversity of patients (Narayanan et al. 2014; Newson and Thiagarajan 2019; Hayempour 2013; Thilakavathi et al. 2019; Venables, Bernat, and Sponheim 2008).

Similarly, findings on gamma activity are mixed. Some studies do not find significant changes, possibly due to limitations in analysis methods (Narayanan et al. 2014; Pachou et al. 2008), while others indicate a promising correlation between gamma band activity and the pathology of schizophrenia (Whittington et al. 2011).

Quantitative EEG studies have highlighted a slowing in the individual alpha peak frequency in schizophrenia patients, indicating a reduction in the frequency of the strongest alpha oscillation (around 10 Hz) observed during rest (Ramsay et al. 2021). A meta-analysis of quantitative EEG in schizophrenia also identified distinct variations in spectral power across frequency bands, including increased delta and theta waves, decreased alpha waves, and increased beta and gamma waves. These changes are particularly pronounced in the delta wave, primarily in the frontocentral area. While these patterns can help distinguish schizophrenia from healthy states, they share similarities with other mental disorders like depression and dementia, reducing their diagnostic specificity. Although quantitative EEG is effective in differentiating schizophrenia from normal states, distinguishing between various psychiatric conditions remains challenging (Kim et al. 2015).

Results also indicate that resting state EEG frequency abnormalities are evident in schizophrenia patients and their biological relatives, but are largely absent in bipolar disorder patients, which are often studied alongside schizophrenia patients, due to similarities in the disorder (Venables, Bernat, and Sponheim 2008).

Table 2.1 contains a short summary of a selection of papers, detailing the findings regarding EEG in schizophrenia.

Title	**Delta**	**Theta**	**Alpha**	**Beta**	**Gamma**
The status of spectral EEG abnormality as a diagnostic test for schizophrenia (Boutros et al. 2008)	increase	increase	decrease	increase	-
Brain Rhythms Connect Impaired Inhibition to Altered Cognition in Schizophrenia (Pittman-Polletta et al. 2015)	-	-	Altered coordination	Altered coordination	decrease
Diagnostic utility of quantitative EEG in unmedicated schizophrenia (Kim et al. 2015)	increase	increase	decrease	-	insignificant
Resting state EEG power and coherence abnormalities in bipolar disorder and schizophrenia (Kam et al. 2013)	increase	increase	decrease	increase	-
Resting State Electroencephalogram Oscillatory Abnormalities in Schizophrenia and Psychotic Bipolar Patients and Their Relatives from the Bipolar and Schizophrenia Network on Intermediate Phenotypes Study (Narayanan et al. 2014)	increase	increase	-	increase (fast alpha)	increase
Genetic and Disorder-Specific Aspects of Resting State EEG Abnormalities in Schizophrenia (Venables, Bernat, and Sponheim 2008)	increase	increase	-	increase	-
EEG Frequency Bands in Psychiatric Disorders: A Review of Resting State Studies	increase	increase	decrease	-	-
Working Memory in Schizophrenia: An EEG Study Using Power Spectrum and Coherence Analysis to Estimate Cortical Activation and Network Behavior (Pachou et al. 2008)	-	increase	insignificant	decrease	decrease
EEG power spectrum analysis for schizophrenia during mental activity (Thilakavathi et al. 2019)	increase	-	decrease	increase	-

Table 2.1: Short summary of specific findings regarding brain rhythm abnormalities in schizophrenia

EEG stands out as a promising tool for studying schizophrenia and its underlying causes due to its ability to capture the brain's electrical activity with high temporal resolution. It offers insights into the neural oscillations and patterns that may be disrupted in schizophrenia, potentially allowing researchers to identify specific biomarkers associated with the disorder. The observed abnormalities in EEG frequency bands, such as changes in delta, theta, alpha, and gamma activities, provide crucial clues to the functional differences in the brains of individuals with schizophrenia. Despite the methodological and diagnostic variability that complicates the interpretation of EEG data (Narayanan et al. 2014; Newson and

Thiagarajan 2019), its potential to reveal the disorder's underlying pathology and contribute to a better understanding of its etiology makes EEG a valuable tool in the field of psychiatric research.

2.4 Graph Theory

Graph theory is a powerful and versatile mathematical framework used to describe complex networks. These networks can range from individual neurons in the brain, connected by dendrites and axons, over macroscopic brain areas linked by white matter tracts, to cities on a map connected by roads. To translate any network into the framework of a graph, each unit (such as a neuron, brain area, or city) is represented as a node (or vertex), the fundamental element of a graph. The connections between each node (such as axons, white matter tracts, or roads) are represented as lines, called edges, that form pairwise connections between the nodes.

There are different types of graphs, that are classified by the characteristics of their edges. The edges of a graph can be *directed*, meaning that information traverses the edges in only one direction, such as from node A to node B, forming a *directed graph*. Alternatively, they can be *undirected*, allowing information to flow bidirectionally, from A to B and from B to A, forming an *undirected graph*. Edges can take on binary values, simply indicating that two nodes are connected or unconnected (there either is a road between two cities or not) in a *binary graph*, or they can be weighted, indicating the strength of a connection (how many lanes has the road) with numeric values forming a *weighted graph*.

Graphs and their individual elements exhibit various properties by which they can be classified and characterized. These properties help to understand the structure and behavior of the graph as a whole, as well as the roles and relationships of individual nodes and edges:

The *degree* of a node is determined by the number of edges terminating in that node and, therefore, ranges from zero for an isolated node, to an upper limit constrained only by the network's size. It is a simple metric to estimate the importance of a node in a network. High-degree nodes are called *hubs*, and often play an essential role within a network, influencing its connectivity and dynamics (Wilson 2009; Power et al. 2010). The degree of a node is defined as

$$k_i = \sum_{j \in N} a_{ij} \tag{2.1}$$

where k_i is the node degree, N is the set of all nodes in the graph and a_{ij} is an element of the adjacency matrix, representing either a binary value, or an edge weight (Rubinov and Sporns 2010).

A *path* is a sequence of edges connecting two nodes, with the condition that no node in the path is passed more than once. The path length is determined by counting the number of edges in the path between two nodes. The shortest path, therefore, is the path that requires the fewest edges to connect two nodes (Power et al. 2010). In a weighted graph, where higher weight values represent stronger connections, some inverse of the weights can be used to estimate the weighted path length. The *characteristic path length* is the average shortest path in a network. It indicates the ease of information transfer between the nodes of a graph and is inversely related to the efficiency of the network (Power et al. 2010; Bullmore and Sporns 2009). The characteristic path length is defined as

$$L = \frac{1}{n} \sum_{i \in N} L_i = \frac{1}{n} \sum_{i \in N} \frac{\sum_{j \in N, j \neq i} d_{ij}}{n-1} \tag{2.2}$$

where n is the total number of nodes in the graph, d_{ij} is the shortest path between two nodes i and j and N is the set of all nodes in the network (Rubinov and Sporns 2010).

In comparison, the *global efficiency* is defined as

$$E = \frac{1}{n} \sum_{i \in N} E_i = \frac{1}{n} \sum_{i \in N} \frac{\sum_{j \in N, j \neq i} d_{ij}^{-1}}{n-1} \tag{2.3}$$

Long paths tend to have an outsized contribution in the calculation of the characteristic path length when compared to short paths, leading to problems in disconnected networks (the path between disconnected nodes is defined as having infinite length), while the global efficiency is dominated by the shortest paths, making it a more meaningful metric for disconnected networks (Rubinov and Sporns 2010).

Betweenness centrality quantifies how often a node lies on the shortest path between two other nodes. It is a crucial measure for information flow and can mark potential points of vulnerability in a network (He and Evans 2010). A more sophisticated measure of centrality is the eigenvector centrality. It not only captures the quantity of a nodes connections, but also their quality, with connections to well connected nodes being of higher value than connections to less connected nodes (Farahani, Karwowski, and Lighthall 2019).

Betweenness centrality is defined as:

$$b_i = \frac{1}{(n-1)(n-2)} \sum_{\substack{h,j \in N \\ h \neq j, h \neq i, j \neq i}} \frac{\rho_{hj}(i)}{\rho_{hj}}, \tag{2.4}$$

where ρ is the number of shortest path between the nodes indicated by the indices (Freeman 1978; Rubinov and Sporns 2010).

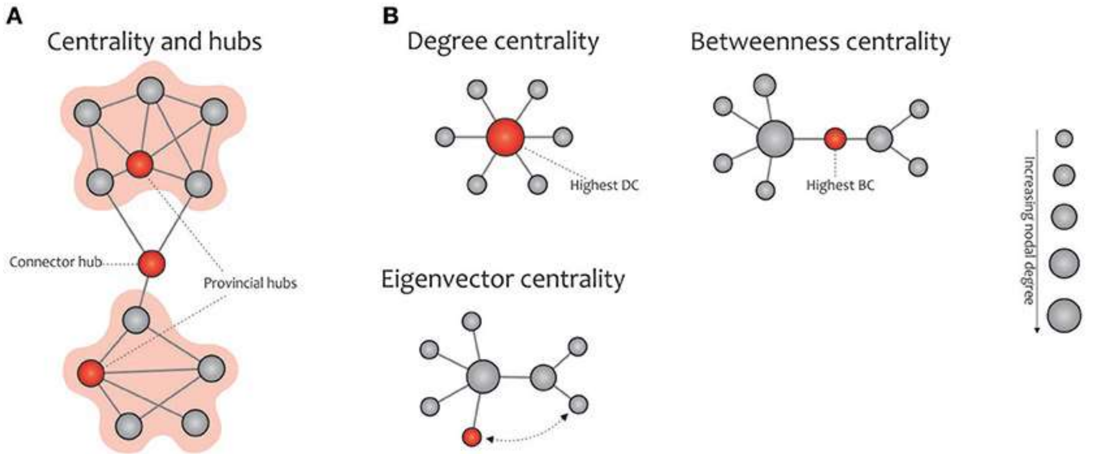

Figure 2.3: This image showcases simple examples of graphs highlighting the principles of degree centrality, eigenvector centrality, and betweenness centrality, alongside the identification of network hubs. Each node's size corresponds to its centrality measure (Farahani, Karwowski, and Lighthall 2019).

The node connectivity on a local level is quantified by the *clustering coefficient*, indicating how dense the connections are among a node's immediate neighbors (i.e. the number of triangles around a node) and therefore the potential for functional segregation in an anatomy-based network.

$$C = \frac{1}{n} \sum_{i \in N} C_i = \frac{1}{n} \sum_{i \in N} \frac{2t_i}{k_i(k_i - 1)}, \tag{2.5}$$

where C_i is the clustering coefficient of a single node, t_i is the number of triangles through node i and k_i is the degree of node i (Watts and Strogatz 1998; Rubinov and Sporns 2010).

For an individual node, the clustering coefficient is calculated by dividing the number of actual connections between its neighbors (triangles) by the total possible connections among them. For the entire network, the clustering coefficient can be the average of all individual nodes' clustering coefficients. A high clustering coefficient indicates a network in which nodes tend to create tightly knit groups with many interconnections. It is related to the effectiveness of local information transfer within a network (Power et al. 2010). The average clustering coefficient is normalized on a per-node basis, which can lead to a disproportional influence of lower degree nodes. Conversely, a traditional form of the clustering coefficient, termed *transitivity*, is normalized across the entire network, thereby avoiding this issue.

A completely random graph would have short path lengths and low clustering, while a highly ordered lattice-type graph would have long path lengths and high clustering. It is, however, possible for a graph to have a high clustering coefficient while at the same time retaining short path lengths. This property is called the *small worldness* of a graph (Watts and Strogatz 1998). There are different mathematical definitions of small worldness. (Humphries and Gurney 2008) defines it as:

$$\sigma = \frac{\frac{C}{C_{\text{rand}}}}{\frac{L}{L_{\text{rand}}}} \tag{2.6}$$

where C and C_{rand} are clustering coefficients and L and L_{rand} are characteristic path lengths of the tested matrix and a random matrix of the sames size.

Networks with high clustering and short path lengths tend to exhibit greater robustness against random failures. This is because dense local connections offer alternative routes for network flow (M. v. d. Heuvel et al. 2008). In the field of neuroscience, high clustering coefficients are thought to indicate functionally specialized modules, whereas a short characteristic path length suggests minimal numbers of synapses in cortico-cortical connections that bridge any two modules. This small-world topology likely reflects a necessary equilibrium between anatomical segregation and integration (Meehan and Bressler 2012).

Another, more versatile metric to characterize small worldness is *small world porpensity* (SWP). SWP quantifies the extent to which a network displays small-world characteristics. It does this by comparing the network's clustering coefficient and path length to those of both lattice and random networks (Muldoon, Bridgeford, and Bassett 2016). The SWP is calculated as:

$$SWP = 1 - \sqrt{\frac{\Delta_C^2 + \Delta_L^2}{2}} \tag{2.7}$$

Where Δ_C represents the fractional deviation of the clustering coefficient from a lattice network, and Δ_L represents the fractional deviation of the path length from a random network. This approach allows for a more nuanced and accurate assessment of small-world properties in weighted networks, overcoming the density dependence issues of previous metrics. The SWP ranges from 0 to 1, with values closer to 1 indicating stronger small-world characteristics (Muldoon, Bridgeford, and Bassett 2016).

Groups of nodes in a network that are more densely connected to each other than to the rest of the network are known as *communities*. The quality of community structure is assessed by a metric called *modularity*. It is defined as:

$$Q = \sum_{u \in M} \left[e_{uu} - \left(\sum_{v \in M} e_{uv} \right)^2 \right] \tag{2.8}$$

In this definition the network is subdivided into nonoverlapping modules M. e_{uv} are the edges that connect nodes in module u to nodes in module v (Newman 2003).

Modularity quantifies the density of links within communities compared to the density of links between different communities. It is calculated as the fraction of the edges that fall within the given groups minus the fraction that would be expected, if the edges were distributed randomly, while node degrees were kept constant. This measurement highlights the network's structure by evaluating the arrangement and density of edges, thereby identifying non-random patterns of connection (Power et al. 2010; Newman 2003).

Two nodes in a graph are adjacent if there is a single edge joining them together. A graph is fully described by a complete list of its nodes and edges. The mathematical formalism describing a graph takes the convenient shape of a matrix, termed adjacency matrix. Each node is represented by a row and a column of entries, and each entry represents an edge that joins two nodes together. The entries are ones and zeros in a binary graph and numerical values in weighted graphs, adding an additional level of depth by quantifying the strength of connections (Power et al. 2010; Wilson 2009).

This approach reduces a complex system to its simplest form, while retaining and emphasizing the structure of the underlying network and its properties, highlighting the topological organization of the network.

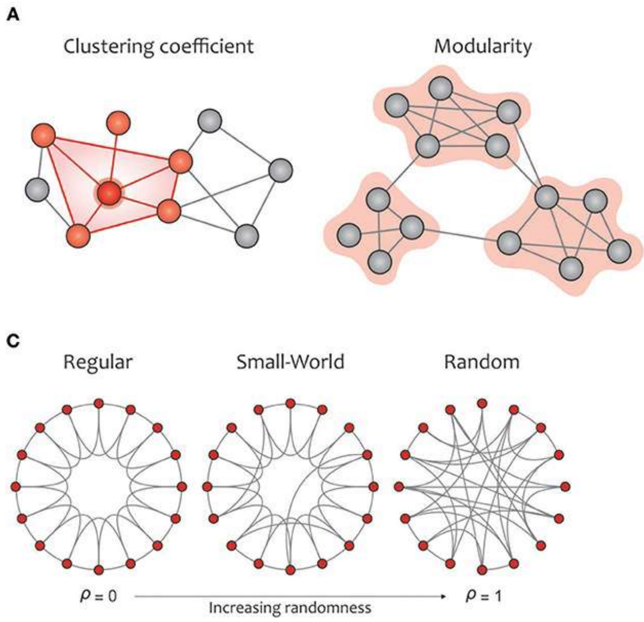

Figure 2.4: The simple graphs in this figure showcase the concepts of the clustering coefficient, modularity, shortest path as well as the difference between regular-, small-world- and random networks (Farahani, Karwowski, and Lighthall 2019).

2.5 Diffusion Tensor Imaging and Fractional Anisotropy

Diffusion Tensor Imaging (DTI) is an advanced MRI technique that allows for the visualization and quantification of white matter tracts in the brain. This non-invasive method provides valuable insights into the structural connectivity of the brain by measuring the diffusion of water molecules within tissue.

DTI works by applying magnetic field gradients in multiple directions to measure the movement of water molecules. In brain tissue, this diffusion is not uniform in all directions due to the presence of cellular structures, particularly in white matter tracts. The diffusion tensor model represents this anisotropic diffusion as an ellipsoid, where the long axis indicates the primary direction of diffusion, which typically aligns with the orientation of white matter fibers (Figley et al. 2022).

Fractional anisotropy (FA) is a key metric derived from DTI data. It is a scalar value between 0 and 1 that quantifies the degree of anisotropy in a given voxel (Basser and Pierpaoli 1996; Özarslan, Vemuri, and Mareci 2005). An FA value of 0 indicates isotropic diffusion (equal in all directions), while a value of 1 represents highly anisotropic diffusion (restricted to a single direction). In the context of white matter tracts, high FA values typically indicate well-organized, densely packed axons with intact myelin sheaths, whereas low FA values may suggest less organized fibers, demyelination, or increased extracellular space.

FA is particularly useful for assessing white matter integrity and has been widely used in studies of brain development, aging, and various neurological and psychiatric disorders (Siasios et al. 2016).

DTI and FA measurements have greatly contributed to the understanding of structural brain connectivity.

DTI data can be used to reconstruct 3D representations of white matter pathways, allowing for the visualization of major fiber tracts, through a process called tractography (Annavarapu, Kathi, and Vadla 2019), and by combining DTI with graph theory approaches, researchers can map and analyze whole-brain structural connectivity networks.

While DTI and FA provide valuable insights into white matter structure, there are limitations. DTI assumes a single fiber orientation per voxel, which can be problematic in areas of crossing fibers. FA values can be affected by various factors, including axon density, myelination, and fiber organization, making interpretation complex (Figley et al. 2022). Tractographic methods suffer from a 'gyral bias', a systematic error where fiber tracking algorithms show a tendency to preferentially terminate on gyral crowns rather than in the sulcal walls or fundi of the brain. This bias results in an overestimation of connectivity to gyral crowns by a factor of 1.5 to 5 and an underestimation of connectivity to sulcal regions (Schilling et al. 2017).

Advanced diffusion imaging techniques, such as high angular resolution diffusion imaging and diffusion kurtosis imaging, are being developed to address some of these limitations and provide more detailed information about white matter microstructure.

2.6 Brain Connectivity

In the context of network neuroscience, the term *connectivity* describes how neurons, brain regions, and networks within the brain are linked to facilitate the communication necessary for the brain to perform its various functions. It is a crucial concept for understanding how information is processed and integrated across different brain regions, to give rise to cognition, emotion, and sensory processing. There are several types of connectivity, all shedding light on different aspects of brain organization.

Structural connectivity in the brain refers to the network of physical and anatomical connections between neurons and brain regions, primarily through synaptic connections and white matter tracts. These axonal connections facilitate the transmission of electrical and chemical signals, in the case of white matter tracts, over long distances, thereby integrating disparate regions of the brain. Structural connectivity is a fundamental concept for exploring and understanding the brain's wiring, and provides a static map of the brain's neuronal networks (Sporns 2007).

Brain structure is complex and can be analyzed at various scales. Mapping the entire brain at the microscale is impractical due to the sheer volume of components involved, given that the cortex alone contains an estimated 10^{10} neurons and 10^{13} synaptic connections. Moreover, such detailed recreation may be unnecessary, as substantial evidence suggests that the brain's functionality emerges from the coordinated activity of large populations of neurons working in concert within the extensive network of the brain. A more viable approach to explore brain function as a whole might be to model the brain on a macroscale, focusing on neuron populations or entire brain regions and their connecting pathways(Sporns, Tononi, and Kötter 2005).

In contrast to structural connectivity, *functional connectivity* describes the statistical relationships and temporal correlations between neuronal activity in separate brain regions. It maps how different brain regions coactivate and synchronize their activity at rest or during specific tasks and is studied using imaging modalities such as blood oxygen level dependent fMRI or EEG (Sporns 2007).

Effective connectivity incorporates aspects of both structural and functional connectivity to understand the causal interactions and dynamic flow of information within a brain network (Sporns 2007).

Structural connections in the brain are good predictors of functional connectivity, indicating that direct anatomical pathways underlie many observed patterns of neural activity. However, indirect interactions also contribute to the formation of functional connections and are not directly mirrored by structural pathways. These indirect connections can introduce often observed deviations of functional maps from structural maps in brain networks (Bullmore and Sporns 2009).

The mathematical representation of brain network connectivity is motivated by graph theory and typically takes the form of an adjacency matrix, which can be analysed via graph theoretical methods. Brain regions are delineated by a parcellation suited to the task at hand and abstracted into the form of nodes. These nodes are represented by the rows and columns of the adjacency matrix. The entries in the matrix represent the edges of the network. In an unweighted network, these edges assume binary values: 1 signifies the presence of a connection, while 0 denotes its absence. Conversely, in a weighted network, the numerical value of the edges quantifies the connection strength, offering a more nuanced depiction of the network's architecture (Power et al. 2010; Sporns 2007). A major simplification in the graph-theoretical representation of a brain network, is that all nodes are considered identical, disregarding potential differences between the regions they represent (Sporns 2018).

The graphs created from structural connectivity are generally sparse, meaning that most possible connections are not realized, and stable over time. In contrast, functional connectivity graphs are often dense and highly variable over short time spans (Sporns 2018).

When analyzed through the lens of graph theory, structural brain connectivity networks representing large-scale anatomical topology, reveal properties such as small-world organization, balancing efficient local processing with global integration (Watts and Strogatz 1998). They exhibit a high clustering coefficient, indicating tight clusters of neurons for specialized processing, combined with a short path length, enabling rapid information transfer to and from distant regions. Scale-free properties are observed, with a few highly connected hubs facilitating network resilience and efficiency. Modularity within these networks reflects functional specialization, segregating into communities that perform specific tasks, yet work cohesively. These properties are thought to be instrumental for the brain's robust, efficient communication and adaptability (Sporns 2007; Bullmore and Sporns 2009).

The small-world structure of the brain is believed to emerge through the satisfaction of two competing requirements. On one hand, any biological system aims to minimize wiring costs, and therefore avoids long distance connections due to the higher metabolic penalty they incur. On the other hand, optimizing the efficiency of global information transfer is essential (Bullmore and Sporns 2009). This balancing act results in a network of tight clusters with high connection density, interconnected by sparse long-range connections, resulting in the short path lengths and high clustering characteristic of small world networks (Lynn and Bassett 2019; Bullmore and Sporns 2012).

2.6.1 Connectivity in Schizophrenia

The disconnection hypothesis proposed by Friston in 1998, suggested that schizophrenia is, at least partly, a result of brain disconnectivity, and has been expanded upon in subsequent research. The disorder is accompanied, if not fully characterized, by significant alterations in white matter integrity and brain network organization, as evidenced by investigations using modalities such as fMRI, EEG, and structural MRI (Heuvel, Martijn, and Fornito 2014; O'Donoghue et al. 2017; Narr and Leaver 2015; Konrad and Winterer 2007). Studies investigating altered brain structure in individuals with schizophrenia have found widespread changes in various structures, particularly in white matter, including volumetric and morphological alterations as well as compromised structural integrity (Kubicki et al. 2007). Diffusion-weighted imaging analyses have demonstrated reductions in white matter volume and structural connectivity, particularly affecting connections between the frontal, temporal, and parietal regions (Heuvel, Martijn, and Fornito 2014).

White matter abnormalities were extensively documented in various brain regions, through DTI studies, manifesting as decreased FA, a measure indicating the directional dependence of water diffusion in tissues. Instances of reduced FA were found in the internal capsule, the prefrontal and temporal lobes, involving fiber bundles like the uncinate fasciculus, cingulum bundle, and corpus callosum, as well as in the fornix and the superior occipito-frontal fasciculus, corona radiata, inferior fronto-occipital fasciculus, superior longitudinal fasciculus, inferior longitudinal fasciculus, optic radiations, hippocampus and cerebellum, indicating widespread diffusion abnormalities (Wheeler and Voineskos 2014; M. Kubicki et al. 2005; Marek Kubicki et al. 2005).

General reductions in white matter volume and morphology were also observed, especially in key areas such as the deep frontal, temporal, and occipital lobes, the fornix, and the cingulate bundle (Canu, Agosta, and Filippi 2015).

In addition, significant microstructural alterations have been identified in critical white matter tracts, also including the uncinate fasciculus, arcuate fasciculus, cingulum, and corpus callosal genu tract, indicating their role in the pathology of schizophrenia (Heuvel, Martijn, and Fornito 2014).

Brain Area	**Changes**
Prefrontal cortex	Decreased FA, increased mean diffusivity
Temporal lobes	Decreased FA, increased mean diffusivity
Uncinate fasciculus	Decreased FA
Cingulum bundle	Decreased FA
Arcuate fasciculus	Decreased FA
Corpus callosum	Decreased FA
Internal capsule	Decreased FA
Cerebellar peduncles	Decreased FA
Frontal lobes	Reduced connectivity strength, altered network metrics
Parietal lobes	Reduced connectivity strength, altered network metrics

Occipital lobes	Reduced connectivity strength, altered network metrics
Insular regions	Reduced connectivity strength, altered network metrics
Thalamic radiations	Reduced connectivity strength, altered network metrics
Superior longitudinal fasciculus (SLF)	Decreased FA
Inferior longitudinal fasciculus (ILF)	Decreased FA
Inferior fronto-occipital fasciculus (IFOF)	Decreased FA
Superior occipito-frontal fasciculus	Decreased FA
Fornix	Decreased FA
Superior frontal gyrus	Altered structural and functional connectivity, reduced efficiency and modularity
Precuneus	Altered structural and functional connectivity, reduced efficiency and modularity
Cingulate cortex	High centrality nodes
Anterior limb of the internal capsule (ALIC)	Decreased FA
Corona radiata	Decreased FA

Table 2.2: List of brain areas and white matter structures that show abnormalities in schizophrenia according to information gathered from (Ellison-Wright et al. 2014; Bullmore and Sporns 2012; Cabral et al. 2013; M. Kubicki et al. 2005; Canu, Agosta, and Filippi 2015; Wheeler and Voineskos 2014; Kubicki et al. 2007)

Voxel-based morphometry and tract-based diffusion studies have shed light on specific white matter alterations that contribute to the pathology of schizophrenia, revealing a compromised microstructure and potential reductions in myelination and tract organization. These collective findings highlight the extensive impact of white matter abnormalities in schizophrenia, leading to decreased connectivity and structural integrity throughout the brain (Heuvel, Martijn, and Fornito 2014).

White matter abnormalities in schizophrenia form the anatomical basis for widespread disruptions in structural connectivity network metrics, as identified through graph theoretical analysis. The observed microstructural changes suggest a compromised foundation for neuronal communication, which is crucial for coherent brain function (Narr and Leaver 2015). Graph theoretical analysis further elucidates the potential consequences of these white matter disruptions, revealing decreased network segregation and integration (Gao et al. 2023). This manifests itself as altered clustering coefficient and reduced local efficiency, indicating impaired local interconnectedness, with specific alterations observed especially in frontal and temporal brain regions, alongside an increase in characteristic path length and a decrease in global efficiency, reflecting impaired integration and longer paths for information transfer across the brain. The increases in path length are most prominent in the frontal, temporal and occipital regions (Micheloyannis 2012; Heuvel, Martijn, Mandl, et al. 2010). This can be interpreted as a deterioration of specialized modules, entailing a higher wiring cost and decreased nodal robustness. Consequently, the brain network shifts away from the optimal small-world organization, characteristic of healthy brain networks, towards more costly, less efficient and less well integrated configurations (Gao et al. 2023; Micheloyannis 2012). Betweenness centrality of frontal hubs in patients is significantly reduced, indicating that these regions play a diminished role as central hubs within the overall network architecture (Heuvel, Martijn, Mandl, et al. 2010). Additionally the connection density of rich-clubs is reduced in schizophrenia (O'Donoghue et al. 2017; Park and K. Friston 2013), indicating reduced centrality in the association cortices and changes in the distribution of hemispheric hubs (Y. Zhang et al. 2012). Decreases in connectivity strength are centered on a frontal-parietal-occipital network.

Graph Metric	**Change Schizophrenia**	**Primarily Affected Brain Regions**
Clustering Coefficient	Reduced	Frontal, Temporal
Local Efficiency	Reduced	Frontal, Temporal
Characteristic Path Length	Increased	Frontal, Temporal, Occipital
Global Efficiency	Reduced	General Brain Network
Betweenness Centrality	Reduced	Frontal Hubs
Connection Density of Rich-Clubs	Reduced	-
Connectivity Strength	Reduced	Frontal-Parietal-Occipital Network

Table 2.3: Changes in Graph Metrics of Structural Connectivity in Schizophrenia

This aligns with the *disconnection hypothesis*, proposing disruptions in the coordinated activity and connectivity of distributed brain networks, rather than isolated regional abnormalities, as major contributing factors to the illness. These findings highlight the role of network disorganization in the pathophysiology of schizophrenia, marking a shift away from the optimal small-world organization towards less efficient, less integrated configurations (Gao et al. 2023; Micheloyannis 2012).

2.7 Computational Neuroscience and Brain Modeling

Computational neuroscience is a multidisciplinary field that merges principles from neuroscience, mathematics, and computer science to understand the complex workings of the brain. This chapter provides an overview of computational neuroscience and brain modeling, beginning with a brief historical perspective on the evolution of the field. The rationale behind brain modeling is explored and various modeling approaches are discussed, ranging from microscopic scales involving detailed neural dynamics to macroscopic scales focusing on larger brain regions and their interactions. Key techniques such as neural mass modeling, which simplifies the collective behavior of neurons, and brain network modeling, are examined in detail. Through these discussions, the chapter aims to elucidate the diverse methodologies employed in computational neuroscience and their critical role in advancing our understanding of the brain (Rattay, Greenberg, and Resatz 2002; Rattay 1990).

2.7.1 Historical Perspective

The evolution of neuroscience can be classified into several epochs. Its origin can be traced back to the ancient Egyptians and Greeks, where it started as a philosophical endeavour. Philosophers like Alcmaeon of Croton and Plato speculated about the origin of the mind, but their approach relied solely upon logical reasoning, as well as reductionist and rational thinking, lacking empirical evidence but nonetheless laying a groundwork for exploring consciousness and its origins (Fan and Markram 2019).

The Anatomists of the Renaissance began the systematic exploration of the brain's structure, creating detailed drawings and trying to draw first correlations between specific brain structures and functions, slowly transitioning from philosophy to empiricism (Fan and Markram 2019).

The 19th century saw the emergence of experimental neuroscience. The electrical nature of nerve signals was discovered and techniques to study electrical brain activity and structure-function relationships were developed. The study of traumatic brain injuries, such as the case of Phineas Cage, lead to increased understanding of structure-function relationships. The detailed microscopic study and subsequent illustrations of the Neuron by Santiago Ramón y Cajal established the foundation of the neuron doctrine (Fan and Markram 2019; Yuste 2015).

The theoretical phase, starting in the twentieth century, saw an overlap with the anatomical phase. Researchers began applying models from mathematics and physics to experimental data to create a deeper understanding of the inner workings of the brain through mathematical abstraction (Bassett, Zurn, and Gold 2018). Alan Hodgkin's and Andrew Huxley's work on the giant squid axon combined theoretical physics, mathematics and experimental data to create a set of equations that described how action potentials in neurons are initiated and propagated by the movement of ions across the cell membrane. This pioneering effort provided a quantitative description of the mechanisms governing the functioning of the neuron and marked the advent of simulation neuroscience (Fan and Markram 2019; Bassett, Zurn, and Gold 2018; Rattay 1990).

The brain is a complex assembly of numerous individual units interconnected by pathways that facilitate signal transfer. Early neuroscience focused on discovering and understanding these individual units, aiming to attribute distinct functions to specific physical entities. This approach was partially successful, as certain brain areas were found to predominantly facilitate specific functions. However, over time, a more nuanced picture emerged. To generate complex behaviors and higher brain functions, the network that binds these disparate units together, plays an equally important role as the individual units themselves. It appears that the brain is more than just the sum of its parts (Fan and Markram 2019).

Following this insight, after the initial focus on single neurons, researchers began to explore how neurons interact with each other within brain networks. In the 1960s and 1970s, scientists started to simulate small networks of neurons, using computers to understand how interactions between neurons could lead to more complex patterns of activity (Yuste 2015). These efforts were significantly advanced by the development of cable theory and compartmental modeling, which facilitated the simulation of electrical properties along dendrites and axons, providing insights into how neural circuits process information. From these early efforts, the field of network neuroscience emerged, treating the brain as a complex network and seeking to understand the functionality of the brain by studying its structural and connectivity patterns through network analysis and graph theory (Fan and Markram 2019).

The field of neuroinformatics set upon managing and analysing the vast datasets provided by the development of new imaging technologies, and the ever increasing computational power steadily increased its capabilities in managing big data (Fan and Markram 2019).

Simulation neuroscience builds upon all the previous phases, integrating vast amounts of experimental data about the function and structure of the brain and merging them into computer models to accurately simulate the brain's behavior, test hypotheses about brain function, and understand disease mechanisms, forming a new frontier in neuroscience (Fan and Markram 2019).

2.7.2 The Rationale Behind Brain Modeling

The shear complexity of the human brain, with its billions of neurons, trillions of connections, electrical and chemical synapses, and intricate molecular dynamics makes deciphering its working mechanisms a formidable challenge. Histological studies provide insights into the biological makeup of its various cells and tissues, revealing the logic behind the brain's remarkable structure. In vitro studies shed light on the cellular and molecular mechanisms underpinning neuronal function and brain processes, allowing researchers to observe how neurons communicate, how synapses form and function, and how various cellular components contribute to the workings of neural networks. In vivo brain imaging techniques, such as fMRI and positron emission tomography, enable us to observe the dynamics of the brain under different conditions and infer structure function relationships.

Simulation Neuroscience uses computational models to simulate the brain's structure, function, and dynamics. It can integrate data from both in vivo and in vitro studies to create detailed models that capture the complexity of the brain at various levels, from molecular interactions and cellular processes to neural circuits and overall brain function.

By doing so, it can help overcome limitations set by other methods of neuroscience. In vitro Studies, while offering detailed insights at the cellular or molecular level, often cannot replicate the full complexity of living systems, including the intricate interactions and feedback mechanisms present in a living brain. Simulation neuroscience can take the findings from in vitro studies and incorporate them into larger models of brain function, allowing researchers to explore how cellular-level phenomena impact brain-wide processes (Yuste 2015).

In vivo studies are limited by the resolution of imaging techniques and ethical considerations that restrict the extent of experimental interventions. Simulation neuroscience can use data from in vivo studies to construct and validate models that predict how complex neural networks operate and interact, facilitating experiments that are not feasible in living organisms due to technical or ethical constraints.

Simulation neuroscience can serve as a virtual testing ground for hypotheses about brain function and the mechanisms underlying neurological disorders. By simulating brain activity, researchers can predict outcomes of experimental manipulations or therapeutic interventions, explore scenarios difficult or impossible to replicate in vivo or in vitro, and conduct virtual experiments in a fraction of the time it would take to do them in real life. It represents a third pillar of neuroscience research that complements traditional experimental approaches, offering new avenues for discovery and innovation in understanding the brain.

2.7.3 Modeling Approaches

The field of computational neuroscience leverages a variety of models to understand the intricate relationships within the brain, each model offering unique insights into its structure and function. This chapter discusses the different approaches available to model complex systems like the brain. A model is a simplified representation of a system, or object, that captures its essential features and relationships. Models are used to abstract and reduce complexity, making it easier to understand, analyze, and predict the behavior of the real-world phenomena they mimic. They never depict reality in all its detail, but represent a compromise to reduce a system to its essentials, to improve understanding of a specific aspect, and thereby represent a balancing act between performance, accuracy and realism. The choice of the modeling approach, which delineates the type and level of abstraction is highly dependent on the objective being pursued.

Models can be classified along three different continuums, ranging from data representation to first-principles theory, from biophysical realism to functional phenomenology, and from elementary descriptions to coarse-grained approximations. Where they place on these spectra depends on the modeling approach (Bassett, Zurn, and Gold 2018).

Purely data-driven models are constructed based on empirical data. In neuroscience these models aim to represent observed brain structures and activities as accurately as possible. As mere data representations they are unable to make predictions on how a system behaves or develops. The other side of this spectrum are purely theory-driven models. These are usually derived from first principles and aim to predict how neural systems behave under various conditions, combining network architecture with dynamic equations to describe the evolution of the system. Data-driven models often retain much biological realism and track closely with experimental results, but can not provide information about the dynamics and evolution of a system, like theory-driven models strive to do. Theory-driven models, however often sacrifice neuroanatomical details to abstraction to allow for manageable calculations (Bassett, Zurn, and Gold 2018).

Models with an emphasis on biophysical realism incorporate detailed anatomical and physiological data. These models aim to accurately reflect the physical properties and interactions within the brain, including representations of physical entities, such as neurons and their dynamics. They make use of rich empirical findings about the brains' physical nature, but can be computationally demanding and hard to interpret. On the opposing side, there are functional phenomenological models with a focus on capturing the functional relationships between brain regions without necessarily adhering to their exact physical counterparts, often using statistical measures of functional connectivity. They provide interpretability and simplicity, but are difficult to correlate with physical brain structure (Bassett, Zurn, and Gold 2018).

The final dimension to classify a model considers scale. Elementary models, with a focus on the fine-grained details of neural interactions at the level of individual neurons and synapses stand in opposition to coarse-grained models, that simplify the brain's complexity by averaging or approximating the properties of large groups of neurons. Where elementary models are helpful for understanding the fundamental mechanisms of neural processing, coarse grained models are well suited for exploring large-scale brain dynamics and functional connectivity (Bassett, Zurn, and Gold 2018).

Most models fall somewhere between the extremes of these spectra and so does the model that is used built for this thesis. Where they fall is determined by many factors, like the subject of research, the available data or the computational resources.

2.7.4 Neural Mass and neural field Models

Neural mass models describe the average activity of populations of neurons with matching characteristics and coordinated behaviour, often focusing on the dynamics of specific types of neural interactions, such as excitatory and inhibitory connections within a localized region. These models typically abstract away the spatial structure of neural populations, instead representing them as point-like entities. The assumption is, that explicit structural or temporal features of single neurons are irrelevant for capturing complex mesoscopic dynamics, applying the concept of universality from statistical physics, that posits that the laws governing large systems are largely independent from the laws governing its small scale constituents (Ritter et al. 2013). Connections between single neurons of a population are exchanged for connections of the mean activity of populations. This kind of model usually incorporates two different types of mathematical transformations. A transformation from waves to pulses at the neuron's soma, which is generally described by a static sigmoid function, and a linear transformation from pulses to waves at the synaptic level within the neural ensemble. The wave-to-pulse operator links the mean firing rate directly to the average postsynaptic depolarization, assuming an immediate response. Meanwhile, the pulse-to-wave operator is determined by synaptic kinetics, modeling the average postsynaptic reaction as a linear convolution of the incoming spike rate (David and K. J. Friston 2003). This approach simplifies the complexity of neural interactions to a few key variables and parameters, making it particularly useful for modeling EEG or MEG signals where the spatial resolution is limited. Neural mass models are well suited for capturing the essential dynamics of neural populations, such as oscillatory behavior and wave propagation, using a relatively small number of equations (Sanz-Leon et al. 2015; Sanz Leon et al. 2013).

Neural field or mean field models, on the other hand, extend the concept of neural mass models by incorporating spatial continuity and interactions over a continuous field. These models describe how neural activity varies not only over time but also across space, allowing for the simulation of complex spatial patterns of brain activity, such as waves of activity moving across the cortex. Neural field models represent tissue-level models that depict the spatiotemporal progression of averaged variables like synaptic voltage or firing rate activity across neuron populations. They are governed by partial differential equations that account for both the local interactions within neural populations and the long-range connections between different brain regions. This makes neural field models particularly suited for studying the spatial aspects of brain dynamics, such as the propagation of activity waves and the formation of activity patterns over larger brain areas (Sanz-Leon et al. 2015; Sanz Leon et al. 2013).

In summary, while neural mass models focus on the temporal dynamics of aggregated neuronal activity without explicit consideration of spatial distribution, neural field models incorporate both the spatial and temporal evolution of brain activity, offering a more detailed representation of how neural processes unfold across the brain's complex landscape (Sanz-Leon et al. 2015; Sanz Leon et al. 2013).

2.8 The Virtual Brain

The Virtual Brain (TVB) is a sophisticated, open source platform designed to simulate the dynamics of large-scale brain networks, leveraging biologically realistic connectivity data derived from neuroimaging techniques like DTI and DSI. It is the product of a colaborative effort of several institutions like Charité – Universitätsmedizin Berlin, Aix-Marseille University and The Human Brain Project. The platform facilitates the inference of neurophysiological mechanisms through modeling, spanning various brain scales, which are fundamental to producing large-scale neuroimaging signals such as fMRI, EEG, and MEG (Ritter et al. 2013). TVB provides a neuroinformatics tool with a brain simulator at its core, featuring a wide array of local dynamics models. Users can access TVB through a browser-based graphical user interface for a more guided experience or utilize its full capabilities via a Python package. The scripting interface enables users to integrate its functionality with custom scripts and external libraries, providing flexibility for advanced applications.

2.8.1 Motivation

The TVB project emerged in response to the limitations of contemporary network simulations, which predominantly focused on microscopic and mesoscopic scales, infusing detailed biophysical information but often overlooking global brain dynamics. This approach facilitates understanding of localized brain activity, but falls short in capturing the full spectrum of brain dynamics that arises from the complex interplay of different brain regions. The development of TVB was motivated by the idea to fill this gap and develop an efficient and flexible neuroinformatics platform that operates at the macroscopic level of brain organization, using realistic connectivity, to reproduce and probe a wide variety of brain dynamics (Sanz Leon et al. 2013).

Traditional neural field modeling often resorted to using homogeneous (translationally invariant) connectivity, primarily due to the unavailability of detailed large-scale brain connectivity data. This approach mainly emphasized the temporal domain of brain organization, without touching on the spatiotemporal organizational structure critical to understanding global brain dynamics (V. Jirsa et al. 2002). Furthermore, the symmetry of the connectivity in these earlier models lead to constraints on the range of observable dynamics (V. Jirsa et al. 2002). TVB introduces a top-down modeling approach to whole brain dynamics, where the underlying network is characterized by its structural large-scale connectivity, extracted from brain imaging data, and mesoscopic models that govern the intrinsic dynamics of the nodes (Sanz Leon et al. 2013).

Large-scale brain dynamics are fundamentally expected to mirror the underlying anatomical connectivity linking brain areas (Deco, V. K. Jirsa, and McIntosh 2010). However, structural connectivity is not the sole determinant of brain network dynamics and transmission delays also play a crucial role in shaping these dynamics (Knock et al. 2009). Homogeneous approximations, while suitable for mesoscopic descriptions of brain activity, proved to be less effective in addressing full brain network dynamics prompting the integration of biologically realistic DTI-based connectivity into full brain modeling (Sanz Leon et al. 2013).

The strengths of TVB lie in its integration of empirical data at multiple scales, its ability to create personalized brain models through integration of brain imaging data, its advanced simulation capabilities that leverage the implementation of biologically realistic connectivity with connection weights and delays, and its support of a large selection of local dynamics models, as well as its ability to interact with other widely used tools and packages.

The evolution of TVB, dedicated to identifying and reproducing realistic whole brain network dynamics based on empirical connectivity and neural field models, reflects a broader vision to look beyond models of localized brain activity to a comprehensive framework that encompasses the entire brain. By doing so, TVB aims to facilitate a deeper understanding of the brain's complex dynamics and foster advancements in neuroscience research and clinical applications (Sanz Leon et al. 2013).

2.8.2 The Modeling Principle of TVB

TVB is designed to simulate brain wide dynamics, investigate the emergence of higher-level phenomena as a consequence of segregation and integration of neuronal populations, explore their underlying neurophysiological mechanisms and aid in the formulation and testing of hypotheses regarding the functioning of the brain as a network (Ritter et al. 2013). This chapter provides a quick overview detailing the modeling approach that forms the foundation a simulation in TVB is based upon.

TVB models brain activity at a macroscopic level as bottom-up interactions between mesoscopic brain-processing units, connected by long range and optionally short range connectivity. The integration of multimodal imaging data, provides connectivity as well as data from individual neurons and neuronal populations, that enter a simulation through local dynamics models, to form a coherent framework that encompasses the entirety of the brain (Ritter et al. 2013).

In TVB, macroscopic, salient brain regions, which consict of large neural populations, are represented through nodes. Each node is equipped with a mesoscopic local dynamics model, creating its own intrinsic dynamics and mimicking the neural activity of the neural population. These local dynamics models usually are neural mass models of varying complexity, ranging from phenomenological approximations, to detailed, neurophysiologically based descriptions of neural activity. Theses models simplify the behavior of large groups of neurons into more manageable, functionally relevant dynamics, thereby translating the micro- to the mesoscale, whilst sacrificing some detail on the way. A necessary compromise, with the goal of bridging the gab between the microscopic world of single neurons as sources of electrical activity and the macroscopic world of whole brain dynamics, by leveraging an intermediate step in the mesoscale (Sanz Leon et al. 2013; Ritter et al. 2013; Woodman et al. 2014).

The regional nodes are coupled via structural connectivity, derived from DTI tractography, with the aim of simulating macroscopic effects by connecting mesoscopic entities. These non-local and heterogeneous connectivities provide connection weights, scaling the strength of the connections between nodes, and connection lengths, which, due to finite transmission speed, introduce transmission delays that are essential to shaping brain network dynamics (Woodman et al. 2014; Sanz Leon et al. 2013; Ritter et al. 2013).

The long range connections represented by the structural connectivtiy matrix represent axonal projections from pyramidal neurons. Therefore, these connections are purely excitatory. However, incoming activity can excite inhibitory populations in the target, thereby creating inhibition (Sanz Leon et al. 2013).

The activity represented by the state variables of the local dynamics models is transmitted from node to node via the connections formed by the long range connectivity, but before entering a model, they have to be rescaled to a form appropriate to the population model at that node. This rescaling is achieved by passing the state variables through a coupling function (Sanz Leon et al. 2013).

Networks in TVB can be described at two distinct spatial scales, which result in two types of simulations. Region based simulations rely solely on the structural connectivity for long range connections, as described earlier. Short range connections are subsumed in the local dynamics models and not treated independently. This results in a coarse grained approximation of the whole brain network on the order of centimeters (Sanz Leon et al. 2013; Ritter et al. 2013; Woodman et al. 2014).

Surface based simulations take a more finegrained approach. This type of simulation uses the triangular surface mesh of the cortex, to simulate cortico cortical activity. In surface based simulations, each triangle of the surface mesh contains a local dynamics model. Lateral connections between the cortical surface models are facilitated by a local connectivity kernel. This kernel is translationally invariant and assigns weight to the connections between surface nodes according to their geodesic distance on a scale of millimeters. Typically these kernels use Gauß functions, that taper of exponentially with distance and have a defined cut off distance, where the coupling falls to zero. This way close cortical units exert a strong influence on each other, whereas distant units do not influence each other at all. Applying this method results in a much more detailed spatial sampling of cortical activity, creating an approximation of cortical activity that is spatially continuous, neural-field-like, but also drastically increases computation times (Sanz Leon et al. 2013; Ritter et al. 2013; Woodman et al. 2014).

In this type of model, long range and short range connectivity coexists. Short range connectivity facilitates lateral, intracortical signal transfer, whlie long range connectivity provides time delayed, intercortical input from far off cortical or subcortical regions, that are represendted by regional nodes (Sanz Leon et al. 2013; Ritter et al. 2013; Woodman et al. 2014).

The integrators implemented in TVB provide standard numerical solutions, both deterministic, and stochastic for the implementation of noise, to the equations of the local dynamics models (Sanz-Leon et al. 2015).

Recording and processing of the simulated signals in TVB is implemented via so-called monitors and happens simultaneously with the simulataion. These monitors represent a measuring process that is applied to the simulated neural activity. Several monitors are available, providing different functionalities. The raw monitor simply records all neural activity, represented by the state variables of the neural models at all nodes, without any processing, quickly accumulating large amounts of data that might be limited by disk space.

Biophysically inspired monitors, serve two purposes simultaneously. They transform the simulated activity into a form that is directly comparable to experiments by using spatial, temporal or spatiotemporal kernels on the output to recreate biophysical measurements, and also perform a significant downsampling of the raw data resulting in considerable data reduction (Sanz Leon et al. 2013; Ritter et al. 2013; Woodman et al. 2014).

The EEG monitor specifically uses a temporal average as the temporal kernel and a lead field matrix as the spatial kernel (Woodman et al. 2014). The neural source activity is projected onto EEG space by using forward models. TVB assumes that source activity can be well estimated by only considering excitatory neurons, whose dendritic trees are positioned roughly perpendicular to the cortical surface. Theses neurons generate equivalent current dipoles (Woodman et al. 2014). The forward model is computed by first defining each vertex of the cortical mesh as a source dipole. Their orientations are chosen so that each vertex normal, points to the outside of the cortex. TVB uses a three compartment head model constructed from anatomical data to incorporate volume conduction effects. Under theses assumptions the lead field matrix is calculated, with the purpose of projecting each source of neural activity onto the EEG electrodes (Sanz Leon et al. 2013; Ritter et al. 2013; Woodman et al. 2014).

Each of these components is defined as a class in the TVB framework:

1. The local dynamics model, has the form of a set of differential equations that capture the dynamics of neural activity of a brain region. These models vary in their complexity and their capabilities and have to be carefully chosen, depending on the goal of the simulation.

2. The connectivity class represents the anatomical connections, mainly white matter tracts derived from DTI that model the long range connections that couple individual local dynamics models to form a network. It can also provide weights to scale the signal transfer between individual nodes, and transmission delays.

3. The coupling function transforms the signal that travels from one node to another, via the pathways formed by the structural connectivity, into an adequate shape, before it enters the equations of the local population model.

4. The integrator defines the numerical model that is used to solve the differential equations.

5. The monitor is an object that is used to capture the outputs of the simulation. By incorporating forward models TVB can translate the simulated neural activity into signals comparable to those measured by various neuroimaging modalities, such as EEG, MEG, and fMRI, thus making the data more interpretable and reducing the the raw output data to a smaller size.

To run a simulation, objects have to be created from these classes to then combine them in a simulator object.

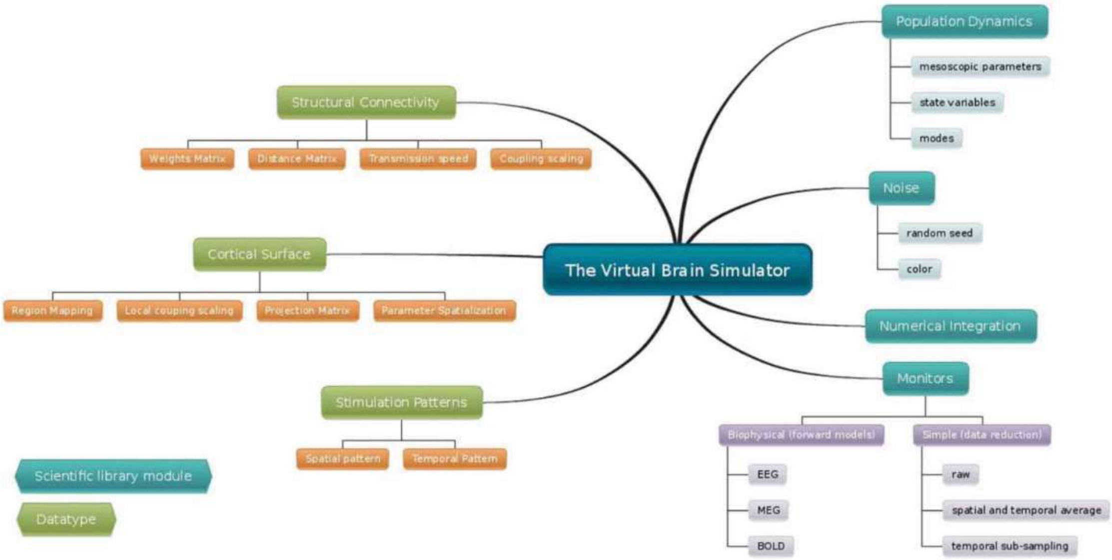

Figure 2.5: This diagram is a visual interpretation of the inputs the simulator object requires to set up a simulation (Sanz Leon et al. 2013)

2.8.3 Data Requirements

Building a simulation in TVB, requires various data objects, each serving a unique purpose in creating a comprehensive brain network model. These data objects can be created by processing raw structural data from brain imaging, extracting the necessary information, and molding it into the specific data structure unique to TVB.

The raw data to build a model from scratch includes structural MRI and DTI images. The structural MRI, usually T1/T2 weighted scans, are used to differentiate the brains soft tissue types and digitally recreate the brains anatomy. The DTI data are used to extract the white matter tracts that form the basis for the structural connectivity.

The raw data undergoes several preprocessing steps, in which the structural MRI is parcelled and several triangular surface meshes, representing the border regions between tissue types, are extracted. White matter tracts are extracted from DTI data and converted into a structural connectivity matrix. The format TVB requires is a collection of text files with a specific naming convention, that are compacted into Zip folders. Each surface is stored in a separate zip folder with three text files:

- **Vertices:** containing the coordinates of each corner point of a triangle as triplets.

- **Triangles:** containing triplets indexing the vertices.
- **Normals:** containing the orientation of the surface normals to each triangle of the mesh.

The connectivity zip folder must contain at least three text files:

- **Centres:** containing the region labels and coordinates of the region nodes.
- **Weights:** containing the weights matrix.
- **Tract_lengths:** containing the tract lengths matrix.

The connectivity zip folder can hold additional information, also as text files, supplying information about average orientations, about whether a node is cortical or subcortical, or about whether a node is in the left or right hemisphere.

The minimally required preprocessed structural data set to perform a basic simulation in TVB consists of a surface mesh, a parcellation, region centers, region mapping, and a connectivity matrix. The surface mesh represents the cortical surface, while the parcellation and region centers further define the brain's structural divisions on the surface and assign nodes to the correct region. The region mapping links each triangle of the surface mesh to a specific brain region delineated by the parcellation, and the connectivity matrix describes the strength and direction of connections between these regions. To perform more advanced simulations, the minimal dataset can be expanded on by adding skull and skin surface meshes to create a head model, a tracts matrix containing tract lengths, detailed information about units (areas, lengths, connectivity strengths), data on various sensors like EEG and MEG (locations, labels), as well as a lead-field matrix forming the link between the cortical surface, the regional nodes and a chosen sensor array. EEG Locations and region mapping have to be provided as simple text files, and the projection matrix as a matlab file.

2.8.4 Local Dynamics Model

The local dynamics model is responsible for creating neural activity at the site of each node of the model. It describes how each brain area responds and evolves over time based on its intrinsic properties and incoming signals, by describing the collective behavior of neural populations at a mesoscopic scale, and bridges the gap

Minimal Structural Dataset	Complete Structural Dataset
Surface mesh Parcellation Region centres Region mapping Connectivity matrix	Surface mesh Parcellation Region centres Region mapping Connectivity matrix
	additional connectivity details Head model surfaces Tracts matrix Units information (areas, lengths, connectivity strengths) EEG/MEG/iEEG sensors information

Table 2.4: Comparison of Minimal and Complete Structural Datasets for TVB Simulations

between individual neurons and whole-brain activity. Incorporation of biophysical parameters that reflect real neural properties, facilitates more physiologically accurate simulations. The following chapter briefly introduces the Jansen and Rit model, which was used as a local dynamics model in this simulation.

The Jansen and Rit Model

The Jansen and Rit model is a physiologically inspired neural mass model that was developed by merging ideas from previous works by Lopes da Silva (1974), introducing the concept of neural populations involving thalamocortical relay cells and interneurons with feedback loops to uncover the origin of alpha waves, Katznelson (1981), emphasizing the importance of cortico-cortical connections and especially long-range excitatory connections through pyramidal neurons, and more. The model aimed to simulate the electrophysiological phenomena observed in EEG, with an emphasis on alpha activity, using a lumped parameter approach focusing on cortical columns inhabited by a large number of neurons (Jansen, Zouridakis, and Brandt 1993). The model was able to successfully simulate alpha activity and, after ”sensory stimulation”, evoked potentials (Grimbert and Faugeras 2006).

The model describes neuronal dynamics as an interaction between three different types of neural populations in the cortical column: feed forward pyramidal neurons, excitatory interneurons, and inhibitory interneurons.

The pyramidal cells are excitatory, receive external input from neighboring or distant columns, and are able to project signals out of their local region. The excitatory interneurons, interpreted as layer IV spiny stellate cells following Friston et al. (K. J. Friston and Dolan 2010) and the inhibitory interneurons form excitatory and inhibitory feedback loops with the pyramidal cells within a column (Aburn et al. 2012). The balanced feedback relationship between pyramidal cells and interneurons leads to rhythmic activity. Delays and the interactions between these feedback loops are crucial for the emergence of different rhythms, allowing for the complex oscillatory patterns observed in EEG signals.

External input entering a pyramidal cell is represented as a pulse density $p(t)$, which can be random (representing nonspecific background activity) or deterministic (representing specific activity originationg from other cortical units) (Grimbert and Faugeras 2006).

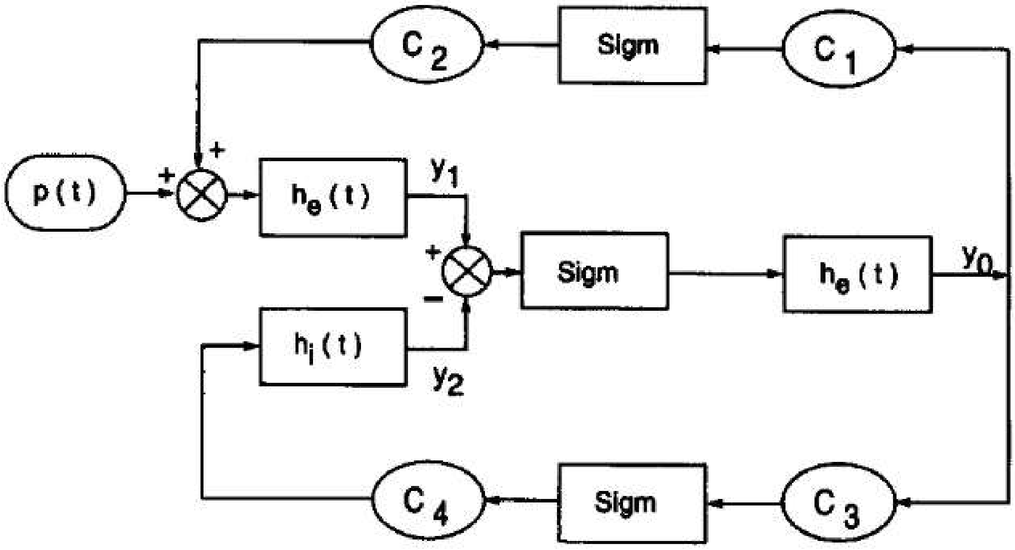

Figure 2.6: Schematic representation of the Jansen and Rit model for alpha generation

In the model, each group of neurons is represented by two functional units. The first unit, known as the postsynaptic potential block, processes the incoming average pulse density of the action potentials and converts it into an average postsynaptic membrane potential. This potential can be either excitatory or inhibitory, depending on the nature of the synaptic input. The postsynaptic potential block essentially acts as a linear filter and performs a linear transformation, characterized by a specific impulse response, to perform this conversion. The transformation functions for the excitatory and inhibitory case are as follows (Jansen and Rit 1995):

$$h_e(t) = \begin{cases} Aate^{-at} & \text{if } t \geq 0 \\ 0 & \text{if } t < 0 \end{cases} \tag{2.9}$$

$$h_i(t) = \begin{cases} Bbte^{-at} & \text{if } t \geq 0 \\ 0 & \text{if } t < 0 \end{cases} \tag{2.10}$$

Variable	Description
A, B	Maximum amplitude of the excitatory/inhibitory postsynaptic potential
a, b	Lumped representation of the sum of the reciprocal of the time constant of passive membrane and all other spatially distributed delays in the dendritic network for excitatory/inhibitory synapses

Table 2.5: Description of the variables in equations (2.9) and (2.10)

The second functional unit is a sigmoid function that converts a population's average membrane potential into an average pulse density of action potentials generated by the neurons (Jansen and Rit 1995).

$$Sigm(v) = \frac{2e_0}{1 + e^{r(v_0 - v)}} \tag{2.11}$$

Variable	Description
e_o	Maximum firing rate of the neural population
v_o	Postsynaptic potential at which a 50% firing rate is achieved
r	Steepness of the sigmoidal transformation

Table 2.6: Parameters of equation (2.11)

Four connectivity constants C_{1-4} represent the connections between pyramidal cells and interneurons. These constants account for the total number of synaptic connections from interneurons to axons and dendrites of the cortical column (Jansen and Rit 1995).

Every postsynaptic potential unit leads to two second order differential equations in the shape of

$$\ddot{y}(t) = Aax(t) - 2a\dot{y}(t) - a^2y(t) \tag{2.12}$$

that each can be rewritten into two first order differential equations

$$
\begin{aligned}
\dot{y}(t) &= z(t) \\
\dot{z}(t) &= Aax(t) - 2az(t) - a^2y(t)
\end{aligned}
\tag{2.13}
$$

Here, $x(t)$ represents the input signal and $y(t)$ represents the output signal.

With equation (2.13) the states of the model can be fully described by the following six differential equations:

$$
\begin{aligned}
\dot{y_0}(t) &= y_3(t) \\
\dot{y_3}(t) &= Aa\text{Sigm}[y_1(t) - y_2(t)] - 2ay_3(t) - a^2y_0(t) \\
\dot{y_1}(t) &= y_4(t) \\
\dot{y_4}(t) &= Aa\{p(t) + C_2\text{Sigm}[C_1y_0(t)]\} - 2ay_4(t) - a^2y_1(t) \\
\dot{y_2}(t) &= y_5(t) \\
\dot{y_5}(t) &= Bb\{C_4\text{Sigm}[C_3y_0(t)]\} - 2by_5(t) - b^2y_2(t)
\end{aligned}
\tag{2.14}
$$

with y_{1-3} representing the output of the postsynaptic potential units (Jansen and Rit 1995).

The Jansen and Rit model has been used in many different configurations, since its development to simulate EEG rhythms and other phenomena. Variations in input, coupling strengths and network structure yield a broad spectrum of behaviours, that go beyond the original intention of simulationg alpha activity and evoked potentials. Coupled networks of Jansen and Rit models have produced various types of oscillatory activity, including delta and theta activity and spike-wave discharges reminiscent of epilepsy (Ahmadizadeh et al. 2018). The wide spectrum of brain waves in the repertoire of this model and its roots in biophysically inspired mechanisms make it an ideal candidate for the purpose of this work.

The Jansen and Rit Model in TVB

The original Jansen and Rit model implements Ordinary Differential Equations (ODEs) for each connection between neural masses, adding complexity and detailed interaction mechanisms. Specifically, it includes additional postsynaptic potential blocks for each connection, leading to 16 ODEs for a two-column model. In contrast, the TVB implementation simplifies this by using ODEs only per neural mass, omitting the extra postsynaptic potential blocks and replacing them with delays and sigmoid functions. This results in an approximation, where global coupling and noise are handled differently. TVB introduces noise via a stochastic integrator and uses the parameter *mu* as the mean input firing rate, rather than directly through *p(t)*. This simplification allows for efficient large-scale simulations but loses some of the detailed connection dynamics present in the original Jansen and Rit model. The TVB approach does not replicate the exact system described in the original paper, particularly in multicolumn setups due to these methodological differences, but aims to yield an approximation that is as close as possible to the original model, while adhering to the modeling principles embedded in TVB.

3 MATERIALS AND METHODS

3.1 Data and Data Processing

This section provides a short overview on where the data used for this project was acquired from, and how it was processed to yield a dataset compatible with TVB.

3.1.1 Structural Connectivity Matrices

The dataset used to create the average structural connectivity at the center of the simulation was obtained from braingraph.org (Kerepesi et al. 2017). It consists of 1064 structural connectivity datasets that were generated from MRI scans, made available through the human connectome project. The dataset is available for download on the homepage under the name *'86 nodes set, 1064 brains, 1 000 000 streamlines, 10x repeated & averaged (18 MB)'*. It contains structural connectivities extracted from MRI data of 1064 brains and is parcellated into, contrary to what the name of the dataset suggests, 83 nodes (70 cortical, 13 subcortical), following the *Desikan Killiani atlas* (Desikan et al. 2006). Node 83, the brainstem, was removed to resolve compatibility issues in subsequent processing steps. The files are presented in a standardized GraphML format, defining nodes and edges by several attributes that can be accessed as text files. Each node is specified by a set of seven attributes, five of which were relevant for the creation of the adjacency matrices and were extracted from the data sets. The attributes that were used to create the nodes of the adjacency matrix are *dn_position_x*, *dn_position_y*, and *dn_position_z* containing the coordinates of each node in a three-dimensional vector space, *dn_name* supplying the label for each node as well as the brain-hemisphere they are located in and *dn_region*, specifying if a node is cortical or subcortical.

The relevant attributes for extracting the edges from the data set are *number_of_fibers*, indicating the number of fibers running between two brain regions, *FA_mean* indicating the mean fractional anisotropy measured for the fibers between two regions, *fiber_length_mean*, indicating the length of the fibers as well as *source* and *target*, specifying the region where the measured tract originates and the region where it terminates.

attribute	description
dn_position_x	x coordinate of the node position
dn_position_y	y coordinate of the node position
dn_position_z	z coordinate of the node position
dn_name	specifier for the hemisphere and node name
dn_region	specifier for cortical and subcortical regions
source	node of origin for a specific tract/edge
target	target node for a specific tract/edge
number_of_fibers	number of fibers measured for an edge connecting two nodes
FA_mean	mean fractional anisotropy of tracts between two nodes
fiber_length_mean	mean length of the fibers connecting two nodes

Table 3.1: Description of attributes from braingraph.org data sets containing the relevant information to create adjacency matrices.

The information contained in the braingraph.org datasets was extracted file by file using a custom python script. For each file, three matrices were created. Two matrices containing the FA values and the fiber counts respectively, that were used to create the weights matrix, and one matrix containing the tract lengths. The weight of each edge is represented as an entry in the weights matrix and scales the connection strength between two nodes in the simulation. It was estimated by element-wise multiplication of the FA matrix and the fiber count matrix, using the fiber count as the prime measure of connection strength and FA, which quantifies tract integrity, to scale it. This approach was chosen because, according to (Huang and Ding 2016), FA alone, while being a widely applied measure in this context, is not a good measure of the strength of anatomical connectivity, because it ignores fiber count.

After creating a weights- and a tract matrix for each of the 1064 brains in the dataset, an average weights matrix and an average tract matrix were created by calculating the mean for each entry, over all matrices. A small number of entries in some of the matrices were *Not a Number* (NaN) values, that were dealt with by skipping them in the computation of the mean. This approach was deemed appropriate, considering that the number of NaN values was very small compared to the total number of entries. The entry containing the most NaN values (16 instances), counted over all 1064 matrices, was the edge connecting area 69 to 28 (lh.temporalpole and rh.temporalpole), so this edge in the average matrix is only a mean of 1048 values. Due to the same reason, the edge between 68 and 27 (lh.entorhinal and rh.entorhinal) is average of 1054 values, seven edges are an average of 1062 entries and two edges are an average of 1063 entries.

This process resulted in two matrices, an average weights matrix and an average tract length matrix, already in the correct format required by TVB.

3.1.2 Surface Data

The next step in preparing the data for the simulation was extracting surfaces from anatomical MRI images, namely a cortical surface, an inner skull surface, an outer skull surface and a scalp surface.

Obtaining these surfaces was necessary for a number of reasons, the main reason being the requirements of the *convert2TVB* pipeline, the final leg of the *TVB preprocessing pipeline*, which was used to create TVB ready datasets for the simulation. The TVB preprocessing pipeline uses multimodal MRI datasets from anatomical, functional and diffusion-weighted MRI as inputs and computes structural connectivities, brain surfaces, electrode positions, lead field matrices and more, in the specialized format that is used in the TVB simulation framework, as output (Schirner et al. 2015). Since the goal in this work is to run simulations on an average structural connectivity, the full pipeline could not be used and the format of the custom connectivity- and tract matrices was not compatible with the requirements for the input of the *convert2TVB* script. Therefore proxy data (surfaces, tracts etc. that would have been created in previous steps of the pipeline, if the full pipeline had been used) had to be created to be entered as input in the convert2TVB section of the pipeline. to generate a TVB ready dataset around the custom connectivity matrices.

The dataset that was used, had been obtained from *OpenNeuro*, and was previously used in the paper *Modeling brain dynamics in brain tumor patients using The Virtual Brain* (Aerts et al. 2018). It contains anatomical T1 weighted and diffusion weighted images of tumor patients and controls. One of the control datasets, that best fit the specifications, was selected. Surface meshes were computed on the basis of the T1 weighted anatomical image using the open source software *freesurfer* (Fischl 2012). Freesurfer's recon-all command performs a series of automated processing steps including motion correction, intensity normalization, talairach transformation, skull stripping, brain tissue and structure segmentation, cortical surface reconstruction and refinement, and anatomical parcellation of the cortical and subcortical regions. This is a time consuming process that lasts several hours and produces suitable surface meshes that can be further processed for TVB.

Additionally tracts and weights were extracted from the diffusion weighted image using *MRtrix3*, also a requirement as a proxy dataset for the convert2TVB pipeline.

Both scripts were run on WSL2 (Windows subsystem for Linux).

Pre-Processing Pipeline

Before successfully running the *convert2TVB* script, several modifications had to be made to the code to remedy issues due to depreciation of parts of the code and to correctly integrate the proxy data. Additionally, the surface meshes representing the cortical surface and the inner skull had to be manually modified. Due to an artefact, likely created during freesurfer processing, the boundaries of the cortical surface and the inner scull surface were locally protruding outwards, crossing the boundary of the outer skull surface (see figure 3.1), producing an error during the creation of the head model.

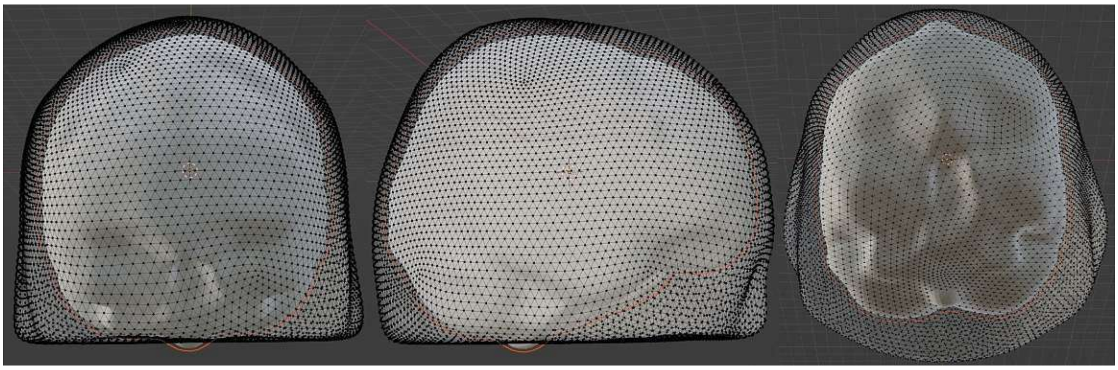

Figure 3.1: Images of the surfaces created with freesurfer and imported into blender. On the bottom the protrusions of the cortical surface (gray) and the inner skull surface (orange outline) are visible as they cross the boundary of the outer skull surface (triangle mesh).

To make the necessary modifications, the surface meshes were converted into an object format readable by the 3D modeling software blender, using a custom python script. In blender, the protruding areas on the caudal surfaces of the cortical and inner skull meshes were smoothed by hand, resolving the boundary crossing issue. Then the surfaces were converted back into the format expected by the *convert2TVB* pipeline. With the surfaces and tracts complete, the convert2TVB processing pipeline was successfully run, generating a comprehensive set of TVB-ready data. The pipeline performs the following steps:

1. **Create Cortical Surface and Region Mapping**: Generates cortical surface meshes by combining the meshes created with freesurfer, maps the nodes of a connectivity matrix to the vertices of the cortical surface mesh and adds a parcellation.

2. **Compute Source Space**: Establishes the source space for the simulation, defining where neural activity is generated.

3. **Compute Boundary Element Model and EEG Locations**: Creates a boundary element model for accurate forward modeling and determines the locations of EEG sensors. The EEG montage used was MNE's *biosemi64* montage.

4. **Compute Forward Solution**: Calculates the forward solution, essential for projecting neural activity time-series into sensor space.

5. **Save Files in TVB Format**: Outputs all necessary files in the format required by TVB.

The finished data set includes a connectome file, surface meshes of the boundaries between cortex and inner skull, between inner skull and outer skull, between outer skull and skin and between skin and air, as well as a region mapping file, sensor locations and an EEG projection matrix. Region mapping is used to map the nodes specified by connectivity to the vertices of the cortical surface mesh. The region mapping is crucial for correlating the nodes with the vertices of the cortical surface. The cortical surfaces and boundary element model are used to construct a head model, which supports tools like FieldTrip in generating precise forward models for EEG. These models are essential for computing the lead-field matrix, which projects neural activity time-series into sensor space.

After reordering the nodes of the custom tract- and the weights matrix, to match the order of the nodes of the MRtrix3 lookup table used in the pipeline, they were added to the data set, replacing the matrices created from the proxy data.

Implementation of white matter alterations

White matter alterations, regularly observed in patients with schizophrenia, manifest as reduced FA in affected white matter tracts in diffusion tensor imaging studies.

The first step to integrate these alterations into the TVB simulation, was to identify all the tracts that were affected, by conducting a comprehensive literature search. The literature on this topic does not provide fully unambiguous information, with some contradicting studies regarding specific tracts. The information gathered in the literature search was compiled into a list of eleven white matter tracts that are resolved with reduced FA in MRI studies. Tracts that were in doubt, due to contradictory studies or unclear phrasing, were still included in the list. The so identified white matter tracts had to be matched with the cortical parcellation at the basis of the structural connectivity. A further literature search was conducted to identify which nodes were likely connected by which white matter tracts. Papers exploring this topic rarely used the same or a similar brain atlas for parcellation, and mostly used more coarse grained atlases. For this reason, the nodes of the structural connectome had to be mapped to each of the parcellations used in the studies exploring the origins and terminations of white matter tracts by hand. Due to these parcellation mismatches some overlaps occurred, where some nodes of the structural connectivity were partly located in more than one area, as delineated by atlases of the white matter tract studies. In these cases the respective node was assumed to form connections with all tracts originating or terminating in the areas they are overlapping with. This information was then used in a custom Python script, to create binary connectivity matrices representing rough approximations of each white matter tract.

Then, all of these tracts were combined into one single matrix representing all affected white matter tracts.

Altering the Structural Connectivity

To modify the weights matrix of the average structural connectivity, the full white matter matrix was further modified. The values of the binary white matter matrix where chosen, somewhat unintuitively, to be one, for connections that were not affected in schizophrenia patients, and zero for connections that were likely to have reduced FA. This way the zeros could easily be replaced by multiplication factors, used to scale down the connections weights (which are the product of FA and fiber count) representing the white matter tracts affected by schizophrenia in the custom weights matrix.

The reduced FA can now be transferred onto the structural connectivity, by element-wise multiplication of the weights matrix, with the white matter matrix and its multiplication factor, to create a new weights matrix that is assumed to be representative of a schizophrenia patient's connectivity.

Applying this method the FA in the original weights matrix was then systematically reduced in steps of two percent, down to 84 percent of the "healthy" value. Graph metrics of each new structural connectivity were computed and analysed. EEG simulations were run with each structural connectivity and the resulting spectra were compared.

3.1.3 Graph-Theoretical Analysis

To explore the graph theoretical metrics of the original and the new weights matrices and how these metrics relate to each other, a custom python script was written, employing the *NetworkX* (Hagberg, Swart, and Schult 2008) toolbox and *brain connectivity toolbox*.

The graph metrics evaluated were characteristic path length, global and local efficiency, mean and local clustering coefficient, transitivity, mean and local betweenness centrality using the *brain connectivity toolbox* and small worldness using *NetworkX*.

The characteristic path length was computed from the weights matrix, not the tract matrix, which contains the actual measured lengths of the tracts, since this matrix remained unchanged through the alterations of the structural connectivity and in this case the characteristic path length is supposed to indicate a sort of *path of least resistance* as opposed to a length in millimeters. The weights in the weights matrix represent a connection strength, higher weights indicating better signal transfer, and are therefore assumed to be inversely related to distance. By inverting the entries of the weights matrix, a so called distance matrix was calculated, from which the characteristic path length was computed.

The *brain connectivity toolbox* offers various options for each graph metric, depending on the nature of the graph to be analyzed. Where possible, the "weighted undirected" (indicated by the "wu" prefix in the library) option was chosen, according to the specifications of the weights matrix.

NetworkX provides two different measures of small worldness, Sigma and Omega. Sigma is defined as

$$\sigma = \frac{C/C_{\text{rand}}}{L/L_{\text{rand}}} \tag{3.1}$$

and Omega is defined as

$$\omega = \frac{L_{rand}}{L} - \frac{C}{C_{lat}} \tag{3.2}$$

Where C is the the average clustering coefficient and L is the characteristic path length of the graph, C_{rand} and L_{rand} are the average clustering coefficient and characteristic path length of an equivalent random graph, and C_{lat} is the average clustering coefficient of an equivalent lattice graph. The algorithm for both Sigma and Omega lets the user specify two parameters, "niter", which specifies the number of rewirings per edge to create the random graph, and "nrand" which specifies the number of random graphs generated to compute average values for C_{rand} and L_{rand}. The default values for "nrand" and "niter" are $nrand = 10$ and $niter = 100$ for computing Sigma and $nrand = 10$ and $niter = 5$ for computing Omega. To reduce the substantial computation time, "niter" was reduced to $niter = 10$ in the calculation of Sigma. This reduced the computation time for each matrix to several hours, but also makes the outcome less meaningful.

3.2 Model Setup

This section provides a comprehensive overview of the simulation setup employed to simulate brain activity in this thesis. The detailed steps cover the selection of the local dynamics model, parameter selection, and tools utilized to execute the simulations and analyze the resulting data.

The model was implemented and run in Python, using TVB's python library in a scripting interface, because it allows for more flexibility in customizing models, compared to the graphical user interface. Other libraries used were Matplotlib for visualization of the results and SciPy for signal processing.

3.2.1 Configuring the Simulation

To build a simulation in TVB, first several python objects must be instantiated from classes provided through the TVB library:

1. **Models object:** This object represents the local dynamics model that produces activity in each node. The choice fell on the Jansen and Rit model, for its ability to produce different brain rhythms. Each of its parameters was individually chosen, orienting on the values used in the original paper by Jansen et. all (Jansen and Rit 1995) as well as other works employing the model (Stefanovski et al. 2019; Spiegler et al. 2010; Ahmadizadeh et al. 2018) and slightly adjusted to the specific purpose of the model (see table 3.2).

2. **Coupling function:** As a coupling function the *SigmoidalJansenRit* function was selected, as it is purpose built to work with this local dynamics model (see table 3.3).

3. **Integrator:** As an integration scheme, the *deterministic Heun* integrator was used, with a time step of $dt = 2^{-4}$.

4. **Monitor:** The recording of EEG signals from the simulation requires an EEG monitor object. The monitor object requires four attributes to be defined, the first three of which requiring files that are part of the TVB ready dataset: The sensors object is created from the EEG_locations file, the projection surface object is created from the projection matrix and the region mapping is created from the region mapping file. The final attribute, the sampling period, was set to 0.976 ms, resulting in a sampling frequency of 1024 Hz. Additionally a reference attribute can be set. For this simulation the *average* attribute was selected, to apply an average reference.

Parameter	Value	Explanation
A	3.25	Maximum amplitude of excitatory postsynaptic potential in mV. Higher values move the theta peak into the alpha range, while lower values destroy the dynamics.
B	22	Maximum amplitude of inhibitory postsynaptic potential in mV. Higher values enhance the theta rhythm, while lower values remove it.
a	0.1	Time constant of excitatory postsynaptic potential decay in ms^{-1}.
b	0.05	Time constant of inhibitory postsynaptic potential decay in ms^{-1}.
v0	5.52	Firing threshold in mV.
nu_max	0.0025	Maximum firing rate in s^{-1}.
r	0.56	Steepness of the sigmoid activation function in mV^{-1}.
J	135	Synaptic efficacy in mV·ms, which influences the magnitude of the response.
a_1	1	Average probability of synaptic contacts in the feedback excitatory loop.
a_2	0.8	Average probability of synaptic contacts in the slow feedback excitatory loop.
a_3	0.25	Average probability of synaptic contacts in the feedback inhibitory loop.
a_4	0.25	Average probability of synaptic contacts in the slow feedback inhibitory loop.
p_min	0.12	Minimum input firing rate in s^{-1}.
p_max	0.32	Maximum input firing rate in s^{-1}.
mu	0.22	Mean input firing rate in s^{-1}.

Table 3.2: List of parameters that were used in the Jansen-Rit Model

5. **Connectivity:** The connectivity object is created by loading the connectivity.zip file from the TVB ready dataset.

After combining these objects in a simulator object and adding the additional attributes of conduction speed for the long range connectivity, chosen as 4 mm/ms and the simulation length in milliseconds, the simulation is configured by running TVB's *configure* method and then started, using TVB's *run* method.

Parameter	Value	Explanation
c_{min}	0.0	Minimum of the sigmoid function
c_{max}	0.005	Maximum of the sigmoid function
midpoint	6.0	Midpoint of the linear portion of the sigmoid
r	0.56	steepness of the sigmoidal transformation
a	5.0	Scaling of the coupling term. This value was settled upon after several test runs.

Table 3.3: List of parameters that were used in SigmoidalJansenRit coupling function

3.2.2 First Simulation Run

Previous test simulations often exhibited strong initial transients, masking the equilibrium dynamics of the system. These occur because the system starts from arbitrary initial conditions that are not representative of the system's equilibrium state. During the initial phase of the simulation, the model's variables and dynamics need time to stabilize and reach a steady state, resulting in irregular and nonrepresentative behavior. To address this, a first, short simulation of 2 seconds was performed, to allow the system to reach its stable dynamic equilibrium state. The result of this simulation was then used to provide initial conditions for subsequent simulations to ensure it starts from a stable point that does not produce initial transients. This was achieved by extracting the final state of this simulation, including time points, state variables, nodes and modes from the simulation's history buffer and combining them into an *initial conditions* object, that could be used as an attribute providing a starting point for further simulations.

3.2.3 Full Length Simulations

A full-length simulation lasted twenty seconds. It was first run with the original custom connectivity matrix (100% FA), and then repeated with matrices, where the FA was gradually reduced by 2% increments in the relevant edges, down to a final matrix with FA reduced to 84% of the original value. These values are not physiological, but were chosen to see if a trend is observable and because of a lack of data providing specific values.

3.2.4 Data Processing and Analysis

To process and analyze the data generated from the simulations, a systematic approach was implemented in python. The primary function responsible for processing the results handles various tasks such as time series extraction, normalization, plotting, and spectral analysis using Fast Fourier Transformation (FFT). This section details the steps involved in processing the simulation data, including the methods used and the rationale behind them.

The function begins by extracting the *time* and *data* variables from the simulation results. The data consists of EEG signals recorded from different channels. The EEG data is then normalized for each channel to ensure that the values lie within a 0 to 1 range. This normalization helps in comparing the relative amplitudes across different channels. The normalized EEG data are plotted for visualization, providing a clear representation of the signals from different channels over time. This is achieved by creating a plot with lanes, where each lane corresponds to a different EEG channel.

To facilitate further analysis, a *TimeSeriesEEG* object is created with the necessary configurations. This object encapsulates the original EEG data, time information, sensor configurations, and other relevant metadata, such as the sampling period.

Spectral analysis is performed using FFT to convert EEG signals in the time domain to the frequency domain. FFT is performed using TVB's *compute fast fourier transform* method with a segment length of 2 seconds, resulting in a frequency resolution of 0.5 Hz, no windowing function, and detrending activated. This analysis helps to identify the dominant frequencies and understand the spectral characteristics of the signals.

The magnitude spectrum up to 60 Hz is then plotted for all sensors, providing a visual representation of the frequency components present in the EEG data. To gain insights into the overall activity, the average magnitude across all sensors is computed and plotted. Peaks in the average magnitude spectrum are identified and annotated. The EEG sensors are grouped by brain areas and hemispheres to analyze the average signals for each group. This grouping helps in highlighting the regional differences in brain activity.

4 RESULTS

4.1 TVB Ready Dataset

The preprocessing steps detailed in the Methods chapter produced a dataset that includes four different surface meshes (cortex, inner skull, outer skull, and scalp), region mapping, the connectome, EEG sensors, and the projection matrix. This dataset is fully compatible with TVB and ready for running simulations.

The heart of the connectome is formed by the weights matrix, which was intentionally left unnormalized. Normalization facilitates intersubject comparability, but since this matrix is an average of many matrices formed from a large number of different subjects and will only be compared to variations of itself, normalization was deemed an unnecessary step.

It was also decided not to prune the edges of the weights matrix by introducing a cut-off for low values. This decision was made because it was unclear if a cut-off value had already been used in the original braingraph.org dataset and because of the large number of connections with very low weights. Introducing even a very low cut-off value would have resulted in the loss of many connections. The reasoning was that, although this might result in false positives remaining in the weights matrix, the averaging process minimizes their influence.

This can easily be seen when comparing the weights matrix, once displaying the edge weights on a linear scale, and once displaying them on a logarithmic scale (see figures 4.1 and 4.2).

A comparison of the two versions of the matrices clearly shows that many of the connections only appear on the logarithmic scale as such, because they have very small weights. This is partly a result of the averaging process. The weight of an edge in the matrix is defined as the product of fibercount and FA. The individual connectivity files obviously never show fiber counts smaller than one and FA only very rarely drops to values below 0.2. Therefore, weight values far below 0.2 are unexpected.

However, the individual connectivity matrices are sparse, and not all connections, particularly the weaker ones, are represented in all, or even most, of the other matrices in the dataset. During the averaging process, these rare connections are progressively devalued but are never completely stricken from the matrix.

The tracts matrix (see figure 4.3), representing the length of connections between

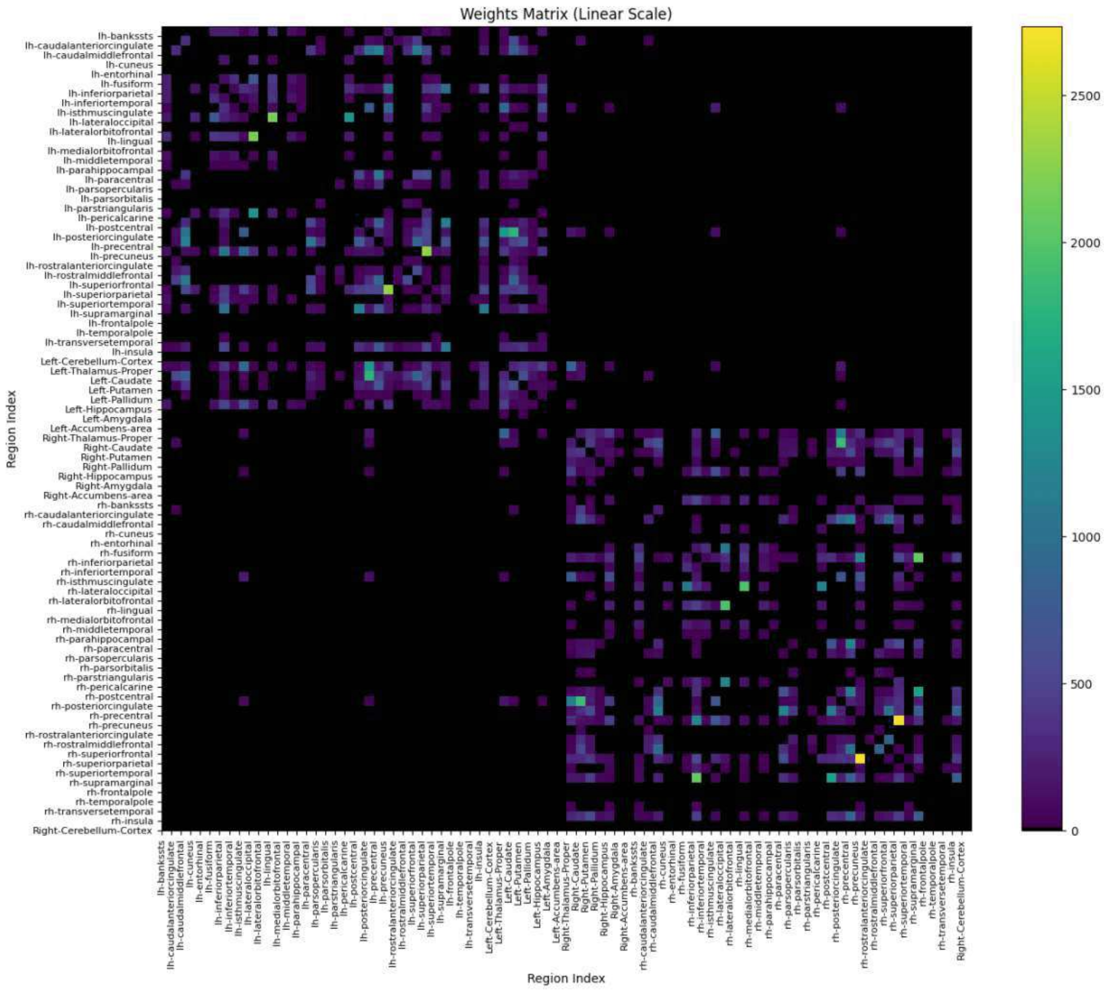

Figure 4.1: Average weights matrix with linear scaling

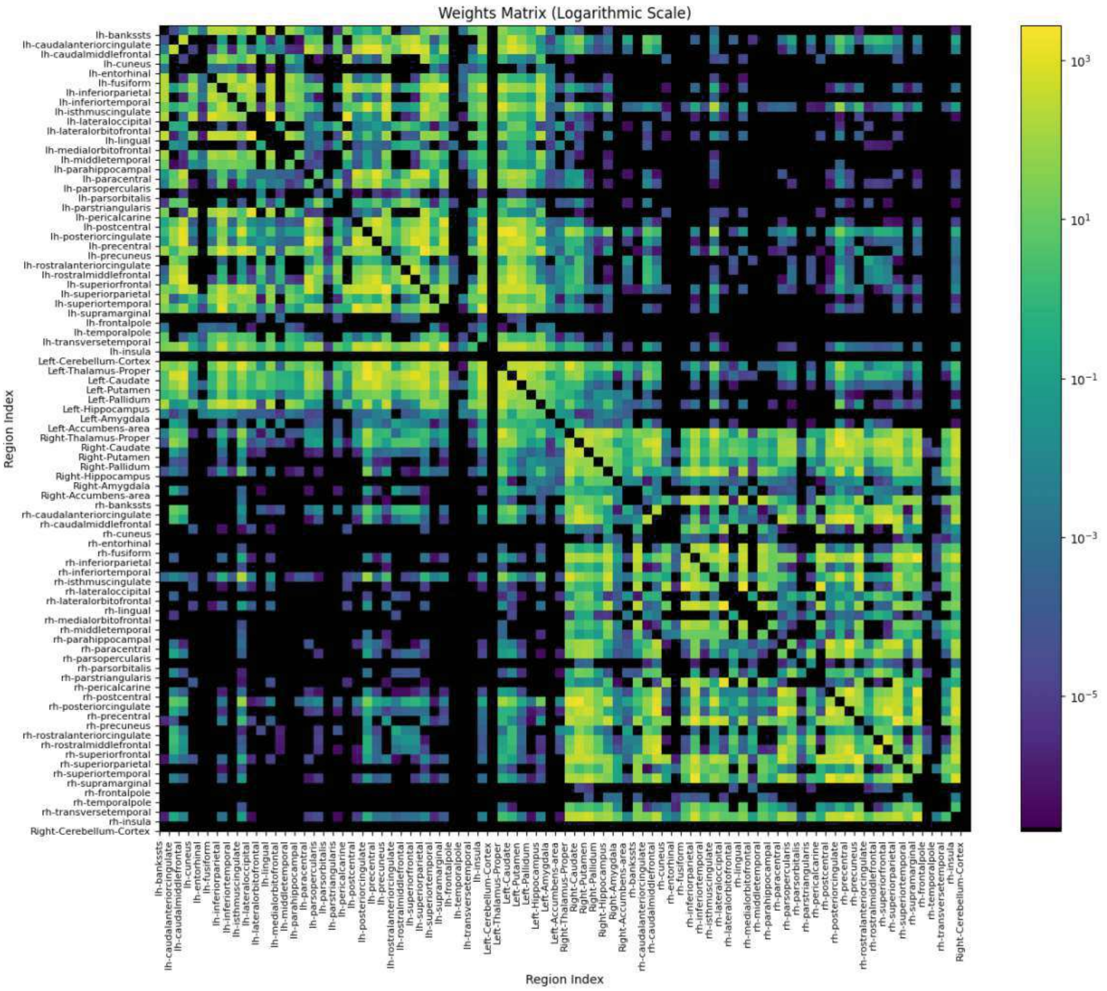

Figure 4.2: Average weights matrix with logarithmic scaling

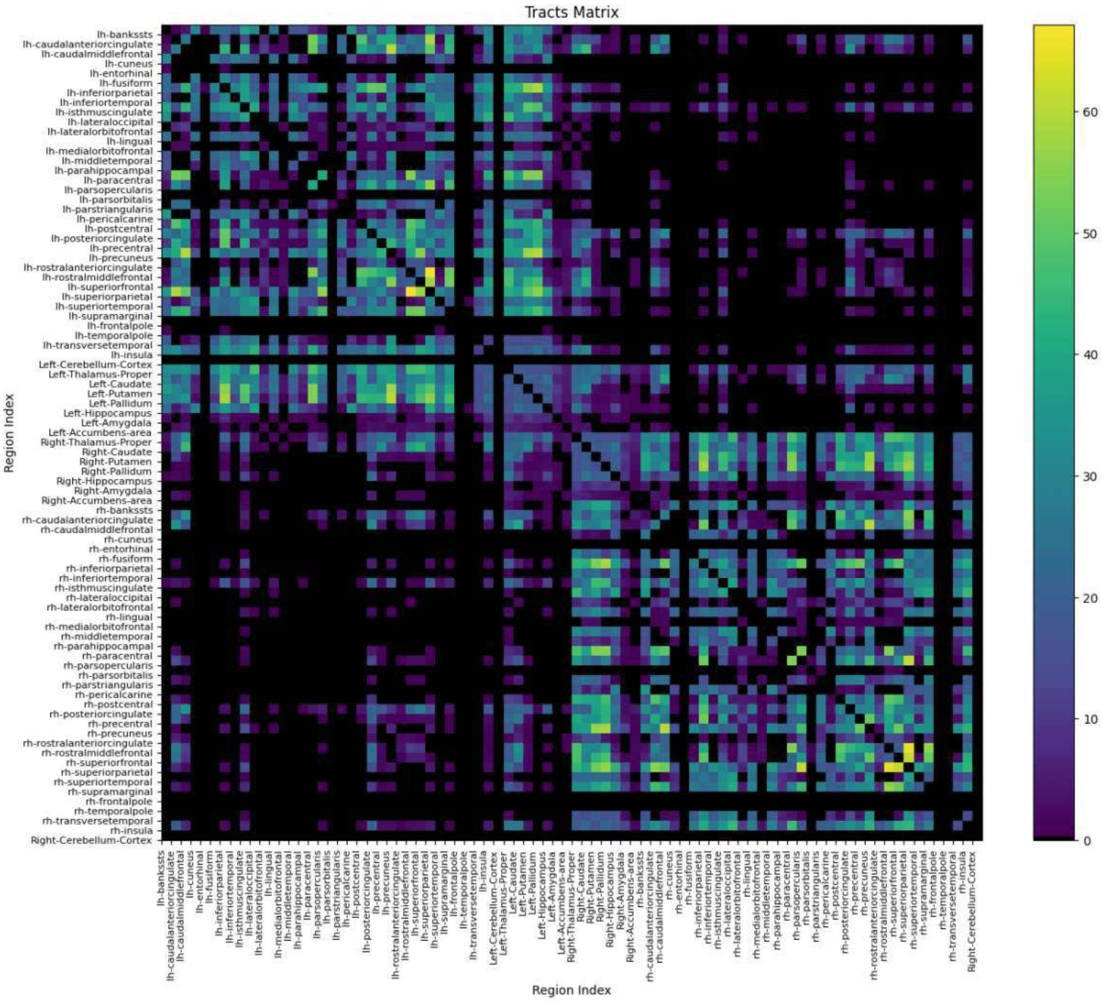

Figure 4.3: Tracts matrix, which shows the lengths of the tracts between nodes and is used to compute transmission delays in the simulation.

node pairs is also an indication that there is a large amount of weaker connections, that would be overlooked on the linear scale.

Both the weights and the tracts matrix are symmetric. The reason for this is that DTI as an imaging modality can only detect fiber tracts indirectly through a probabilistic method (Fan and Markram 2019), but is unable to deduce the direction a signal travels on a fiber.

4.2 White Matter Matrices

The white matter tracts that were found to likely be affected by schizophrenia were the Arcuate Fasciculus (Kenney et al. 2017), Cingulum Bundle, the Fornix, the Anterior and Posterior Limb of the Internal Capsule, the Inferior Fronto-Occipital Fasciculus, the Inferior and Superior Longitudinal Fasciculus, the Thalamic Radiations, Uncinate Fasciculus, and the Corpus Callosum.

The evidence implicating the Arcuate Fasciculus in schizophrenia is ambiguous. Some studies report reduced FA in this tract (Kenney et al. 2017; M. Kubicki et al. 2005; Geoffroy et al. 2014), while other studies report increased FA (Kubicki et al. 2007; Canu, Agosta, and Filippi 2015; Heuvel, Martijn, and Fornito 2014; Klauser et al. 2016), in some studies the effect is observed bilaterally, while other studies report a significant effect only in the left hemisphere (Wheeler and Voineskos 2014; Geoffroy et al. 2014; M. Kubicki et al. 2005).

For simplicity and due to the ambiguity of the evidence, this tract was treated the same as the other tracts in the simulations, bilaterally and with decreased FA.

Several studies show decreased FA in the Cingulum Bundle, again slightly ambiguous, with some studies not finding an effect and some studies limiting the effect to specific areas of the Cingulum Bundle (Whitford et al. 2014) and some studies not specifying specific parts of the tract (Fitzsimmons et al. 2020; Kubicki et al. 2007; Ellison-Wright et al. 2014; M. Kubicki et al. 2005; Canu, Agosta, and Filippi 2015; Klauser et al. 2016).

Several studies find reduced FA Fornix (Wheeler and Voineskos 2014; Canu, Agosta, and Filippi 2015; Ellison-Wright et al. 2014; M. Kubicki et al. 2005; Canu, Agosta, and Filippi 2015).

Several sources report reduced FA in the Internal Capsule (Wheeler and Voineskos 2014; M. Kubicki et al. 2005), or generalized alterations (Canu, Agosta, and Filippi

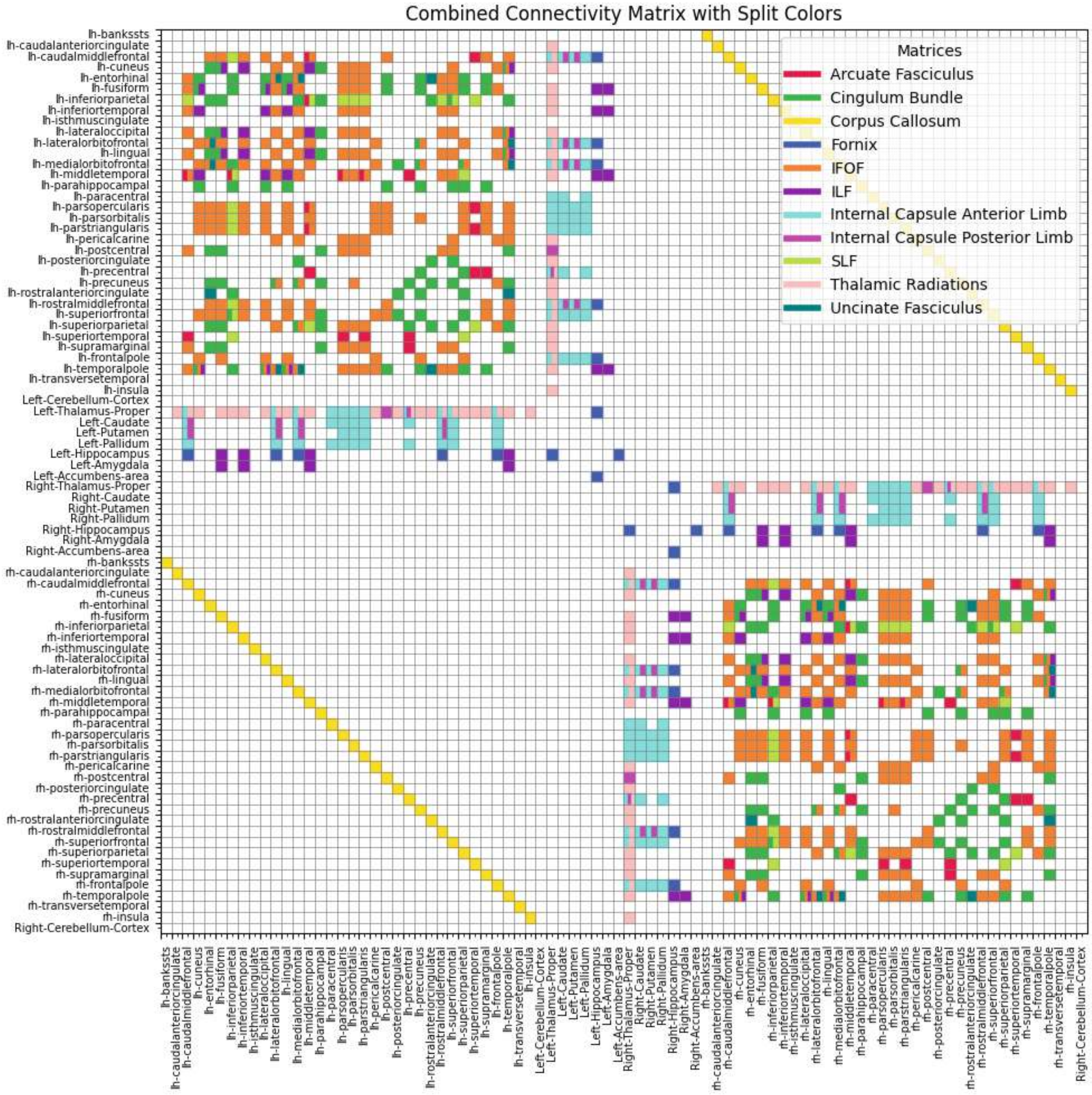

Figure 4.4: Combined binary white matter matrix. The colors of the entries represent different tracts. If edges overlap, and are included in more than one tract, the entry contains several colors.

2015).

Some of them find reductions are specific to the anterior limb of the Internal Capsule (Zou et al. 2008; Canu, Agosta, and Filippi 2015; Ellison-Wright et al. 2014), while others find reductions in the posterior limb as well. Often a lateralization of FA reduction is reported, but there are studies implicating the right hemisphere (Holleran et al. 2013), and others implicating the left hemisphere (Ublinskii et al. 2015; Meng et al. 2019).

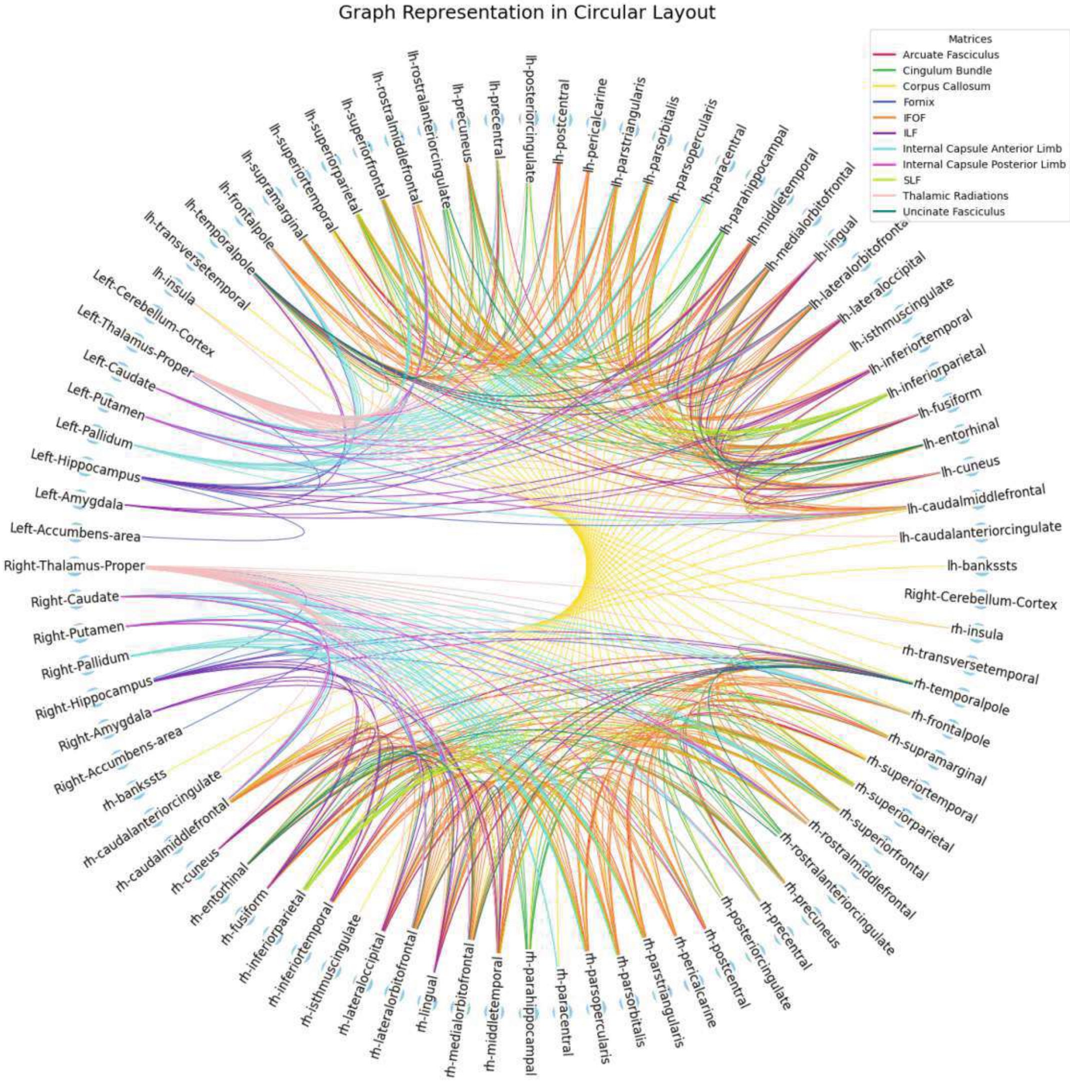

Figure 4.5: Approximated white matter connections in a circular plot. Lines represent the edges connecting two pairs of nodes. The edges are associated to their respective tract by their color.

(Surbeck et al. 2020) and (Canu, Agosta, and Filippi 2015) report reductions of FA in the Inferior Fronto-Occipital Fasciculus, while (Wheeler and Voineskos 2014) only finds reductions in the left hemisphere.

(Canu, Agosta, and Filippi 2015) and (Ellison-Wright et al. 2014) report FA

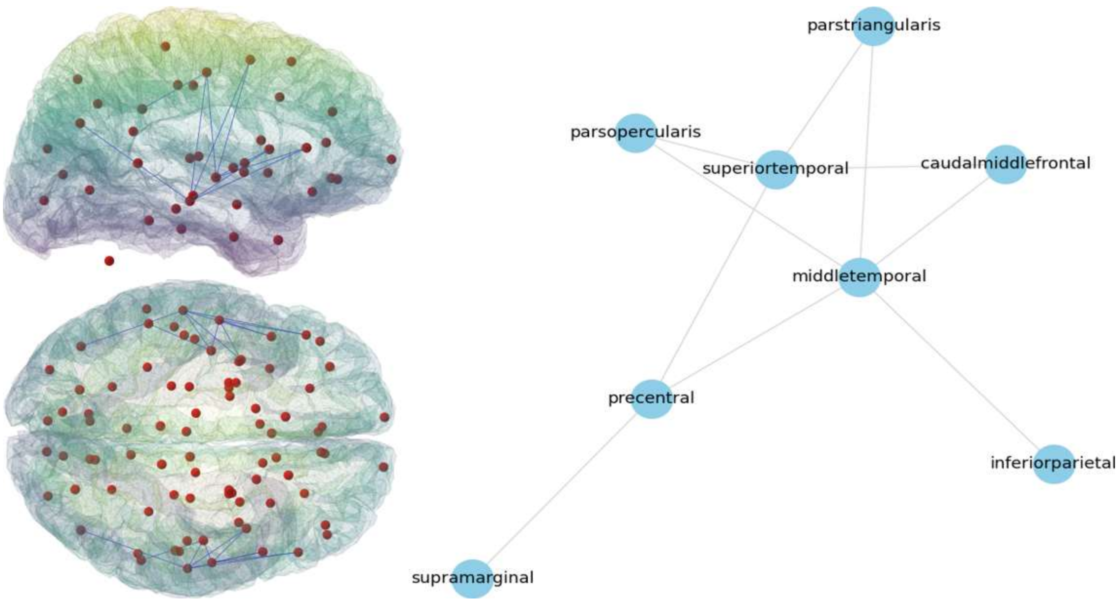

Figure 4.6: Graphical representation of the nodes connected by the Arcuate Fasciculus.

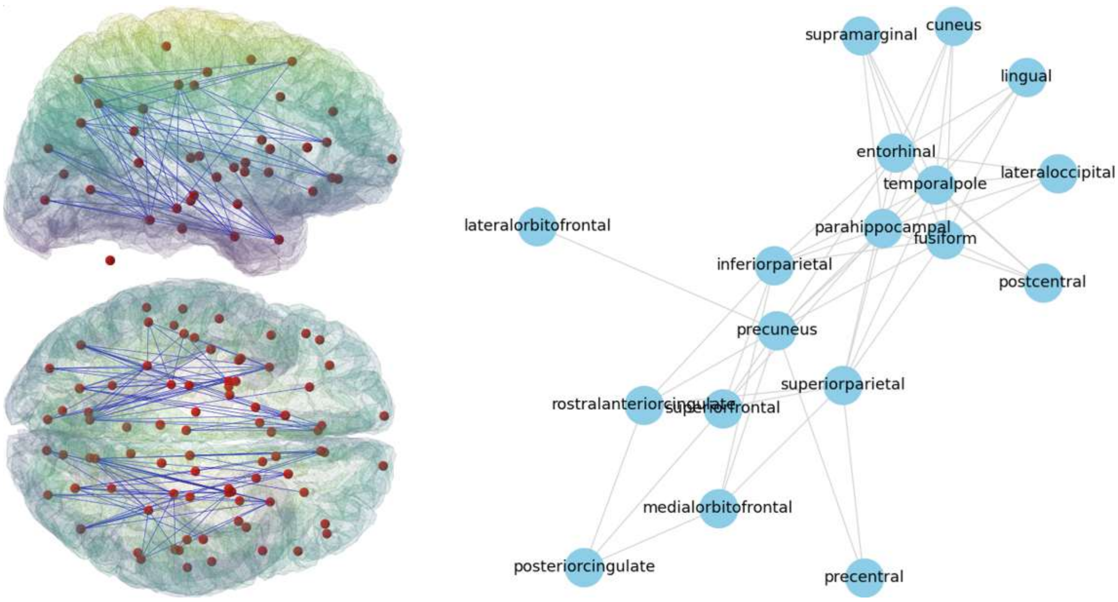

Figure 4.7: Graphical representation of the nodes connected by the Cingulum Bundle.

reductions in the whole Inferior Longitudinal Fasciculus, (Jung et al. 2020) finds FA reductions in the right Inferior Longitudinal Fasciculus, (Holleran et al. 2013)

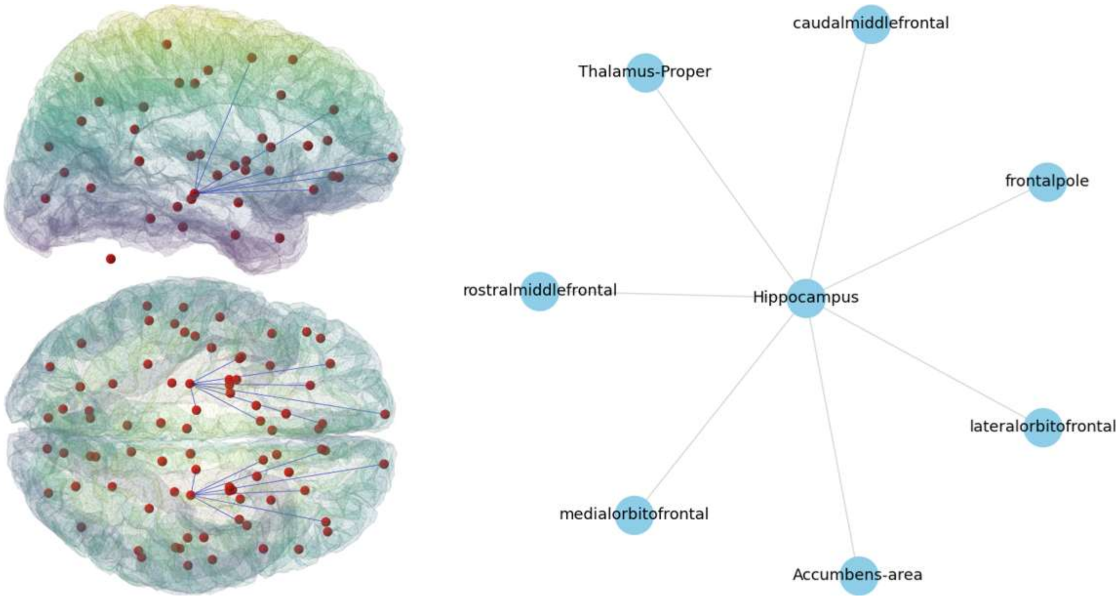

Figure 4.8: Graphical representation of the nodes connected by the Fornix.

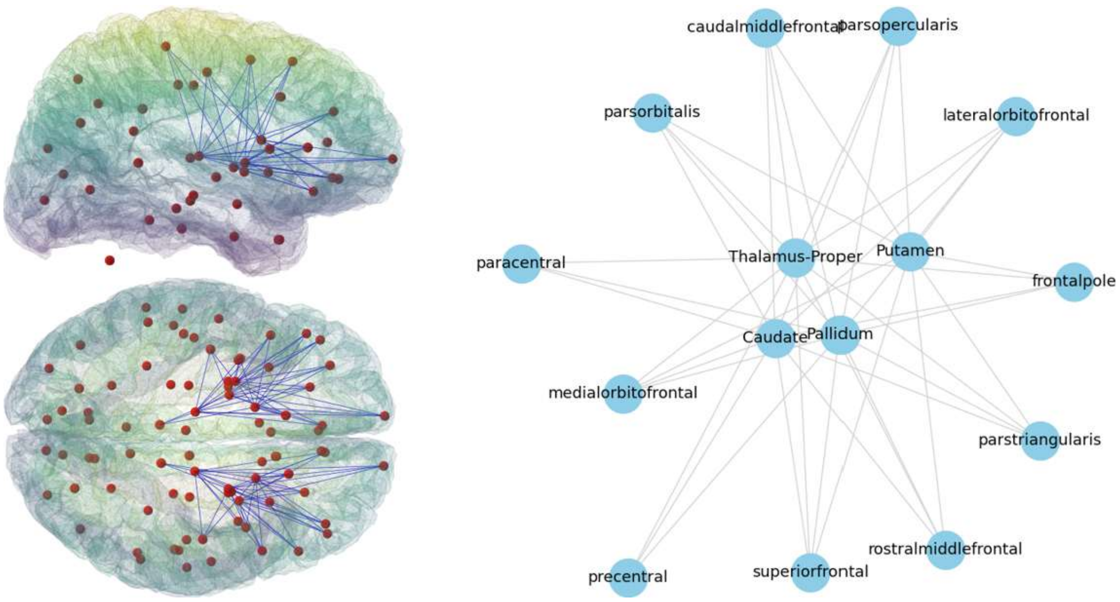

Figure 4.9: Graphical representation of the nodes connected by the Anterior Limb of the Internal Capsule.

finds them only in the right temporal portion of the Inferior Longitudinal Fasciculus and (Wheeler and Voineskos 2014) and (Ashtari et al. 2007) report decreased FA in the left temporal Inferior Longitudinal Fasciculus.

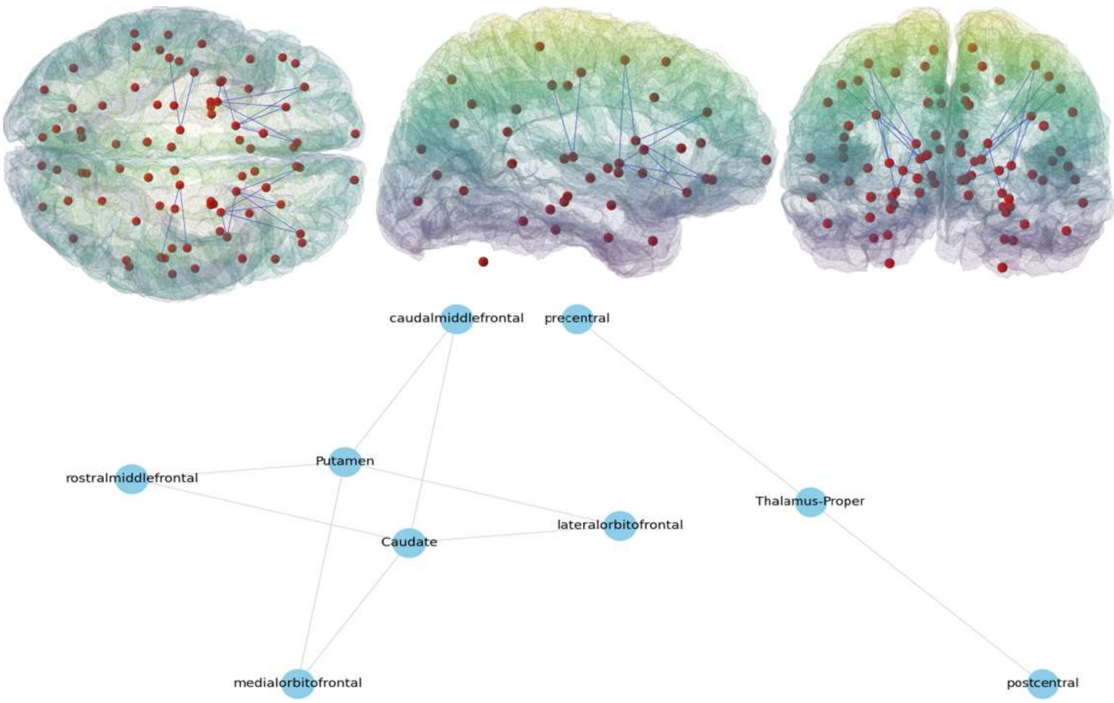

Figure 4.10: Graphical representation of the nodes connected by the Posterior Limb of the Internal Capsule.

Reduced FA is reported in the Superior Longitudinal Fasciculus by (Canu, Agosta, and Filippi 2015), (Ellison-Wright et al. 2014) and (Shergill et al. 2007). (Jung et al. 2020) reports reduction in the Superior Longitudinal Fasciculus in the right hemisphere and (Wheeler and Voineskos 2014) reports reductions in the left hemisphere.

FA decreases in the Thalamic Radiations are reported by (Klauser et al. 2016). (Meng et al. 2019) finds reductions in the posterior Thalamic Radiations, (Canu, Agosta, and Filippi 2015) and (Wheeler and Voineskos 2014) find reductions in the anterior sections of the Thalamic Radiations, (Jung et al. 2020) finds reduced FA in the left anterior sections and (Ellison-Wright et al. 2014) find reductions in the right posterior sections.

Reductions in the FA of the Uncinate Fasciculus are reported by (Wheeler and Voineskos 2014), (Ellison-Wright et al. 2014) and (Shergill et al. 2007). (Jung et al. 2020) finds reductions in FA in the Uncinate Fasciculus of the right hemisphere only.

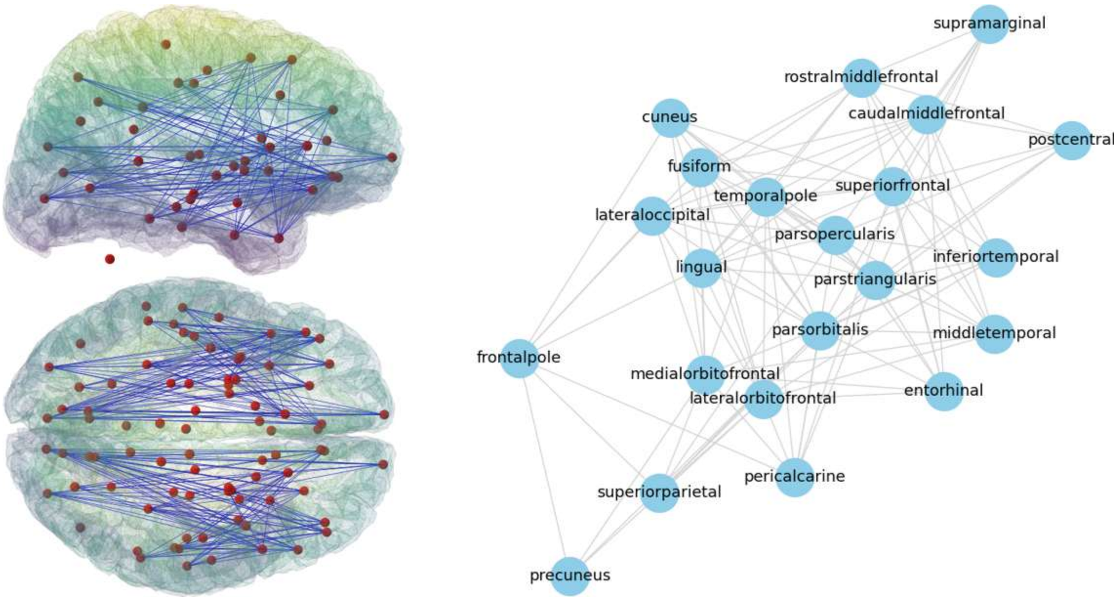

Figure 4.11: Graphical representation of the nodes connected by the Inferior Fronto-Occipital Fasciculus.

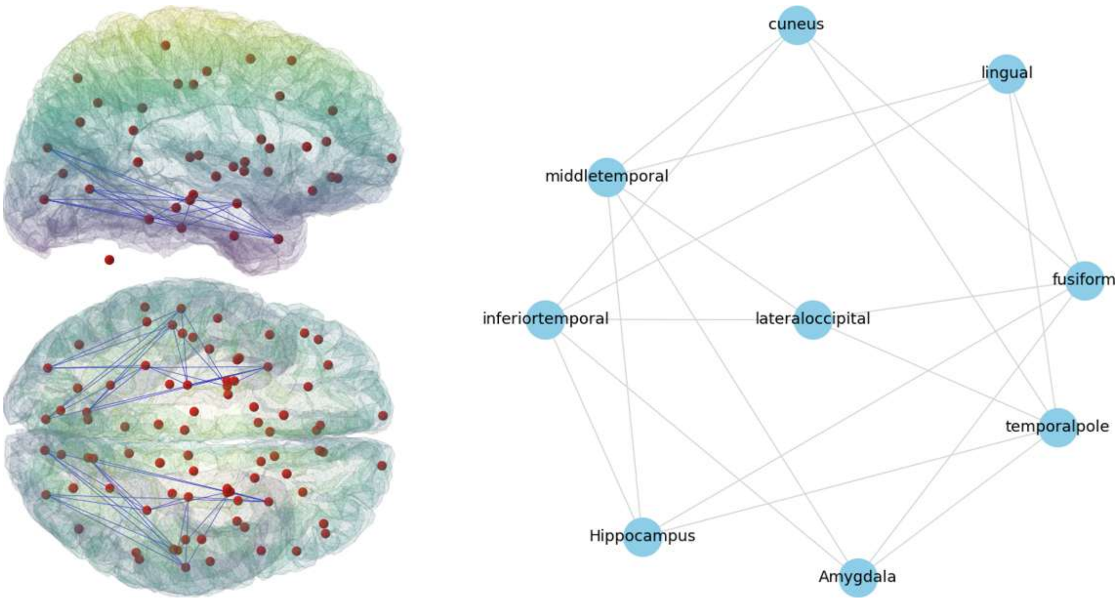

Figure 4.12: Graphical representation of the nodes connected by the Inferior Longitudinal Fasciculus.

FA reductions in the tracts of the Corpus Callosum are reported by (Wheeler

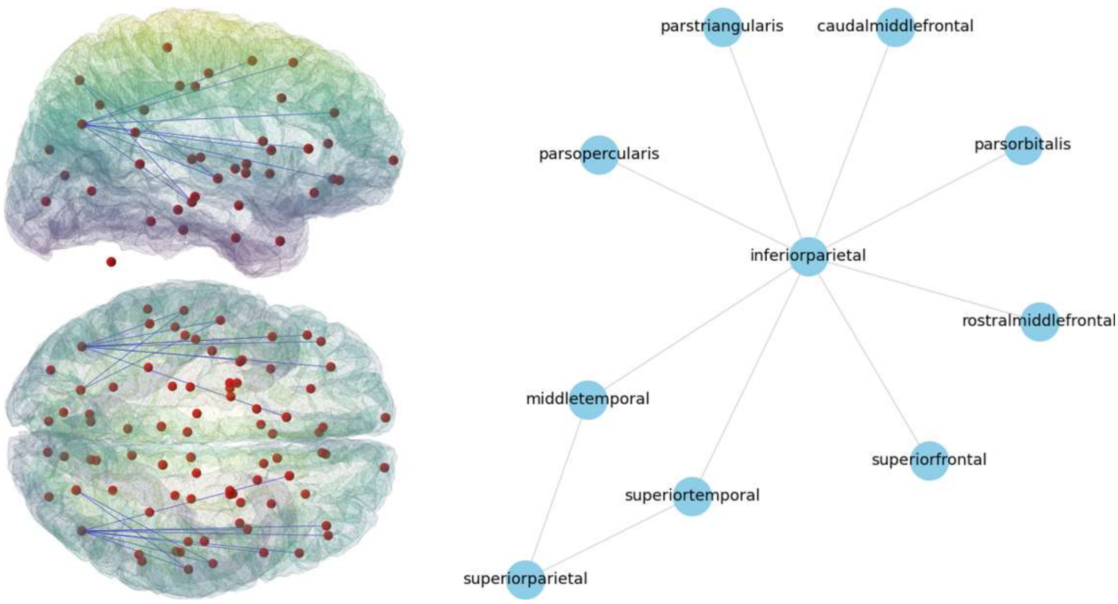

Figure 4.13: Graphical representation of the nodes connected by the Superior Longitudinal Fasciculus.

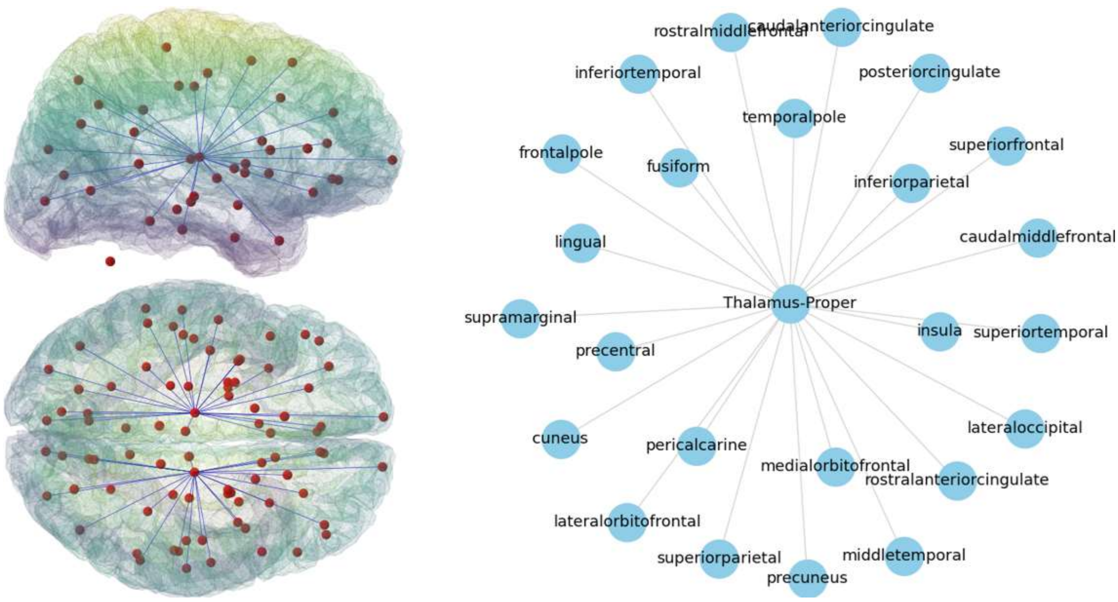

Figure 4.14: Graphical representation of the nodes connected by the Thalamic Radiations.

and Voineskos 2014), (Holleran et al. 2013), (Meng et al. 2019), (Ellison-Wright et al. 2014), (Klauser et al. 2016) and by (Canu, Agosta, and Filippi 2015).

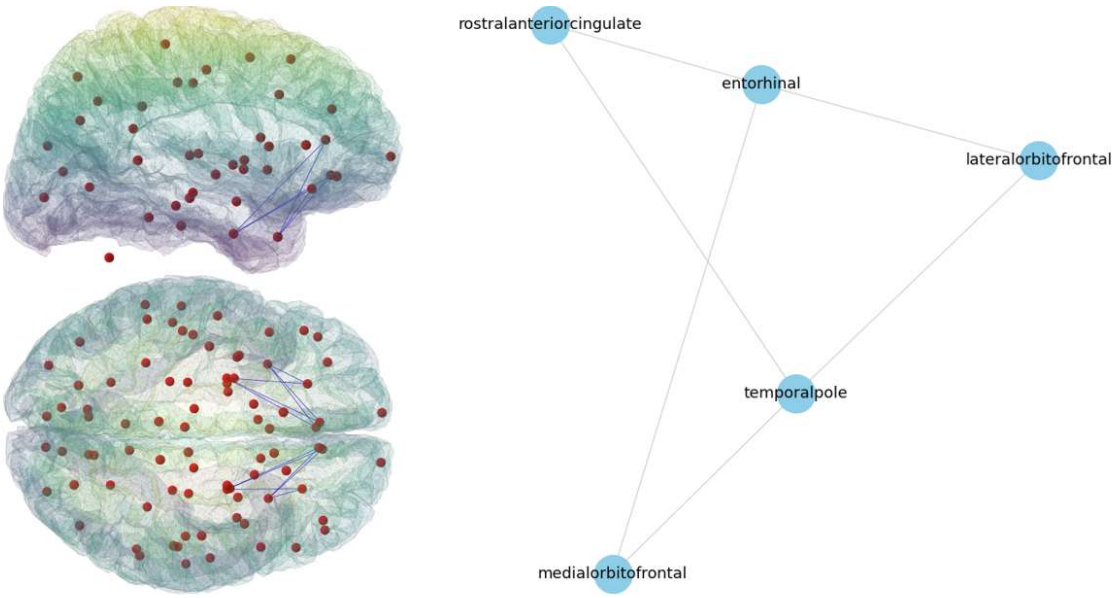

Figure 4.15: Graphical representation of the nodes connected by the Uncinate Fasciculus

The review of the literature shows a general consensus that there are brain wide disruptions in the white matter of schizophrenia patients that can be observed through DTI and reduced FA (Kelly et al. 2017). The body of evidence is equivocal on which specific brain regions are affected and, in a few instances, there is no consensus on the nature of the effect. The quality and quantity of evidence varies depending on the brain region. However, a common observation is a global reduction in FA in the white matter of schizophrenic patients.

The reasons for discrepancies between studies can be manifold, from differences in study design, sample size, or differences in the subject cohorts, ranging from age, medication status and disease progression, to name only a few.

4.3 Graph-Analysis

This chapter examines the effects of progressively reducing FA in specific white matter tracts on key graph metrics of the brain's structural connectivity. By systematically decreasing FA in steps on 2%, this analysis aims to reveal the relationship between white matter degradation and network efficiency, as reflected in metrics such as characteristic path length, global efficiency, clustering coefficient, and others.

4.3.1 Global Metrics

The characteristic path length, which reflects the average shortest path between nodes in the network, increases in very small steps, but gradually, with decreasing white matter integrity (see figure 4.16). A higher characteristic path length indicates less efficient information transfer within the brain network. This suggests that as FA decreases (indicating more compromised white matter), the network becomes less efficient, with longer average paths between nodes. Notably, a substantial increase in path length occurs between 100% and 96% white matter integrity, suggesting a critical threshold beyond which network efficiency significantly deteriorates.

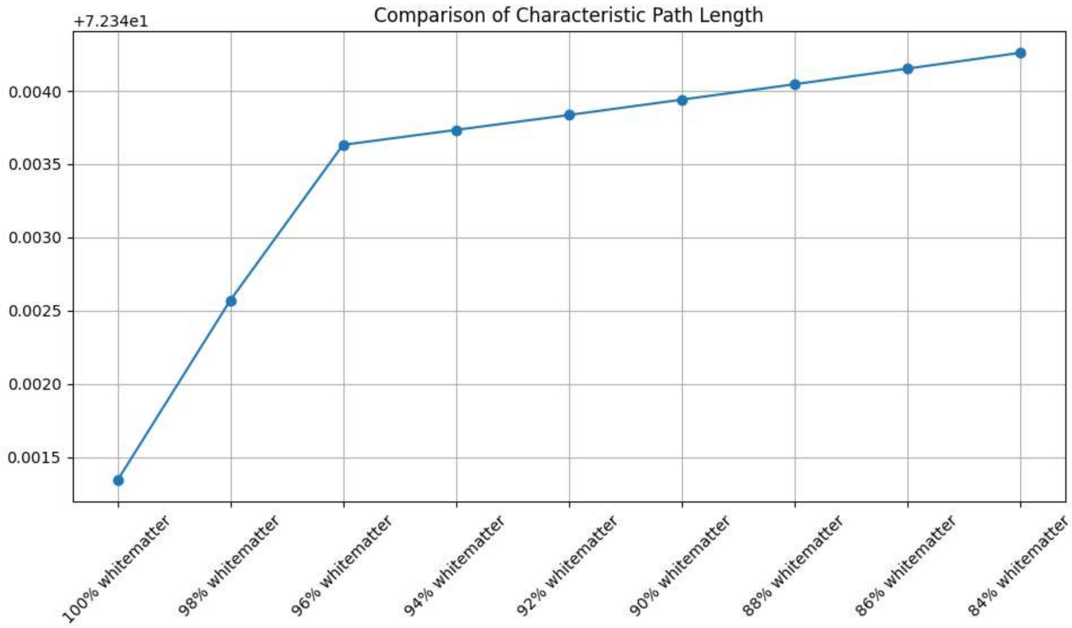

Figure 4.16: Changes in characteristic path length across different levels of white matter integrity, as simulated by reducing FA in specific tracts known to be affected in schizophrenia.

Global efficiency is inversely related to path length, as it is calculated as the average of the inverse of the shortest path lengths between all pairs of nodes.

The graph (see figure 4.17) reveals a linear decline in global efficiency, indicating that as the integrity of white matter is progressively reduced, the brain's network efficiency correspondingly diminishes. Global efficiency, which reflects the brain's capacity for effective information exchange across different regions, is shown to decrease steadily with each step down in FA. This linear trend suggests a direct relationship between white matter integrity and network function,

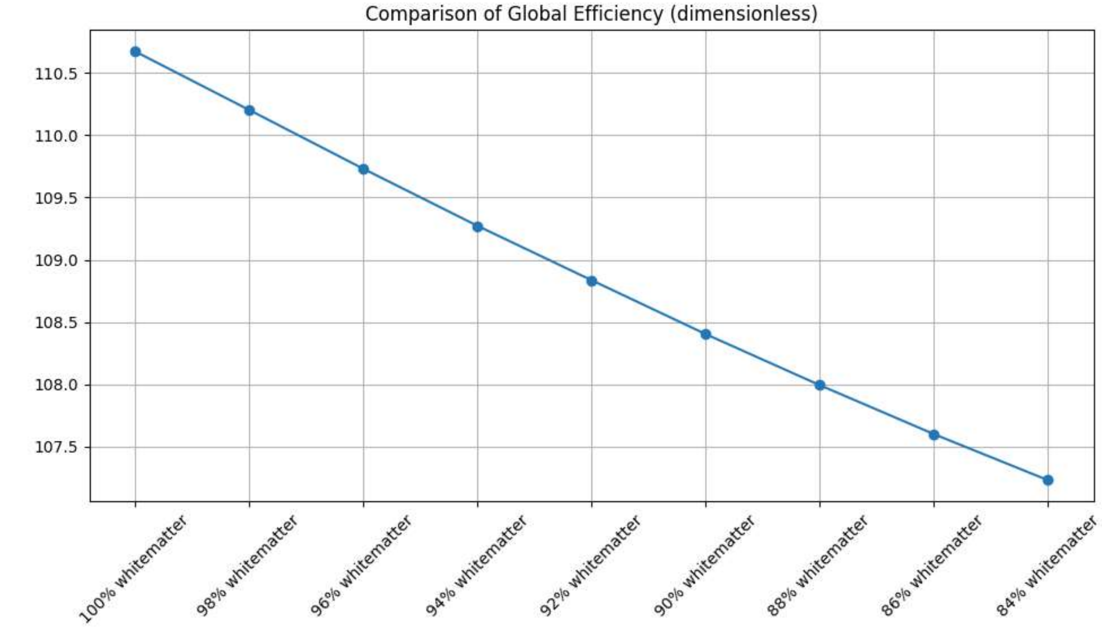

Figure 4.17: Changes in global efficiency as FA decreases in specific white matter tracts associated with schizophrenia.

Betweenness centrality measures the extent to which a node lies on the shortest paths between other nodes in the network. A higher betweenness centrality implies that certain nodes become more critical for the flow of information across the network.

The graph (see figure 4.18) reveals a non-linear increase in betweenness centrality, indicating that, as white matter integrity diminishes, certain nodes or connections become increasingly central to the network's overall connectivity. The sharp rise observed between 96% and 94% white matter integrity suggests a critical point at which the network begins to rely more on fewer nodes, potentially reflecting a loss of network robustness. This trend continues as FA decreases, highlighting a potential of growing network vulnerability .

The clustering coefficient measures the degree to which nodes in the network tend to form clusters. A higher clustering coefficient indicates a higher tendency for nodes to form tightly-knit groups, which is indicative of efficient local information processing and network segregation.

The graph (see figure 4.19) demonstrates a linear decline in the clustering coeffi-

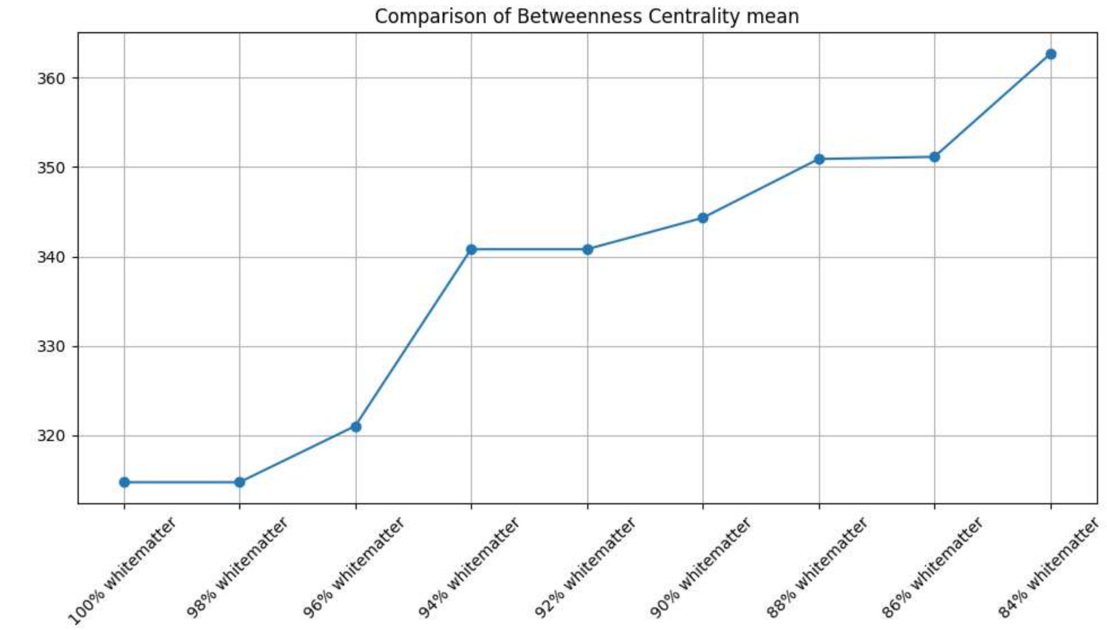

Figure 4.18: Changes in mean betweenness centrality as FA decreases across specific white matter tracts implicated in schizophrenia.

cient, indicating that as white matter integrity deteriorates, the network's tendency to form local clusters diminishes. The observed decline suggests that reduced white matter integrity weakens the network's local connectivity thereby suggesting less segregation and probably less efficient local information processing.

Modularity measures the degree to which a network can be divided into distinct communities or modules. A higher modularity indicates a network with well-defined communities, where nodes within the same module are more densely connected to each other than to nodes in other modules.

The graph (see figure 4.20) reveals a linear decline in modularity, indicating that, as white matter integrity deteriorates, the brain's network structure becomes less modular. The observed decline suggests that reduced white matter integrity leads to a less differentiated network, where the boundaries between different functional modules are weakened.

The small world coefficient measures how closely the brain's network adheres to small-world properties, which balance high local clustering and short path lengths. A network with strong small-world properties is efficient both locally and globally.

Two common measures to quantify small worldness are Omega and Sigma.

Values for Omega range from -1 to 1, with values close to zero indicating small-world properties, while Sigma values exceeding 1 suggest strong small-worldness.

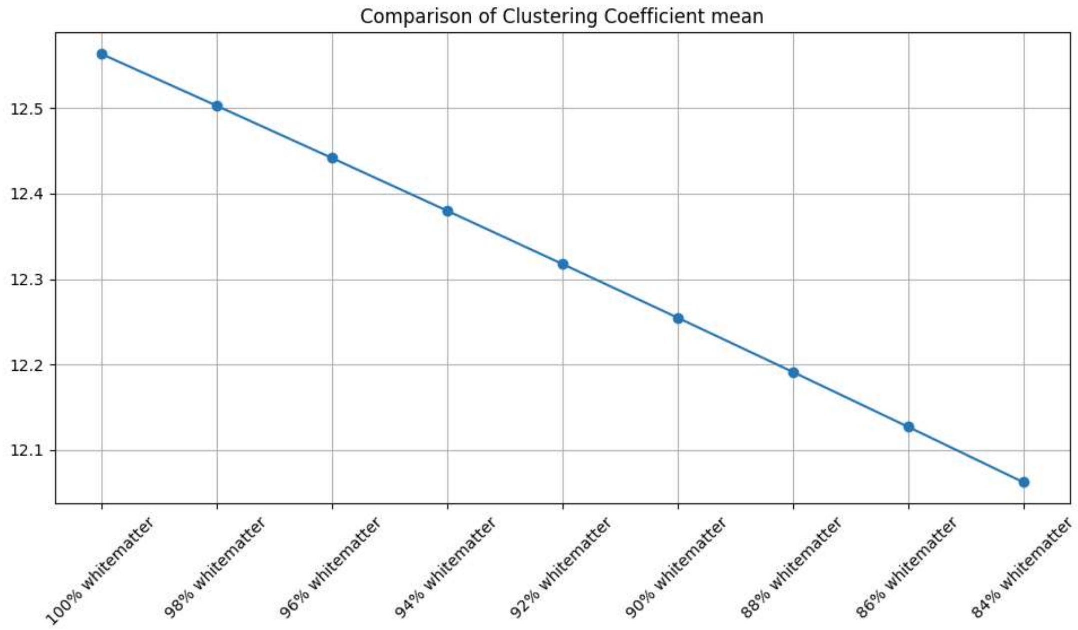

Figure 4.19: Changes in the mean clustering coefficient as connection weights in specific white matter tracts relevant to schizophrenia are decreased.

The initial computation of Omega and Sigma yielded the values indicated by the orange line in figures 4.22 and 4.21. Although the values in both graphs fall within the range indicative of small-worldness, the seemingly random changes of these values, for matrices with continuously decreasing white matter integrity prompted further investigation.

Upon closer examination, it was observed that both the algorithms to compute Sigma and Omega generate random matrices as part of their calculations. In the Sigma algorithm, these random graphs serve as a null model for comparison with the original graph's clustering coefficient and average path length. Similarly, the Omega algorithm uses random graphs to calculate the average shortest path length, providing a baseline for how a network with no inherent structure would behave in terms of path length.

By retroactively introducing a fixed seed for the generation of these random matrices, the fluctuations in the small-worldness values were eliminated, proving that they were indeed a result of the randomization in calculation process.

However, the emergence of constant small-worldness was unexpected, particularly since this metric depends on the characteristic path length and clustering coefficient, both of which were previously observed not to be constant with decreasing white matter integrity.

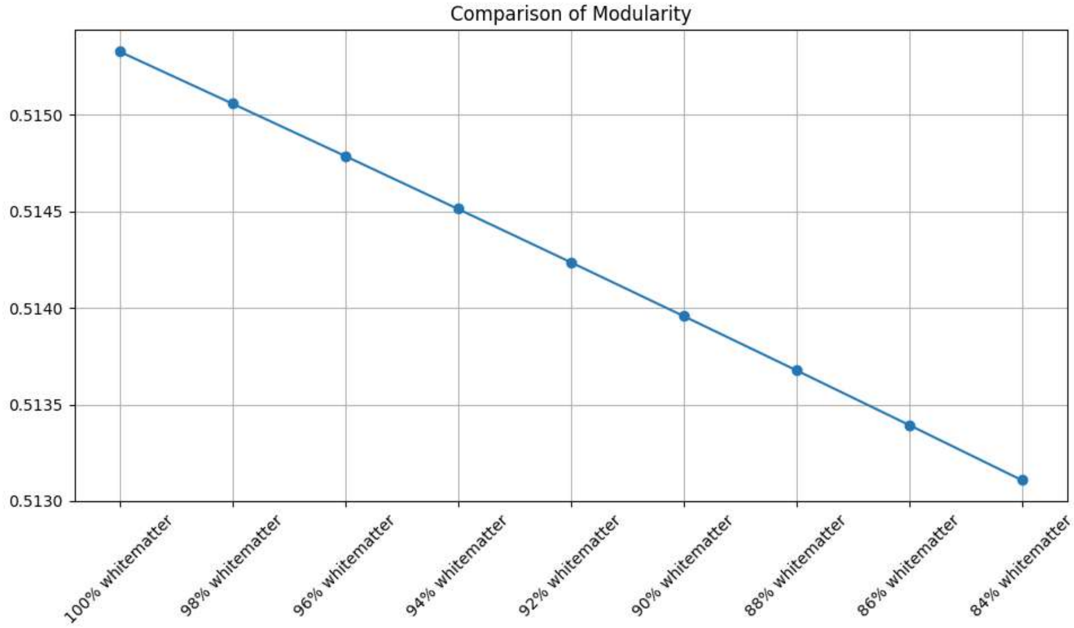

Figure 4.20: Changes in modularity as connection weights in specific white matter tracts relevant to schizophrenia are decreased.

Further investigation revealed that the small-world algorithms provided by *NetworkX* do not take edge weights into account and treat all graphs as binary. This limitation diminishes the effectiveness of these metrics in accurately characterizing the graphs analyzed in this work.

This limitation prompted a search for alternative metrics capable of characterizing small-worldness in weighted graphs. The investigation led to a relatively new concept proposed in 2016 called Small-World Propensity (SWP) (Muldoon, Bridgeford, and Bassett 2016). This metric addresses the shortcomings of previous measures by providing an unbiased assessment of small-world structure in networks of varying densities, including weighted networks.

A network is considered to exhibit small-world characteristics according to this metric if the SWP exceeds a value of 0.6. As shown in figure 4.23, the SWP value calculated for the original networks is significantly lower than this threshold, measuring just below 0.3, and constant over different levels of white matter integrity. Interestingly, when thresholding was applied to the connectivity matrix, the SWP underwent drastic, nonlinear changes. Applying an initial threshold of 2, below which all edges were set to zero, resulted in almost no change in SWP. The first substantial increase in SWP, when gradually increasing the threshold, occurred at a threshold of 2.2. Further increases in the threshold, up to 2.9, again yielded only

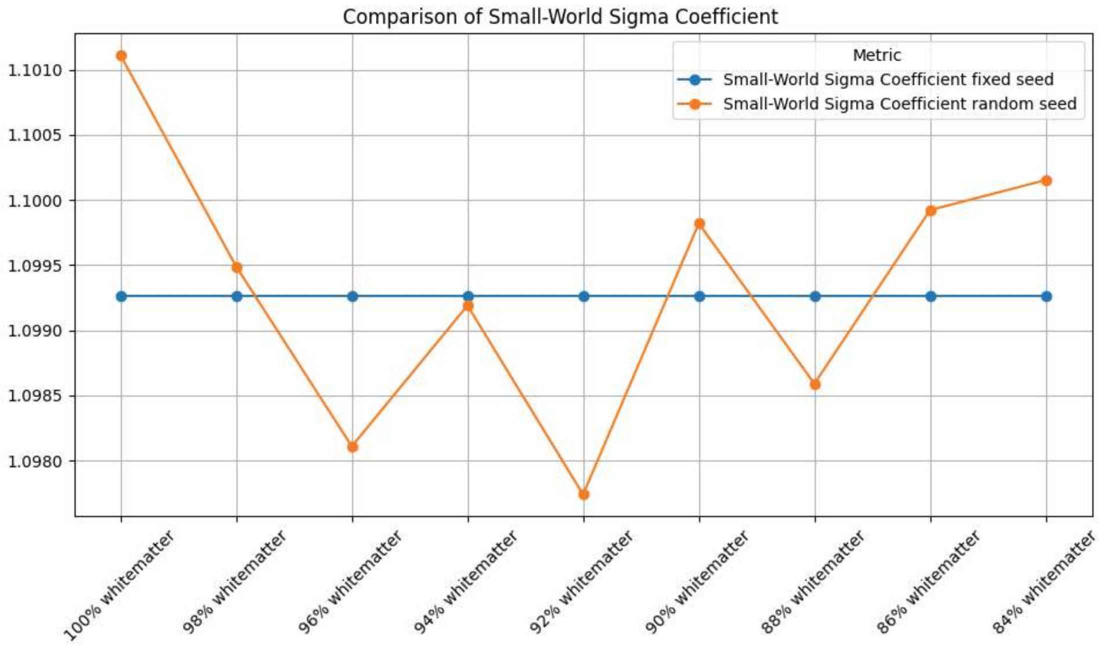

Figure 4.21: Sigma coefficient calculated using the NetworkX library for python

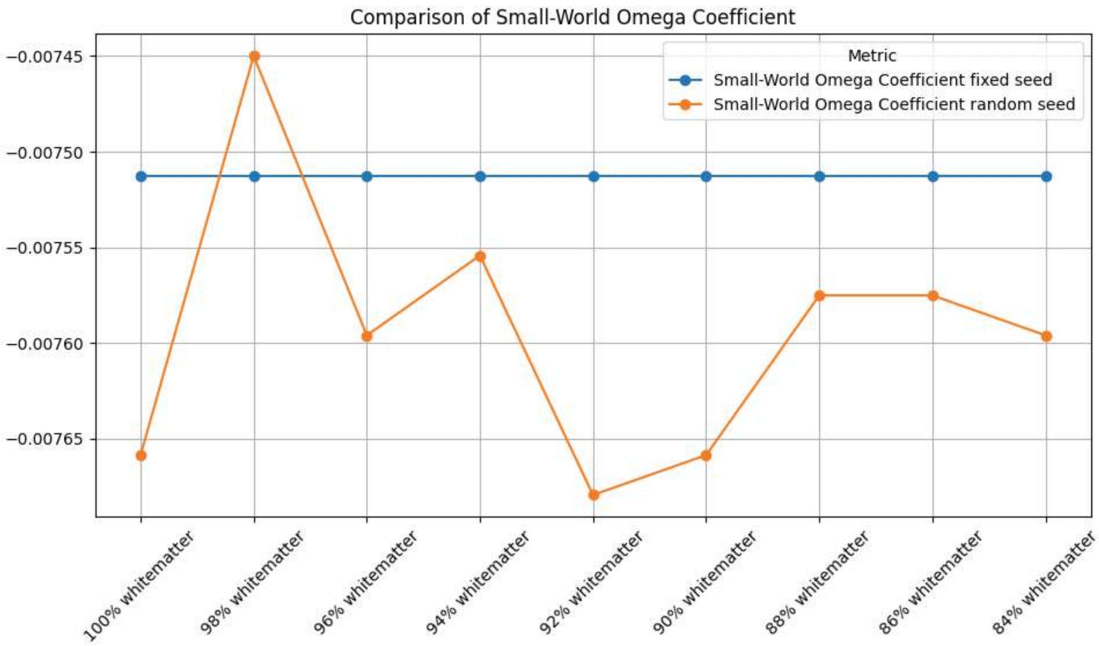

Figure 4.22: Omega coefficient calculated using the NetworkX library for python

modest increases in SWP. However, when the threshold was increased to a value of 3, a significant jump in SWP occured, raising it above the value of 0.6, thereby indicating small-world characteristics.

A critical consequence of this thresholding process is the disconnection of nodes, which coincides with the observed jumps in SWP. The unthresholded network originally had two disconnected nodes. At a threshold of 2.1, the number of disconnected nodes increased to 12, although this did not correspond to any significant change in SWP. Between thresholds of 2.2 and 2.9, the number of disconnected nodes remained at 13, coinciding with the first notable increase in SWP. Finally, at a threshold of 3, the number of disconnected nodes reached 14, which aligns with the second significant increase in SWP.

However, significant changes in SWP correlated to the white matter integrity of the connectivity matrix could again not be observed.

It should be noted that the unthresholded matrix has 3774 edges. This number is reduced to 1416 at a threshold of 2.1 without strongly influencing SWP. At a threshold of 2.2 the number of edges is reduced by 8, to 1408 but SWP jumps to around 5.6, indicating the strong influence of those 8 on the characteristics of the whole network, and one more node gets disconnected (Node 48, Right-Amygdala). When the threshold is increased further, up to 2.9, another 52 edges are lost, reducing the number to 1362, with no significant changes in SWP. Increasing the threshold to 3 eliminates 14 more edges, reducing their number to 1348 (around 35% of the original number), disconnecting one more node (Node 41, Left-Amygdala) and resulting in an increase of SWP to around 0.76. Theses results suggest that a small number of edges and nodes has an outsized influence on the SWP of the graph.

Further increases of the threshold did not increase SWP significantly.

4.3.2 Local Metrics

In this section more local graph metrics will be presented. The metrics were calculated for each node individually. Then the nodes of a specific brain area were averaged to arrive at the values seen in the plots.

Across all brain areas, the node degree appears to decrease as the white matter integrity decreases (see figures 4.24, 4.25 and 4.26). This trend is expected because, as the white matter is compromised, the structural connections between brain regions weaken, reducing the node degree. The node degrees of the left and right Thalamus experience the most significant drop off.

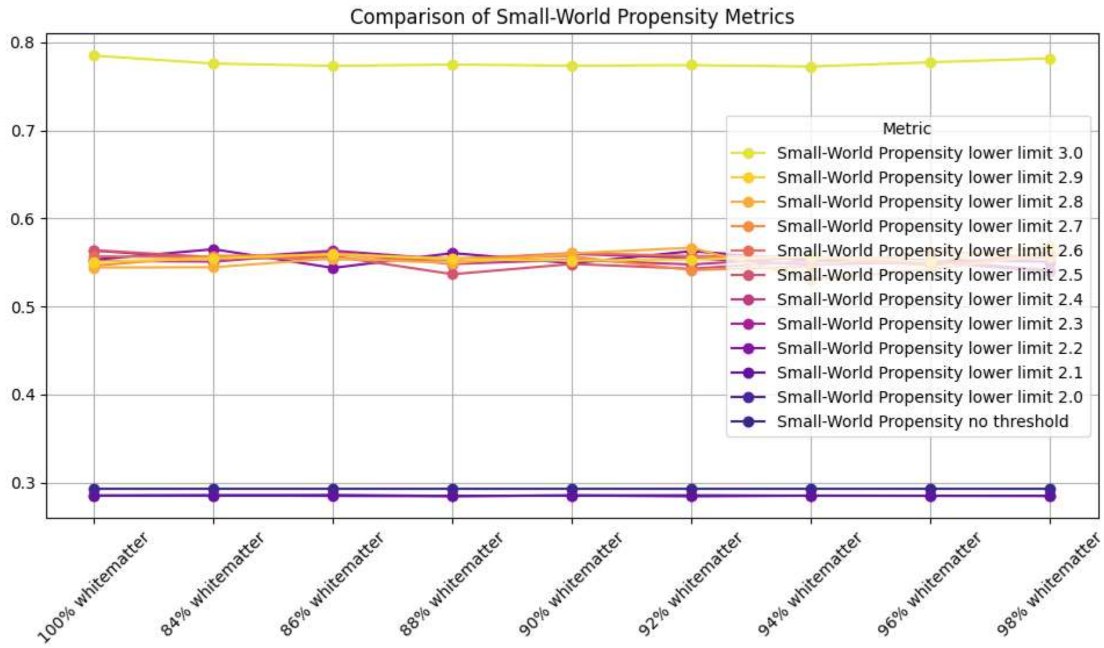

Figure 4.23: Small world propensity for structural connectivity matrices with different white matter integrity as well as with different thresholding levels. Edge weights below these thresholds were set to zero.

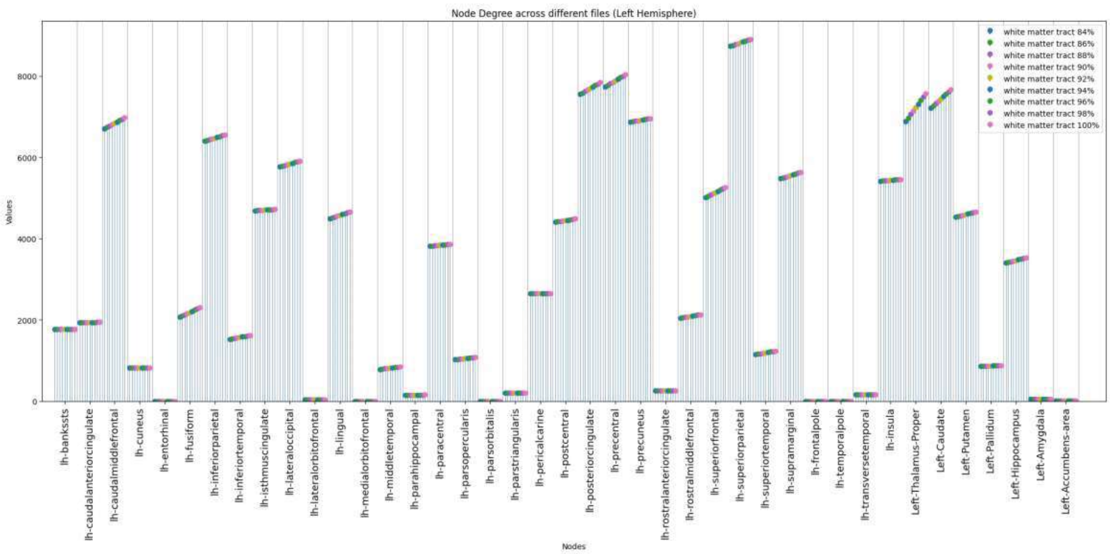

Figure 4.24: Node degree per node, Left Hemisphere.

Graph 4.26 shows the average node degree for different brain areas. A slight decrease in node degree can be observed for all regions except the left and right

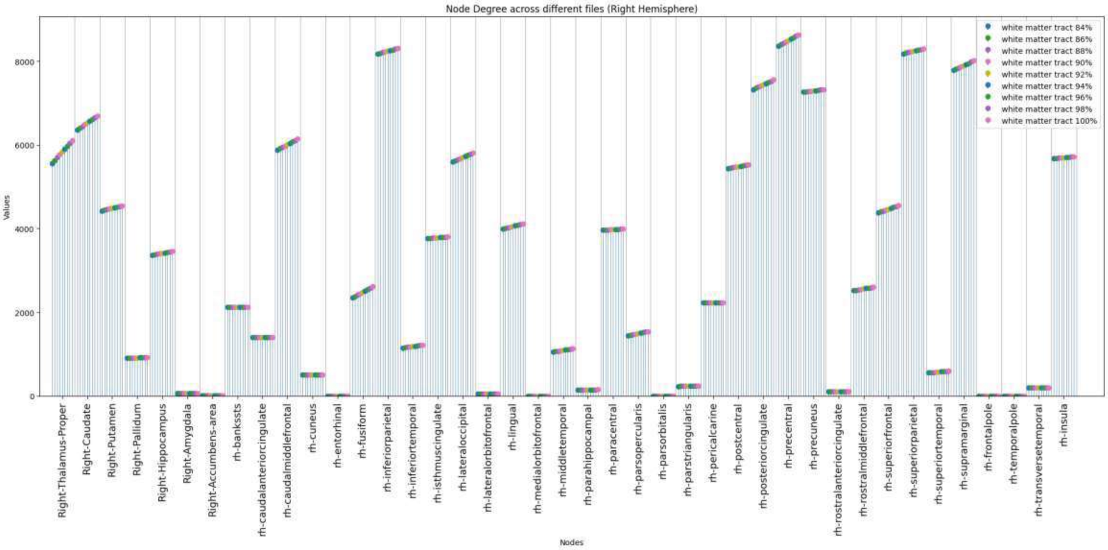

Figure 4.25: Node degree per node, Right Hemisphere.

amygdala. The thalamus shows the steepest decline in node degree.

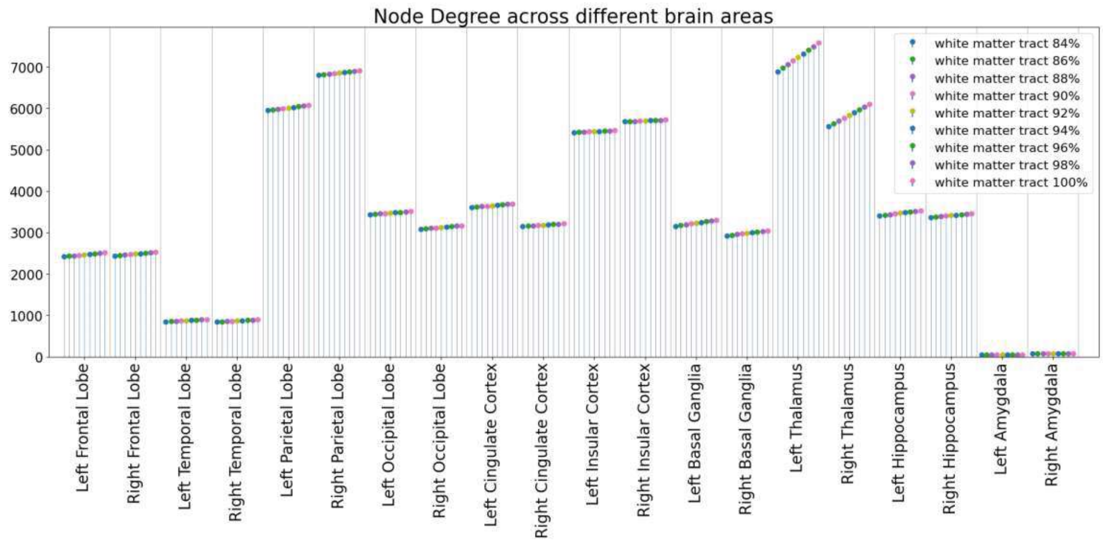

Figure 4.26: Graph showing the influence decreasing white matter integrity exerts on the average node degree in specific macroscopic brain regions.

Graph 4.27 shows how the average efficiency in different areas of the brain model is affected by decreasing white matter integrity, which lead to a steady decrease in efficiency values, most pronounced in the left an right thalamus and absent only in the left and right amygdala. A decrease in efficiency is also a well documented observation in schizophrenia patients (Gao et al. 2023).

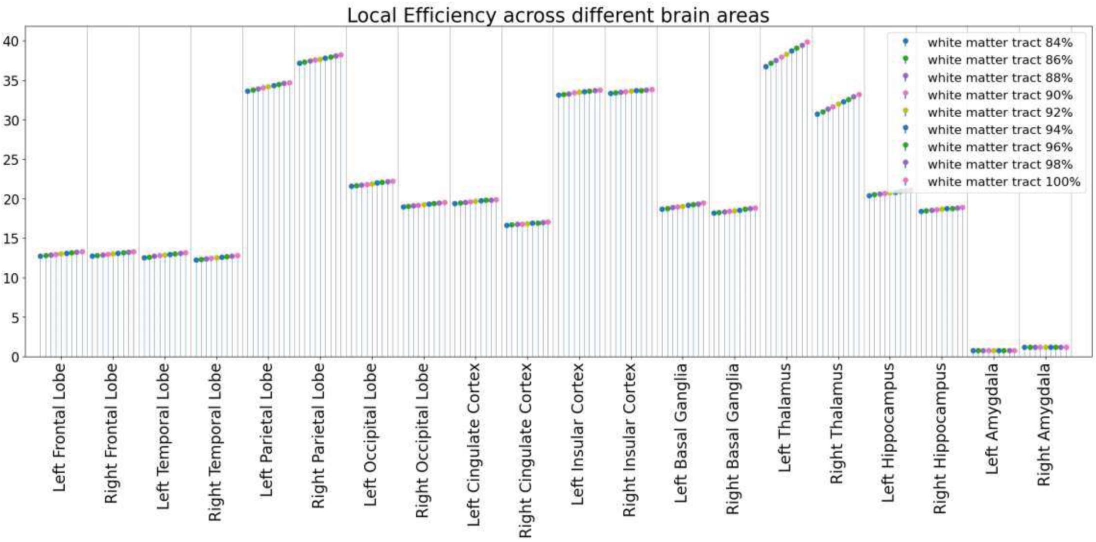

Figure 4.27: Graph showing the influence decreasing white matter integrity exerts on the average local efficiency of nodes in specific macroscopic brain regions.

Graph 4.28 shows the average betweenness centrality values for different brain areas. The highest values by far were calculated for the left and right thalamus indicating its critical role as a hub in the network. Not all brain regions exhibit changes in betweenness centrality with decreasing white matter integrity. Interestingly, most of the changes seem to occur on the left hemisphere of the connectivity model. The left frontal lobe and the left cingulate cortex exhibit a steady increase in betweenness centrality. Smaller increases can be seen in the left parietal lobe, the left occipital lobe, and the right cingulate cortex. Increases in betweenness centrality could indicate a more prominent role in information transfer within theses regions. The left thalamus and left basal ganglia exhibit a decrease in betweenness centrality with decreasing white matter integrity. These decreases could suggests a slightly reduced role of these regions in facilitating communication between different parts of the model. Collectively, theses changes imply a reorganization of the brainmodel's network structure. The hemispherically asymmetric changes in betweenness centrality are especially interesting, since the changes to the structural connectivity matrix were symmetric.

Findings in the literature are inconsistent but generally suggest a decrease in betweenness centrality in schizophrenia. (Y. Zhang et al. 2012) found decreased centrality in association cortices and increased centrality in the primary and paralimbic cortices. (Dimulescu et al. 2021) found decreased betweenness centrality in schizophrenia patients and (Jo et al. 2020) found the mean betweenness centrality to be increased, noting that this finding is inconsistent with current research.

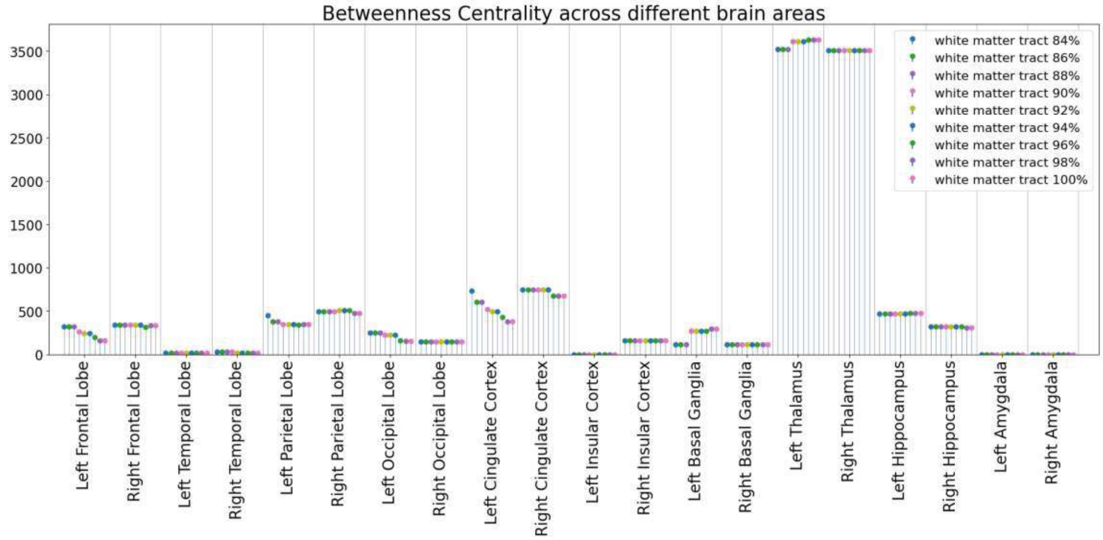

Figure 4.28: Graph showing the influence decreasing white matter integrity excerpts on the betweenness centrality of specific macroscopic brain regions.

Graph 4.29 shows the average clustering coefficient for different brain areas. All regions, except the amygdala experience a decrease of the clustering coefficient, left and right thalamus showing the steepest decline. The trend looks very similar to the trend observed in the node degrees. Regions of reduced clustering are common findings in schizophrenia research (Gao et al. 2023).

A decrease in clustering coefficient suggests reduced local interconnectivity and efficiency in information transfer within local brain regions. This implies a breakdown of specialized modules in the brain, which can lead to increased wiring costs and decreased robustness to nodal damage.

4.4 Simulation Results

This chapter presents the results of the simulations conducted for this thesis. Nine simulations, with the goal of reproducing EEG time series were performed and analyzed. Each simulation run starts from the same initial conditions. The only difference between each simulation is the structural connectivity used in the un-

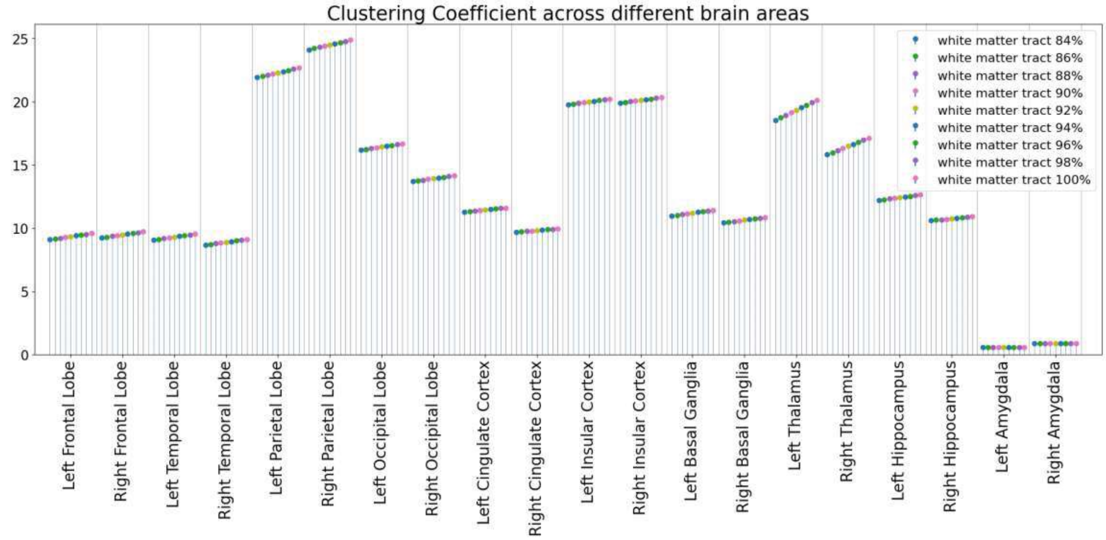

Figure 4.29: Graph showing the influence decreasing white matter integrity exerts on the average clustering coefficient of nodes in specific macroscopic brain regions.

derlying brain model, where deteriorating white matter integrity is modeled by systematically reducing connection strength between specific nodes.

Figure 4.30 shows an exemplary EEG time series that was created during a simulation run using the unaltered structural connectivity. It is twenty seconds long and has a row for each of its 64 EEG sensors. The time series clearly shows oscillations, but varies from the look of a physical EEG measurement. This is in part due to the absence of noise and artifacts that are common in physical EEG time series. The oscillations visible in this image are a superposition of mostly four dominant, narrow frequency bands at 6.0 Hz, 9.5 Hz, 12.5 Hz and a small contribution at 19.0 Hz, which will become obvious in the plots showing the power spectrum (Figure 4.31).

The absence of noise, that was previously noted is even more evident in figure 4.31, especially in the lower frequencies.

Figure 4.31 shows the amplitude spectrum and the average power spectrum for the entire brain model, computed by averaging across the FFT of all sensors of a single time series, in this case of the time series depicted in figure 4.30. Four prominent peaks can be identified. One at 6 Hz in the theta band, one at 9.5 Hz in the low alpha band, one at 12.5 Hz in the high alpha band and a small peak at 19 Hz in the beta band. The presence of peaks at these frequencies suggests that the model is able to capture typical brain rhythms that are observed in physical measurements.

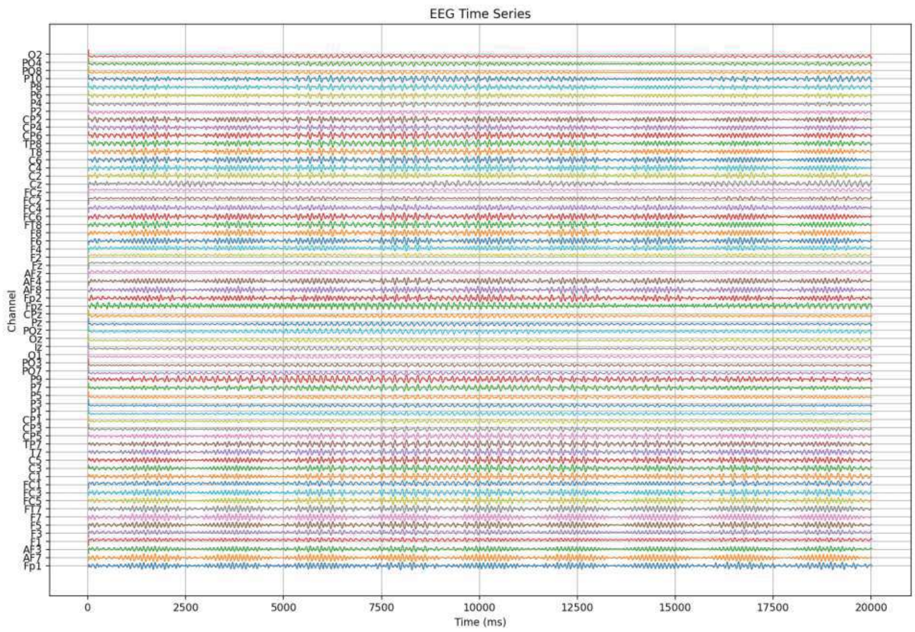

Figure 4.30: EEG time series that was simulated with the unaltered structural connectivity at the core of the model.

Figure 4.32 shows the amplitude spectra and the average power spectra of all nine simulations overlaid in one graph. The structure of the spectra remains unchanged over all datasets, with peaks at the same frequencies and the curves mapping on top of each other almost perfectly. The only difference between the different spectra is a clear, gradual reduction in the amplitude of the theta and low alpha peaks with decreasing white matter integrity and small variations in the high alpha peak.

In figure 4.33 the variation in the amplitude of the peaks is illustrated in more detail. The Theta band experiences a linear increase in amplitude that is inversely related to the integrity of the white matter. Increases in Theta activity are often reported in EEG studies of schizophrenic patients (Narayanan et al. 2014; Newson and Thiagarajan 2019; Thilakavathi et al. 2019). Similar to the Theta band, the amplitude in the Low Alpha band also increases steadily as FA decreases. The High Alpha band amplitude initially shows little change, then a slight increase as FA is reduced further. Physical EEG studies usually show the opposite behaviour. Most studies reveal decreases in alpha activity, but some also report decreases and again other report increases in frontal and decreases in posterior regions (Narayanan et al. 2014; Newson and Thiagarajan 2019; Hayempour 2013; Thilakavathi et al. 2019; Venables, Bernat, and Sponheim 2008). This frontal-posterior split could also not be reproduced. The Beta band amplitude shows a more complicated behaviour with a peak at 98% FA, then a significant drop, with a slight recovery at the lowest FA values.

Figure 4.34 highlights the amplitude spectrum for different brain regions in both hemispheres. The graphs show, that the structure of the spectrum is very similar in each brain region but the amplitudes of the peaks vary drastically both intrahemispherically, between brain regions and interhemispherically between hemispheres.

Figure 4.35 elucidates the hemispheric relationship between the power spectra in the four frequency bands that emerged from the simulation. It shows the peak amplitude as an average of all sensors of one hemisphere. The Z electrodes located on the midline of the scalp were included in both the average amplitudes of the left and right hemispheres.

The amplitude in the Theta band shows a steady increase across both hemispheres as FA decreases, with the left hemisphere consistently showing higher amplitude than the right. The left hemisphere seems to have a stronger reaction to the decreasing FA with a more pronounced amplitude increase.

The amplitude in the Low Alpha band also increases steadily with decreasing FA, with the right hemisphere showing a consistently higher amplitude than the left, contrasting what was seen in the Theta band.

The higher amplitude in the left hemisphere compared to the right suggests lateralization of Theta activity, which could reflect differences in how each hemisphere reacts to the reduced connectivity. The higher Low Alpha amplitude in the right hemisphere suggests a lateralization effect where the right hemisphere might be more involved in maintaining or enhancing alpha activity as structural integrity diminishes.

In the High Alpha band, the left hemisphere shows a more pronounced increase in amplitude with decreasing FA compared to the right hemisphere.

The Beta band amplitude shows a more complex pattern with a peak around 98% FA for the right and 96% FA for the left hemisphere, followed by a sharp decline, and a slight recovery at the lowest FA levels. Both hemispheres exhibit similar patterns, but with slight variations.

Figure 4.36 breaks down the peak amplitude changes in different frequency bands across specific brain regions for both hemispheres in detail. This level of detail provides insights into how different regions contribute to overall brain activity and how these contributions change as white matter integrity decreases.

The amplitude in the Theta band varies across brain regions, with the temporal regions (both left and right) showing the highest amplitudes. The frontal regions also show relatively high amplitudes, while the central, occipital, and parietal regions have lower values. The temporal regions' high Theta amplitude, particularly as FA decreases, suggests that these regions become more involved in slower oscillatory activity as connectivity is disrupted. This is consistent with findings that show increased Theta activity in the temporal lobes in schizophrenia. The frontal regions also show significant Theta activity. The relatively stable activity in the central and occipital regions suggests that these areas are less affected by FA changes in the Theta band.

In the Low Alpha band, the frontal regions show the highest amplitude, with the left frontal region consistently showing a higher amplitude than the right. Temporal regions also exhibit significant activity, but lower than in the Theta band. The dominance of the frontal regions in the Low Alpha band indicates their key role in maintaining Alpha activity. The higher amplitude in the left frontal region aligns with the lateralization of cognitive functions often associated with the left hemisphere.

In the High Alpha band the frontal regions again show the highest amplitude, particularly the left frontal area, followed by the temporal and occipital regions. The central and parietal regions show lower amplitudes. The left frontal, right parietal and right occipital regions show a slight decrease in amplitude.

The more complex pattern of the Beta band shows the highest amplitudes in the frontal region. With decreasing white matter integrity the hemispheric amplitude difference in the frontal lobes diminishes, while it reverses in the temporal lobe.

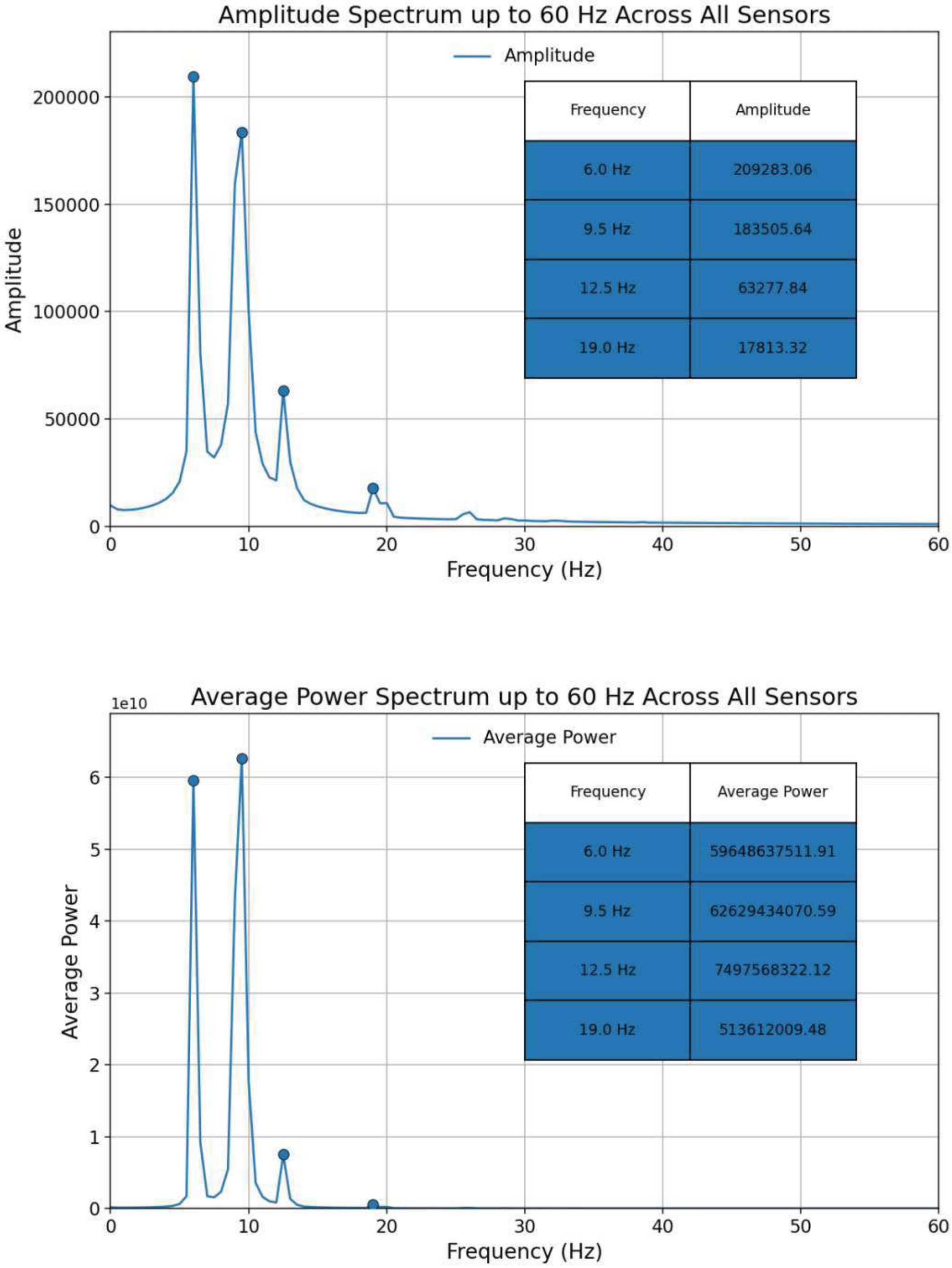

Figure 4.31: Average amplitude spectrum (top) and the average power spectrum (bottom) of the EEG simulation using the unaltered, 'healthy' structural connectivity matrix for the whole brain model, with frequencies ranging from 0 to 60 Hz. Prominent peaks are observed at 6.0 Hz, 9.5 Hz, 12.5 Hz, and 19.0 Hz, corresponding to theta, alpha, and beta frequency bands respectively. This spectrum serves as a baseline for comparison against simulations with altered structural connectivity.

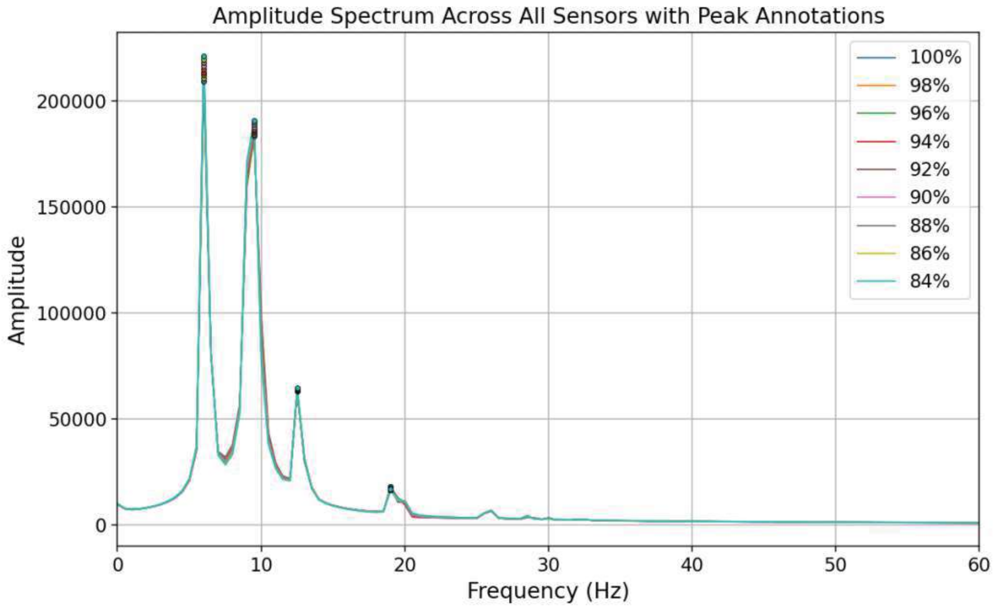

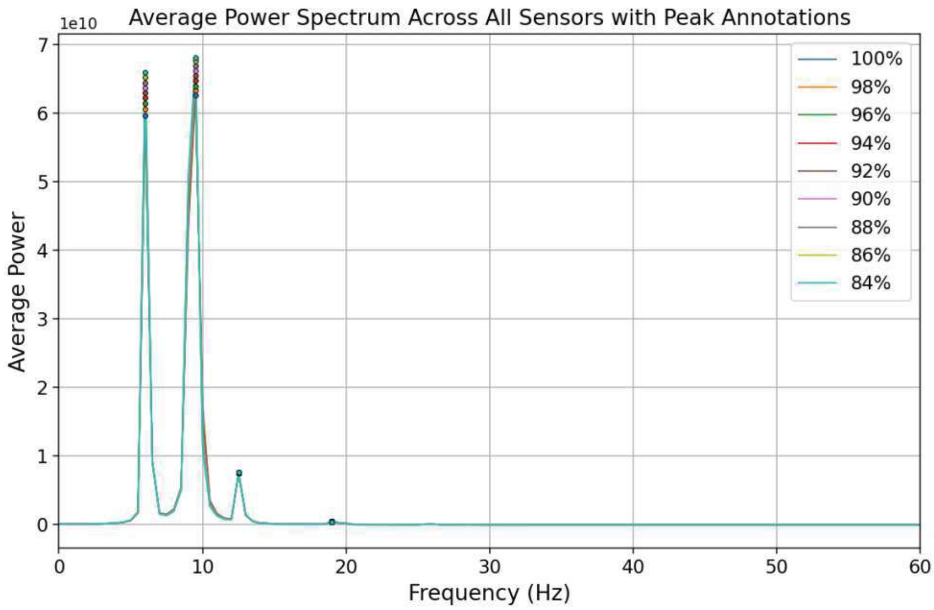

Figure 4.32: Comparisons of the Amplitude spectrum (top) and the average power spectrum (bottom) created in all nine simulation runs using structural connectivity with altered white matter integrity. The frequencies of the respective peaks align and only differ in their amplitudes.

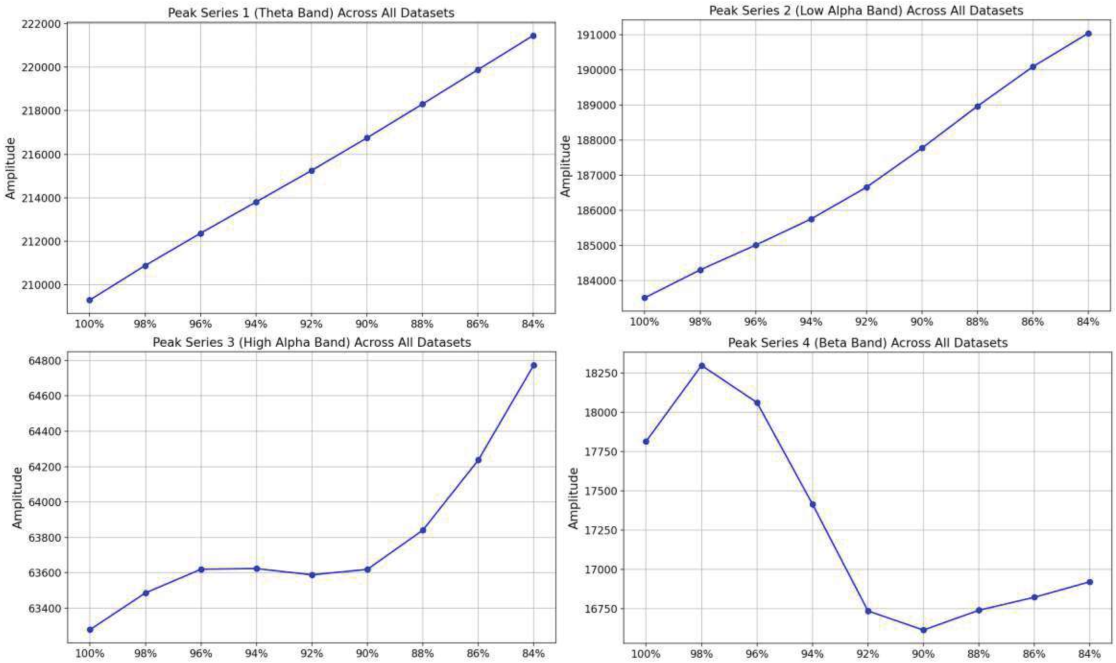

Figure 4.33: Illustration of the peak amplitude changes in the four key frequency bands—Theta (top left), Low Alpha (top right), High Alpha (bottom left), and Beta (bottom right)—across different datasets where FA was reduced by increments of 2% (from 100% to 84%).

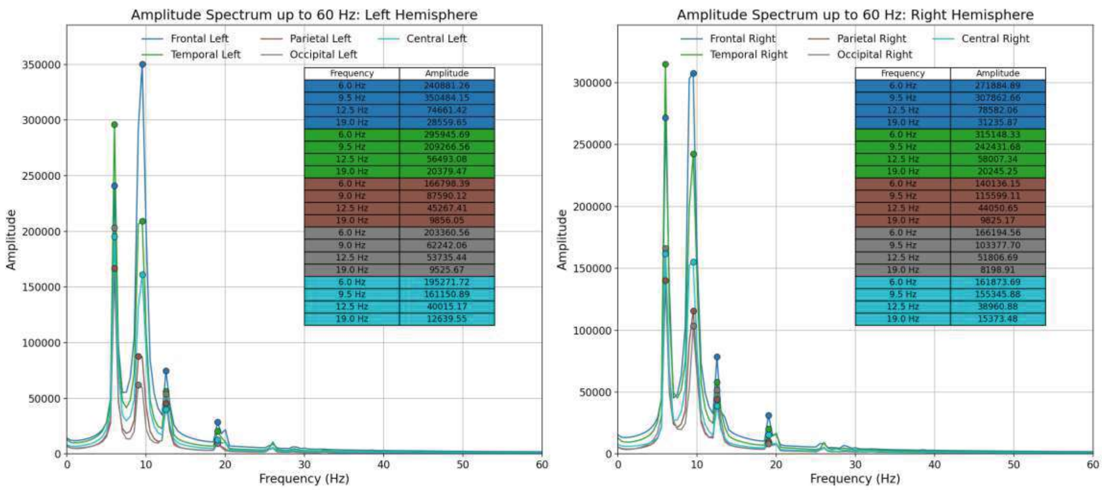

Figure 4.34: Overlaid amplitude spectrum for various brain regions in the left hemisphere (left panel), and corresponding data for the right hemisphere (right panel).

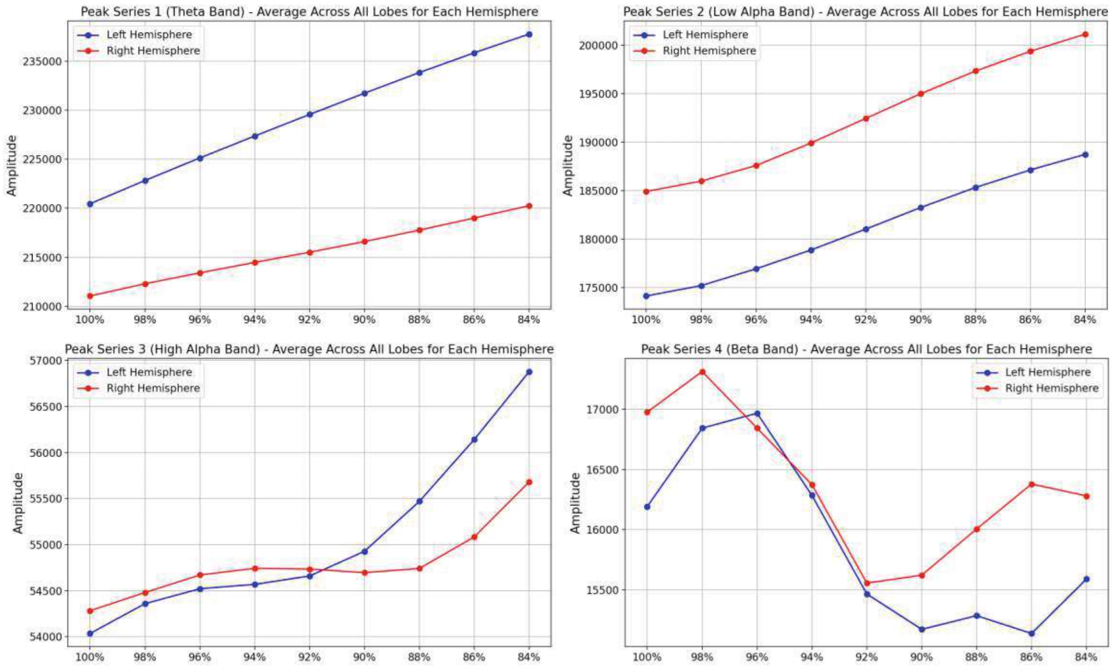

Figure 4.35: Changes in amplitude across the Theta (top left), Low Alpha (top right), High Alpha (bottom left), and Beta (bottom right) frequency bands as FA is gradually reduced from 100% to 84%. The data is averaged across all lobes for each hemisphere.

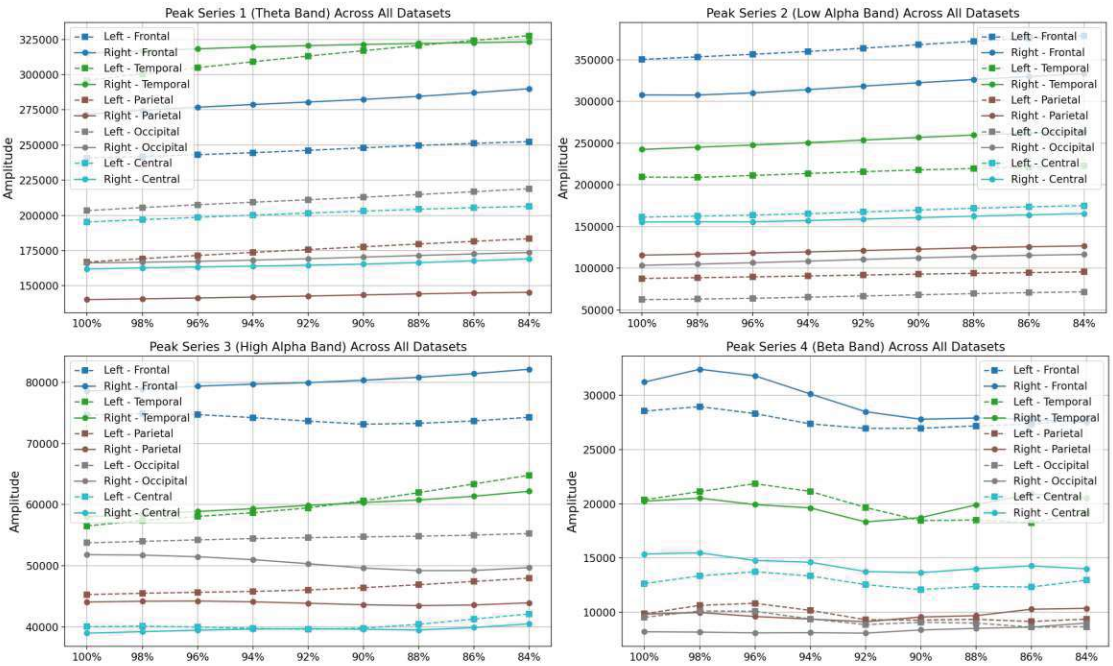

Figure 4.36: Amplitude changes across four frequency bands—Theta (top left), Low Alpha (top right), High Alpha (bottom left), and Beta (bottom right)—as FA is systematically reduced from 100% to 84%. The data is separated by brain region (Frontal, Temporal, Parietal, Occipital, and Central) and hemisphere (Left and Right).

5 DISCUSSION

The primary goal of this thesis was to develop a computational model using *The Virtual Brain* (TVB) platform to simulate EEG signals based on realistic structural connectivity, resembling that of an average human brain. The intention was to then manipulate specific aspects of this structural connectivity, particularly focusing on the effects of white matter integrity, to observe resultant changes in EEG signals and evaluate, if these changes align with expectations from current scientific understanding of schizophrenia to explore the disconnection hypothesis.

The manipulation of the structural connectivity was specifically designed to imitate white matter alterations observed in schizophrenia patients. This was achieved by reducing connection strength through the modulation of FA values, as measured by DTI, in specific tracts. The method was based on the hypothesis that connectivity strength can be modeled, using the product of fiber count and FA of the white matter tracts between two nodes as connection strength values.

To verify if the proposed structural connectivity manipulations resemble the network effects often seen in schizophrenia patients, various graph metrics were computed for each structural connectivity. The observed trends were then compared to metrics from the literature.

The characteristic path length, representing the average shortest path between pairs of nodes in the network, was found to be increased in the schizophrenia-related structural connectivity matrices. An increased characteristic path length is a well-documented finding in schizophrenia research (Micheloyannis 2012; Heuvel, Martijn, Mandl, et al. 2010; Gao et al. 2023).

Global efficiency, a measure of how efficiently information is exchanged across the entire network, was found to be reduced in the schizophrenia-related structural connectivity matrices. The reduction in global efficiency observed in the simulations is consistent with the literature on schizophrenia, where decreased global efficiency has been reported in numerous studies (Gao et al. 2023; Shon et al. 2018).

Global betweenness centrality was found to increase unsteadily with decreasing network integrity. Although findings regarding this metric are mixed, the general trend in the literature points in the opposite direction, to decreasing betweenness centrality (Dimulescu et al. 2021).

The clustering coefficient, which measures the degree to which nodes in a network tend to cluster together, was found to be linearly decreasing alongside with decreasing network integrity. This reduction in clustering coefficient is consistent with numerous studies that have reported similar findings in schizophrenia (Krukow et al. 2019; Shon et al. 2018).

The modularity of the network, which measures the degree to which the network can be divided into relatively independent modules or communities, was found to be decreasing, with decreasing network integrity. Altered modularity, often manifesting as reduced modularity, has been reported in schizophrenia.

The graph metrics computed for the different structural connectivity matrices in this thesis align reasonably well with the broader literature on schizophrenia. The reductions in clustering coefficient, global efficiency, and betweenness centrality, along with increases in characteristic path length, all point towards an increasingly disrupted network structure that is less efficient, less segregated, and less functionally specialized.

The goal was largely accomplished, as the simulations were able to produce EEG signals that reflected changes in white matter integrity, partly consistent with the hypothesized effects observed in the context of schizophrenia. However, the success of the simulation was partial, as the complexity and variability inherent in actual brain function presented challenges that were not fully captured by the model.

The chapter on EEG in schizophrenia outlined several critical abnormalities observed in the EEG patterns of individuals with schizophrenia. These include increased power in the theta frequency band, alterations in alpha band activity (with some studies reporting decreases, others reporting increases), and mixed results in the beta band. These findings reflect disrupted neural oscillations, which are believed to correlate with the underlying pathophysiology of schizophrenia, particularly in terms of connectivity and network dynamics.

The simulation results from this thesis aimed to replicate some of these EEG abnormalities by manipulating the structural connectivity of the brain, particularly focusing on white matter integrity. This approach was based on the hypothesis that disruptions in white matter, as indicated by decreased FA in DTI studies, would lead to changes in EEG signals that resemble those observed in schizophrenia.

The results showed several expected trends in the relationship between reduced white matter integrity and changes in EEG signal amplitude across various frequency bands. These results were partly in line with the hypothesized impact of white matter degradation on frequency bands. The Theta band showed an expected increase, while the alpha and beta bands showed changes, but not necessarily in the expected direction.

1. **Theta band:** Increased power in the theta band has been consistently reported in EEG studies of schizophrenia, often linked to the reduced efficiency of brain networks and disruptions in global brain connectivity. The simulations conducted in this thesis showed a clear increase in the power of the Theta band following the manipulation of white matter integrity. These results align well with the expected outcomes based on EEG studies. The simulated data suggested that as FA was reduced, the neural networks became less efficient, leading to increased low-frequency power, particularly in the theta range.

2. **Alpha band:** The alpha band activity in schizophrenia is often described as being altered, with some studies reporting decreased power and others noting a frontal-posterior split, where frontal regions show increased alpha activity while posterior regions show decreased activity. The simulation produced two peaks in the range of the alpha band which both showed a global increase in power. The high alpha band showed a decrease in alpha power in specific regions such as the left frontal lobe, the right occipital lobe and the right parietal lobe. The model did not reproduce the often reported decrease of the alpha band or the regional variability (frontal-posterior split) observed in some studies.

3. **Beta band:** Beta band activity in schizophrenia has shown mixed results in the literature. The simulated results indicated nuanced changes in Beta band power as white matter integrity was reduced with an initial rise and later drop off. This aligns with some EEG findings, suggesting that reduced structural connectivity impairs the brain's ability to generate and maintain beta oscillations.

A major caveat of this approach is the oversimplification of neural mass models, which, while computationally efficient, can not capture the full range of complex dynamics observed in real brains. The simplified model of the Jansen-Rit neural mass, as implemented in TVB, while sufficient for large-scale simulations, does not replicate the intricate connection dynamics that might be crucial for more nuanced aspects of brain function and dysfunction in schizophrenia. While the model could be used to simulate different neurotransmitter balances, testing for example the glutamate or dopamine hypotheses, by varying parameters controlling the excitation or inhibition of the models' interneurons, this was not attempted in this project.

Moreover, the reliance on averaged structural connectivity matrices from a large dataset posed limitations. Although this approach was intended to create a generalized base model, to which white matter alterations could be introduced, it necessarily lead to a dilution of individual-specific features that might be critical in understanding the variability observed in schizophrenia.

Interpreting the results of this simulation requires much caution, particularly when making inferences about real physical brains. The computational model used is a highly abstracted representation of the brain's complexity. While it can replicate certain macroscopic phenomena, its capability to account for microscopic and mesoscopic interactions and chemical dynamics, such as neurotransmitter fluctuations, that are crucial in understanding the full scope of brain function and its disorders, are limited and were not tested in this simulation. Instead the sole focus of the model is the impact of macroscopic structural connectivity as measured by DTI.

One significant limitation is said reliance on DTI for structural connectivity. DTI, while powerful, provides an indirect and probabilistic reconstruction of neuronal connections. The technique is known for its biases, such as the "gyral bias," where fiber tracking algorithms preferentially trace fibers along gyral crowns, rather than sulcal walls and an unreliability when measuring the tracts in subcortical areas (Fan and Markram 2019). This introduces uncertainties in the structural connectivity matrix that can significantly affect simulation outcomes.

Another potential weak point are the white matter matrices, which can only be seen as a rough approximation of the actual white matter tracts within a human brain. The diverse findings on which tracts are affected in schizophrenia and the unclear allocation of nodes made it necessary to rely on assumptions that likely lead to an overestimation of the tract network implicated in schizophrenia. The reduction of FA by steps of two percent, applied to all tracts affected by reduced FA was an arbitrary choice to simplify the model. In reality the reduction in FA would be not as drastic as it is in the lower end of the simulation.

Additionally, the model's implementation of subcortical structures lacks detail. The reliance on DTI measurements for subcortical tracts and the use of identical local dynamics models for all nodes, including the Thalamus is not ideal. The initial intention of the project to model the Thalamus externally as a spiking neural network, and using this model as an input for the nodes of the Thalamus in a co-simulation proved too expansive for the scope of the thesis.

Several improvements could be made to enhance the realism and reliability of the simulations. Firstly, incorporating a more detailed model, that includes both short-range and long-range connectivity, could better capture the complex dynamics of the brain, especially since the coupling between neighbouring patches of cortex is stronger than long range connections (Breakspear 2017). A surface-based model, for instance, could address the limitations of the current regional model by providing a more detailed spatial sampling of cortical activity, which is crucial for understanding the intracortical connectivity alterations seen in disorders like schizophrenia and lies well within the capabilities of TVB, when sufficient computational resources are available.

Secondly, improving the representation of white matter matrices by incorporating more granular parcellations and using higher-resolution tractography data, or other sources of tract data, could mitigate some of the biases introduced by DTI. A more detailed implementation of FA reductions, using values measured in physical experiments, would add nuance to the simulation and possibly enable simulation results that track more closely with experimental measurements.

Additionally, future simulations could benefit from the inclusion of co-simulations that account for the influence and different dynamics of subcortical structures like the Thalamus, which play a significant role in global brain dynamics. Including chemical imbalances in the simulation, by altering model parameters related to excitation and inhibition, could also provide a more comprehensive model of schizophrenia .

Finally, the simulation is very sensitive to initial conditions. The parameters chosen for this simulation were evaluated via a brute force method. It would be illuminating to find a way to determine proper initial conditions by applying biophysical considerations to the model.

In summary, while this thesis successfully achieved its primary goal of simulating EEG signals based on realistic structural connectivity, and exploring the effects of alterations of said connectivity on the EEG spectrum, several limitations and caveats must be considered when interpreting the results. By addressing these limitations and incorporating the suggested improvements, future simulations could provide accurate and meaningful insights into the effects of structural brain alterations in schizophrenia.

List of Abbreviations

Abbreviation	Full Form
DTI	Diffusion Tensor Imaging
EEG	Electroencephalogram
FA	Fractional Anisotropy
FFT	Fast Fourier Transform
fMRI	Functional Magnetic Resonance Imaging
MRI	Magnetic Resonance Imaging
SWP	Small World Propensity
TVB	The Virtual Brain

Bibliography

Aburn, Matthew J. et al. (2012). "Critical Fluctuations in Cortical Models Near Instability". In: *Frontiers in Physiology* 3. ISSN: 1664-042X. DOI: 10.3389/fphys.2012.00331.

Ackerman, S. (1992). *Discovering the Brain.* Washington (DC): National Academies Press (US).

Aerts, Hannelore et al. (May 2018). "Modeling Brain Dynamics in Brain Tumor Patients Using the Virtual Brain". In: *eneuro* 5.3, ENEURO.0083–18.2018. ISSN: 2373-2822. DOI: 10.1523/eneuro.0083-18.2018.

Ahmadizadeh, Saeed et al. (Mar. 2018). "Bifurcation analysis of two coupled Jansen-Rit neural mass models". In: *PLOS ONE* 13.3. Ed. by Gennady Cymbalyuk, e0192842. ISSN: 1932-6203. DOI: 10.1371/journal.pone.0192842.

Annavarapu, Ramesh Naidu, Srujana Kathi, and Vamsi Krishna Vadla (Jan. 2019). "Non-invasive imaging modalities to study neurodegenerative diseases of aging brain". In: *Journal of Chemical Neuroanatomy* 95, pp. 54–69. ISSN: 0891-0618. DOI: 10.1016/j.jchemneu.2018.02.006.

Ashtari, Manzar et al. (Nov. 2007). "Disruption of White Matter Integrity in the Inferior Longitudinal Fasciculus in Adolescents With Schizophrenia as Revealed by Fiber Tractography". In: *Archives of General Psychiatry* 64.11, p. 1270. ISSN: 0003-990X. DOI: 10.1001/archpsyc.64.11.1270.

Axer, Markus and Katrin Amunts (Nov. 2022). "Scale matters: The nested human connectome". In: *Science* 378.6619, pp. 500–504. ISSN: 1095-9203. DOI: 10.1126/science.abq2599.

Basser, Peter J. and Carlo Pierpaoli (June 1996). "Microstructural and Physiological Features of Tissues Elucidated by Quantitative-Diffusion-Tensor MRI". In: *Journal of Magnetic Resonance, Series B* 111.3, pp. 209–219. ISSN: 1064-1866. DOI: 10.1006/jmrb.1996.0086.

Bassett, Danielle S., Perry Zurn, and Joshua I. Gold (July 2018). "On the nature and use of models in network neuroscience". In: *Nature Reviews Neuroscience* 19.9, pp. 566–578. ISSN: 1471-0048. DOI: 10.1038/s41583-018-0038-8.

Boutros, Nash N. et al. (Feb. 2008). "The status of spectral EEG abnormality as a diagnostic test for schizophrenia". In: *Schizophrenia Research* 99.1–3, pp. 225–237. ISSN: 0920-9964. DOI: 10.1016/j.schres.2007.11.020.

Breakspear, Michael (Feb. 2017). "Dynamic models of large-scale brain activity". In: *Nature Neuroscience* 20.3, pp. 340–352. ISSN: 1546-1726. DOI: 10.1038/nn.4497.

Brown, Alan S. and Florence S. Lau (2016). "A Review of the Epidemiology of Schizophrenia". In: *Modeling the Psychopathological Dimensions of Schizophrenia - From Molecules to Behavior*. Elsevier, pp. 17–30. DOI: 10.1016/b978-0-12-800981-9.00002-x.

Bullmore, Ed and Olaf Sporns (Feb. 2009). "Complex brain networks: graph theoretical analysis of structural and functional systems". In: *Nature Reviews Neuroscience* 10.3, pp. 186–198. ISSN: 1471-0048. DOI: 10.1038/nrn2575.

– (Apr. 2012). "The economy of brain network organization". In: *Nature Reviews Neuroscience* 13.5, pp. 336–349. ISSN: 1471-0048. DOI: 10.1038/nrn3214.

Cabral, Joana et al. (Dec. 2013). "Structural connectivity in schizophrenia and its impact on the dynamics of spontaneous functional networks". In: *Chaos: An Interdisciplinary Journal of Nonlinear Science* 23.4. ISSN: 1089-7682. DOI: 10.1063/1.4851117.

Canu, Elisa, Federica Agosta, and Massimo Filippi (Jan. 2015). "A selective review of structural connectivity abnormalities of schizophrenic patients at different stages of the disease". In: *Schizophrenia Research* 161.1, pp. 19–28. ISSN: 0920-9964. DOI: 10.1016/j.schres.2014.05.020.

Cardno, Alastair G. et al. (Feb. 1999). "Heritability Estimates for Psychotic Disorders: The Maudsley Twin Psychosis Series". In: *Archives of General Psychiatry* 56.2, p. 162. ISSN: 0003-990X. DOI: 10.1001/archpsyc.56.2.162.

Chaddad, Ahmad et al. (July 2023). "Electroencephalography Signal Processing: A Comprehensive Review and Analysis of Methods and Techniques". In: *Sensors* 23.14, p. 6434. ISSN: 1424-8220. DOI: 10.3390/s23146434.

David, Olivier and Karl J. Friston (Nov. 2003). "A neural mass model for MEG/EEG:" in: *NeuroImage* 20.3, pp. 1743–1755. ISSN: 1053-8119. DOI: 10.1016/j.neuroimage.2003.07.015.

Deco, Gustavo, Viktor K. Jirsa, and Anthony R. McIntosh (Dec. 2010). "Emerging concepts for the dynamical organization of resting-state activity in the brain". In: *Nature Reviews Neuroscience* 12.1, pp. 43–56. ISSN: 1471-0048. DOI: 10.1038/nrn2961.

Desikan, Rahul S. et al. (July 2006). "An automated labeling system for subdividing the human cerebral cortex on MRI scans into gyral based regions of interest". In: *NeuroImage* 31.3, pp. 968–980. ISSN: 1053-8119. DOI: 10.1016/j.neuroimage.2006.01.021.

Dimulescu, Cristiana et al. (June 2021). "Structural Differences Between Healthy Subjects and Patients With Schizophrenia or Schizoaffective Disorder: A Graph and Control Theoretical Perspective". In: *Frontiers in Psychiatry* 12. ISSN: 1664-0640. DOI: 10.3389/fpsyt.2021.669783.

Duchatel, Ryan J., Cynthia Shannon Weickert, and Paul A. Tooney (July 2019). "White matter neuron biology and neuropathology in schizophrenia". In: *npj Schizophrenia* 5.1. ISSN: 2334-265X. DOI: 10.1038/s41537-019-0078-8.

Ellison-Wright, Ian et al. (Apr. 2014). "Distribution of tract deficits in schizophrenia". In: *BMC Psychiatry* 14.1. ISSN: 1471-244X. DOI: 10.1186/1471-244x-14-99.

Erkol, Cemre et al. (July 2020). "White Matter Measures and Cognition in Schizophrenia". In: *Frontiers in Psychiatry* 11. ISSN: 1664-0640. DOI: 10.3389/fpsyt.2020.00603.

Fan, Xue and Henry Markram (May 2019). "A Brief History of Simulation Neuroscience". In: *Frontiers in Neuroinformatics* 13. ISSN: 1662-5196. DOI: 10.3389/fninf.2019.00032.

Farahani, Farzad V., Waldemar Karwowski, and Nichole R. Lighthall (June 2019). "Application of Graph Theory for Identifying Connectivity Patterns in Human Brain Networks: A Systematic Review". In: *Frontiers in Neuroscience* 13. ISSN: 1662-453X. DOI: 10.3389/fnins.2019.00585.

Figley, Chase R. et al. (Jan. 2022). "Potential Pitfalls of Using Fractional Anisotropy, Axial Diffusivity, and Radial Diffusivity as Biomarkers of Cerebral White Matter Microstructure". In: *Frontiers in Neuroscience* 15. ISSN: 1662-453X. DOI: 10.3389/fnins.2021.799576.

Fischl, Bruce (Aug. 2012). "FreeSurfer". In: *NeuroImage* 62.2, pp. 774–781. ISSN: 1053-8119. DOI: 10.1016/j.neuroimage.2012.01.021.

Fitzsimmons, Jennifer et al. (Jan. 2020). "Cingulum bundle abnormalities and risk for schizophrenia". In: *Schizophrenia Research* 215, pp. 385–391. ISSN: 0920-9964. DOI: 10.1016/j.schres.2019.08.017.

Freeman, Linton C. (Jan. 1978). "Centrality in social networks conceptual clarification". In: *Social Networks* 1.3, pp. 215–239. ISSN: 0378-8733. DOI: 10.1016/0378-8733(78)90021-7.

Friston, Karl J. and Raymond J. Dolan (Sept. 2010). "Computational and dynamic models in neuroimaging". In: *NeuroImage* 52.3, pp. 752–765. ISSN: 1053-8119. DOI: 10.1016/j.neuroimage.2009.12.068.

Gao, Ziyang et al. (May 2023). "The whole-brain connectome landscape in patients with schizophrenia: A systematic review and meta-analysis of graph theoretical characteristics". In: *Neuroscience and Biobehavioral Reviews* 148, p. 105144. ISSN: 0149-7634. DOI: 10.1016/j.neubiorev.2023.105144.

Geoffroy, Pierre A. et al. (Oct. 2014). "The arcuate fasciculus in auditory-verbal hallucinations: A meta-analysis of diffusion-tensor-imaging studies". In: *Schizophre-*

nia Research 159.1, pp. 234–237. ISSN: 0920-9964. DOI: 10.1016/j.schres.2014.07.014.

Grimbert, François and Olivier Faugeras (Dec. 2006). “Bifurcation Analysis of Jansen’s Neural Mass Model”. In: *Neural Computation* 18.12, pp. 3052–3068. ISSN: 1530-888X. DOI: 10.1162/neco.2006.18.12.3052.

Hagberg, Aric, Pieter J. Swart, and Daniel A. Schult (Jan. 2008). “Exploring network structure, dynamics, and function using NetworkX”. In: *Proceedings of the Python in Science Conference*. URL: https://www.osti.gov/biblio/960616.

Hayempour, Benjamin Jacob (2013). “Neuromolecular Imaging Instrumentation Demonstrating Dysfunctional Brain Function in Schizophrenic Patients”. In: *Journal of Alzheimer’s Disease & Parkinsonism* 03.01. ISSN: 2161-0460. DOI: 10.4172/2161-0460.1000114.

He, Yong and Alan Evans (Aug. 2010). “Graph theoretical modeling of brain connectivity”. In: *Current Opinion in Neurology* 23.4, pp. 341–350. ISSN: 1350-7540. DOI: 10.1097/wco.0b013e32833aa567.

Heuvel, M.P. van den et al. (Nov. 2008). “Small-world and scale-free organization of voxel-based resting-state functional connectivity in the human brain”. In: *NeuroImage* 43.3, pp. 528–539. ISSN: 1053-8119. DOI: 10.1016/j.neuroimage.2008.08.010.

Heuvel, van den, Martijn, and Alex Fornito (Feb. 2014). “Brain Networks in Schizophrenia”. In: *Neuropsychology Review* 24.1, pp. 32–48. ISSN: 1573-6660. DOI: 10.1007/s11065-014-9248-7.

Heuvel, van den, Martijn, René C. W. Mandl, et al. (Nov. 2010). “Aberrant Frontal and Temporal Complex Network Structure in Schizophrenia: A Graph Theoretical Analysis”. In: *The Journal of Neuroscience* 30.47, pp. 15915–15926. ISSN: 1529-2401. DOI: 10.1523/jneurosci.2874-10.2010.

Holleran, Laurena et al. (Oct. 2013). “Altered Interhemispheric and Temporal Lobe White Matter Microstructural Organization in Severe Chronic Schizophrenia”. In: *Neuropsychopharmacology* 39.4, pp. 944–954. ISSN: 1740-634X. DOI: 10.1038/npp.2013.294.

Huang, Haiqing and Mingzhou Ding (Mar. 2016). “Linking Functional Connectivity and Structural Connectivity Quantitatively: A Comparison of Methods”. In: *Brain Connectivity* 6.2, pp. 99–108. ISSN: 2158-0022. DOI: 10.1089/brain.2015.0382.

Humphries, Mark D. and Kevin Gurney (Apr. 2008). “Network ‘Small-World-Ness’: A Quantitative Method for Determining Canonical Network Equivalence”. In: *PLoS ONE* 3.4. Ed. by Olaf Sporns, e0002051. ISSN: 1932-6203. DOI: 10.1371/journal.pone.0002051.

Jaaro-Peled, Hanna et al. (Nov. 2009). “Review of Pathological Hallmarks of Schizophrenia: Comparison of Genetic Models With Patients and Nongenetic

Models”. In: *Schizophrenia Bulletin* 36.2, pp. 301–313. ISSN: 0586-7614. DOI: 10.1093/schbul/sbp133.

Jäkel, Sarah and Leda Dimou (Feb. 2017). “Glial Cells and Their Function in the Adult Brain: A Journey through the History of Their Ablation”. In: *Frontiers in Cellular Neuroscience* 11. ISSN: 1662-5102. DOI: 10.3389/fncel.2017.00024.

Jansen, Ben H. and Vincent G. Rit (Sept. 1995). “Electroencephalogram and visual evoked potential generation in a mathematical model of coupled cortical columns”. In: *Biological Cybernetics* 73.4, pp. 357–366. ISSN: 1432-0770. DOI: 10.1007/bf00199471.

Jansen, Ben H., George Zouridakis, and Michael E. Brandt (Jan. 1993). “A neurophysiologically-based mathematical model of flash visual evoked potentials”. In: *Biological Cybernetics* 68.3, pp. 275–283. ISSN: 1432-0770. DOI: 10.1007/bf00224863.

Jauhar, Sameer, Mandy Johnstone, and Peter J McKenna (Jan. 2022). “Schizophrenia”. In: *The Lancet* 399.10323, pp. 473–486. ISSN: 0140-6736. DOI: 10.1016/s0140-6736(21)01730-x.

Jirsa, V.K. et al. (2002). “Spatiotemporal forward solution of the EEG and MEG using network modeling”. In: *IEEE Transactions on Medical Imaging* 21.5, pp. 493–504. DOI: 10.1109/TMI.2002.1009385.

Jo, Young Tak et al. (Feb. 2020). “Diagnosing schizophrenia with network analysis and a machine learning method”. In: *International Journal of Methods in Psychiatric Research* 29.1. ISSN: 1557-0657. DOI: 10.1002/mpr.1818.

Jongsma, Hannah E et al. (May 2019). “International incidence of psychotic disorders, 2002–17: a systematic review and meta-analysis”. In: *The Lancet Public Health* 4.5, e229–e244. ISSN: 2468-2667. DOI: 10.1016/s2468-2667(19)30056-8.

Jung, Sra et al. (Oct. 2020). “Uncinate fasciculus white matter connectivity related to impaired social perception and cross-sectional and longitudinal symptoms in patients with schizophrenia spectrum psychosis”. In: *Neuroscience Letters* 737, p. 135144. ISSN: 0304-3940. DOI: 10.1016/j.neulet.2020.135144.

Kam, Julia W.Y. et al. (Dec. 2013). “Resting state EEG power and coherence abnormalities in bipolar disorder and schizophrenia”. In: *Journal of Psychiatric Research* 47.12, pp. 1893–1901. ISSN: 0022-3956. DOI: 10.1016/j.jpsychires.2013.09.009.

Kandel, Eric R., ed. (2013). *Principles of neural science*. 5. ed. McGraw-Hill medical. Previous ed.: 2000. - Includes bibliographical references and index. - Description based on print version record. New York: McGraw-Hill Medical. 11709 pp. ISBN: 9781283656245.

Kelly, S et al. (Oct. 2017). “Widespread white matter microstructural differences in schizophrenia across 4322 individuals: results from the ENIGMA Schizophrenia

DTI Working Group". In: *Molecular Psychiatry* 23.5, pp. 1261–1269. ISSN: 1476-5578. DOI: 10.1038/mp.2017.170.

Kendler, Kenneth S. (July 1993). "The Roscommon Family Study: I. Methods, Diagnosis of Probands, and Risk of Schizophrenia in Relatives". In: *Archives of General Psychiatry* 50.7, p. 527. ISSN: 0003-990X. DOI: 10.1001/archpsyc.1993.01820190029004.

Kenney, Joanne P.M. et al. (Nov. 2017). "The arcuate fasciculus network and verbal deficits in psychosis". In: *Translational Neuroscience* 8.1. ISSN: 2081-6936. DOI: 10.1515/tnsci-2017-0018.

Kerepesi, Csaba et al. (June 2017). "The braingraph.org database of high resolution structural connectomes and the brain graph tools". In: *Cognitive Neurodynamics* 11.5, pp. 483–486. ISSN: 1871-4099. DOI: 10.1007/s11571-017-9445-1.

Kim, Jun Won et al. (Mar. 2015). "Diagnostic utility of quantitative EEG in unmedicated schizophrenia". In: *Neuroscience Letters* 589, pp. 126–131. ISSN: 0304-3940. DOI: 10.1016/j.neulet.2014.12.064.

Klauser, Paul et al. (Aug. 2016). "White Matter Disruptions in Schizophrenia Are Spatially Widespread and Topologically Converge on Brain Network Hubs". In: *Schizophrenia Bulletin*, sbw100. ISSN: 1745-1701. DOI: 10.1093/schbul/sbw100.

Knock, S.A. et al. (Sept. 2009). "The effects of physiologically plausible connectivity structure on local and global dynamics in large scale brain models". In: *Journal of Neuroscience Methods* 183.1, pp. 86–94. ISSN: 0165-0270. DOI: 10.1016/j.jneumeth.2009.07.007.

Konrad, A. and G. Winterer (Oct. 2007). "Disturbed Structural Connectivity in Schizophrenia Primary Factor in Pathology or Epiphenomenon?" In: *Schizophrenia Bulletin* 34.1, pp. 72–92. ISSN: 1745-1701. DOI: 10.1093/schbul/sbm034.

Krukow, Paweł et al. (July 2019). "Abnormalities in hubs location and nodes centrality predict cognitive slowing and increased performance variability in first-episode schizophrenia patients". In: *Scientific Reports* 9.1. ISSN: 2045-2322. DOI: 10.1038/s41598-019-46111-0.

Kubicki, M et al. (Jan. 2007). "A review of diffusion tensor imaging studies in schizophrenia". In: *Journal of Psychiatric Research* 41.1–2, pp. 15–30. ISSN: 0022-3956. DOI: 10.1016/j.jpsychires.2005.05.005.

Kubicki, M. et al. (July 2005). "DTI and MTR abnormalities in schizophrenia: Analysis of white matter integrity". In: *NeuroImage* 26.4, pp. 1109–1118. ISSN: 1053-8119. DOI: 10.1016/j.neuroimage.2005.03.026.

Kubicki, Marek et al. (Dec. 2005). "The Application of DTI to Investigate White Matter Abnormalities in Schizophrenia". In: *Annals of the New York Academy of Sciences* 1064.1, pp. 134–148. ISSN: 1749-6632. DOI: 10.1196/annals.1340.024.

Larkum, Matthew E. et al. (July 2018). “A Perspective on Cortical Layering and Layer-Spanning Neuronal Elements”. In: *Frontiers in Neuroanatomy* 12. ISSN: 1662-5129. DOI: 10.3389/fnana.2018.00056.

Lopes da Silva, Fernando (Dec. 2013). “EEG and MEG: Relevance to Neuroscience”. In: *Neuron* 80.5, pp. 1112–1128. ISSN: 0896-6273. DOI: 10.1016/j.neuron.2013.10.017.

Louis, Erik K. et al. (2016). “Electroencephalography (EEG): An Introductory Text and Atlas of Normal and Abnormal Findings in Adults, Children, and Infants”. In: URL: https://api.semanticscholar.org/CorpusID:151886401.

Louis, Erik K. St., Lauren C. Frey, and Jeffrey W. Britton, eds. (2016). *Electroencephalography (EEG). An introductory text and atlas of normal and abnormal findings in adults, children, and infants*. Includes bibliographical references. - Description based on online resource; title from PDF title page (viewed November 28, 2016). Chicago, IL: American Epilepsy Society. 1195 pp. ISBN: 9780997975604.

Luo, Liqun (Sept. 2021). “Architectures of neuronal circuits”. In: *Science* 373.6559. ISSN: 1095-9203. DOI: 10.1126/science.abg7285.

Luo, Yuanyuan et al. (Feb. 2022). “Autoimmune Encephalitis With Psychotic Manifestations and Cognitive Impairment Presenting as Schizophrenia: Case Report and Literature Review”. In: *Frontiers in Psychiatry* 13. ISSN: 1664-0640. DOI: 10.3389/fpsyt.2022.827138.

Lynn, Christopher W. and Danielle S. Bassett (Mar. 2019). “The physics of brain network structure, function and control”. In: *Nature Reviews Physics* 1.5, pp. 318–332. ISSN: 2522-5820. DOI: 10.1038/s42254-019-0040-8.

Marwaha, Steven and Sonia Johnson (May 2004). “Schizophrenia and employment”. In: *Social Psychiatry and Psychiatric Epidemiology* 39.5, pp. 337–349. ISSN: 1433-9285. DOI: 10.1007/s00127-004-0762-4.

Marwaha, Steven, Sonia Johnson, et al. (July 2007). “Rates and correlates of employment in people with schizophrenia in the UK, France and Germany”. In: *British Journal of Psychiatry* 191.1, pp. 30–37. ISSN: 1472-1465. DOI: 10.1192/bjp.bp.105.020982.

McCutcheon, Robert et al. (Dec. 2017). “Defining the Locus of Dopaminergic Dysfunction in Schizophrenia: A Meta-analysis and Test of the Mesolimbic Hypothesis”. In: *Schizophrenia Bulletin* 44.6, pp. 1301–1311. ISSN: 1745-1701. DOI: 10.1093/schbul/sbx180.

McGrath, J. et al. (May 2008). “Schizophrenia: A Concise Overview of Incidence, Prevalence, and Mortality”. In: *Epidemiologic Reviews* 30.1, pp. 67–76. ISSN: 1478-6729. DOI: 10.1093/epirev/mxn001.

Meehan, Timothy P. and Steven L. Bressler (Nov. 2012). “Neurocognitive networks: Findings, models, and theory”. In: *Neuroscience and Biobehavioral Re-*

views 36.10, pp. 2232–2247. ISSN: 0149-7634. DOI: 10.1016/j.neubiorev.2012.08.002.
Meng, Linghui et al. (Feb. 2019). "Widespread white-matter microstructure integrity reduction in first-episode schizophrenia patients after acute antipsychotic treatment". In: *Schizophrenia Research* 204, pp. 238–244. ISSN: 0920-9964. DOI: 10.1016/j.schres.2018.08.021.
Micheloyannis, Sifis (2012). "Graph-based network analysis in schizophrenia". In: *World Journal of Psychiatry* 2.1, p. 1. ISSN: 2220-3206. DOI: 10.5498/wjp.v2.i1.1.
Mountcastle, V. (Apr. 1997). "The columnar organization of the neocortex". In: *Brain* 120.4, pp. 701–722. ISSN: 1460-2156. DOI: 10.1093/brain/120.4.701.
Muldoon, Sarah Feldt, Eric W. Bridgeford, and Danielle S. Bassett (Feb. 2016). "Small-World Propensity and Weighted Brain Networks". In: *Scientific Reports* 6.1. ISSN: 2045-2322. DOI: 10.1038/srep22057.
Narayanan, Balaji et al. (Sept. 2014). "Resting State Electroencephalogram Oscillatory Abnormalities in Schizophrenia and Psychotic Bipolar Patients and Their Relatives from the Bipolar and Schizophrenia Network on Intermediate Phenotypes Study". In: *Biological Psychiatry* 76.6, pp. 456–465. ISSN: 0006-3223. DOI: 10.1016/j.biopsych.2013.12.008.
Narr, Katherine L. and Amber M. Leaver (May 2015). "Connectome and schizophrenia". In: *Current Opinion in Psychiatry* 28.3, pp. 229–235. ISSN: 0951-7367. DOI: 10.1097/yco.0000000000000157.
Newman, M. E. J. (2003). "Fast algorithm for detecting community structure in networks". In: *Physical review. E, Statistical, nonlinear, and soft matter physics.* DOI: 10.48550/ARXIV.COND-MAT/0309508.
Newson, Jennifer J. and Tara C. Thiagarajan (Jan. 2019). "EEG Frequency Bands in Psychiatric Disorders: A Review of Resting State Studies". In: *Frontiers in Human Neuroscience* 12. ISSN: 1662-5161. DOI: 10.3389/fnhum.2018.00521.
Nunez, Paul and Ramesh Srinivasan (2007). "Electroencephalogram". In: *Scholarpedia* 2.2, p. 1348. ISSN: 1941-6016. DOI: 10.4249/scholarpedia.1348.
O'Donnell, Lauren J. and Carl-Fredrik Westin (Apr. 2011). "An Introduction to Diffusion Tensor Image Analysis". In: *Neurosurgery Clinics of North America* 22.2, pp. 185–196. ISSN: 1042-3680. DOI: 10.1016/j.nec.2010.12.004.
O'Donoghue, Stefani et al. (Feb. 2017). "Anatomical dysconnectivity in bipolar disorder compared with schizophrenia: A selective review of structural network analyses using diffusion MRI". In: *Journal of Affective Disorders* 209, pp. 217–228. ISSN: 0165-0327. DOI: 10.1016/j.jad.2016.11.015.
Owen, Michael J, Akira Sawa, and Preben B Mortensen (July 2016). "Schizophrenia". In: *The Lancet* 388.10039, pp. 86–97. ISSN: 0140-6736. DOI: 10.1016/s0140-6736(15)01121-6.

Özarslan, Evren, Baba C. Vemuri, and Thomas H. Mareci (Mar. 2005). "Generalized scalar measures for diffusion MRI using trace, variance, and entropy". In: *Magnetic Resonance in Medicine* 53.4, pp. 866–876. ISSN: 1522-2594. DOI: 10.1002/mrm.20411.

Pachou, Ellie et al. (Aug. 2008). "Working Memory in Schizophrenia: An EEG Study Using Power Spectrum and Coherence Analysis to Estimate Cortical Activation and Network Behavior". In: *Brain Topography* 21.2, pp. 128–137. ISSN: 1573-6792. DOI: 10.1007/s10548-008-0062-5.

Park, Hae-Jeong and Karl Friston (Nov. 2013). "Structural and Functional Brain Networks: From Connections to Cognition". In: *Science* 342.6158. ISSN: 1095-9203. DOI: 10.1126/science.1238411.

Patel, Krishna R et al. (2014). "Schizophrenia: overview and treatment options". In: *Pharmacy and Therapeutics* 39.9, p. 638.

Picchioni, Marco and Robin Murray (2008). "Schizophrenia". In: *Scholarpedia* 3.4, p. 4132. ISSN: 1941-6016. DOI: 10.4249/scholarpedia.4132.

Picchioni, Marco M and Robin M Murray (July 2007). "Schizophrenia". In: *BMJ* 335.7610, pp. 91–95. ISSN: 1468-5833. DOI: 10.1136/bmj.39227.616447.be.

Pittman-Polletta, Benjamin R. et al. (June 2015). "Brain Rhythms Connect Impaired Inhibition to Altered Cognition in Schizophrenia". In: *Biological Psychiatry* 77.12, pp. 1020–1030. ISSN: 0006-3223. DOI: 10.1016/j.biopsych.2015.02.005.

Power, Jonathan D. et al. (Sept. 2010). "The Development of Human Functional Brain Networks". In: *Neuron* 67.5, pp. 735–748. ISSN: 0896-6273. DOI: 10.1016/j.neuron.2010.08.017.

Psychiatric Genomics Consortium, Schizophrenia Working Group of the (July 2014). "Biological insights from 108 schizophrenia-associated genetic loci". In: *Nature* 511.7510, pp. 421–427. ISSN: 1476-4687. DOI: 10.1038/nature13595.

Ramsay, Ian S. et al. (Sept. 2021). "Individual alpha peak frequency is slower in schizophrenia and related to deficits in visual perception and cognition". In: *Scientific Reports* 11.1. ISSN: 2045-2322. DOI: 10.1038/s41598-021-97303-6.

Rattay, Frank (1990). *Electrical Nerve Stimulation. Theory, Experiments and Applications*. Description based on publisher supplied metadata and other sources. Vienna: Springer Wien. 1266 pp. ISBN: 9783709132715.

Rattay, Frank, Robert Greenberg, and Susanne Resatz (Dec. 2002). "Neuron modeling". In: *Handbook of Neuroprosthetic Methods*. CRC Press. ISBN: 9781420040876. DOI: 10.1201/9781420040876.ch3.

Ritter, Petra et al. (Apr. 2013). "The Virtual Brain Integrates Computational Modeling and Multimodal Neuroimaging". In: *Brain Connectivity* 3.2, pp. 121–145. ISSN: 2158-0022. DOI: 10.1089/brain.2012.0120.

Rubinov, Mikail and Olaf Sporns (Sept. 2010). "Complex network measures of brain connectivity: Uses and interpretations". In: *NeuroImage* 52.3, pp. 1059–1069. ISSN: 1053-8119. DOI: 10.1016/j.neuroimage.2009.10.003.

Sanz Leon, Paula et al. (2013). "The Virtual Brain: a simulator of primate brain network dynamics". In: *Frontiers in Neuroinformatics* 7. ISSN: 1662-5196. DOI: 10.3389/fninf.2013.00010.

Sanz-Leon, Paula et al. (May 2015). "Mathematical framework for large-scale brain network modeling in The Virtual Brain". In: *NeuroImage* 111, pp. 385–430. ISSN: 1053-8119. DOI: 10.1016/j.neuroimage.2015.01.002.

Schilling, Kurt et al. (Dec. 2017). "Confirmation of a gyral bias in diffusion <scp>MRI</scp> fiber tractography". In: *Human Brain Mapping* 39.3, pp. 1449–1466. ISSN: 1097-0193. DOI: 10.1002/hbm.23936.

Schirner, Michael et al. (Aug. 2015). "An automated pipeline for constructing personalized virtual brains from multimodal neuroimaging data". In: *NeuroImage* 117, pp. 343–357. ISSN: 1053-8119. DOI: 10.1016/j.neuroimage.2015.03.055.

Shergill, Sukhwinder S. et al. (Mar. 2007). "A Diffusion Tensor Imaging Study of Fasciculi in Schizophrenia". In: *American Journal of Psychiatry* 164.3, pp. 467–473. ISSN: 1535-7228. DOI: 10.1176/ajp.2007.164.3.467.

Shon, Seung-Hyun et al. (June 2018). "Deterioration in Global Organization of Structural Brain Networks in Schizophrenia: A Diffusion MRI Tractography Study". In: *Frontiers in Psychiatry* 9. ISSN: 1664-0640. DOI: 10.3389/fpsyt.2018.00272.

Siasios, Ioannis et al. (Sept. 2016). "The role of diffusion tensor imaging and fractional anisotropy in the evaluation of patients with idiopathic normal pressure hydrocephalus: a literature review". In: *Neurosurgical Focus* 41.3, E12. ISSN: 1092-0684. DOI: 10.3171/2016.6.focus16192.

Silva, Fernando Lopes da (2009). "EEG: Origin and Measurement". In: *EEG - fMRI*. Springer Berlin Heidelberg, pp. 19–38. ISBN: 9783540879190. DOI: 10.1007/978-3-540-87919-0_2.

Spiegler, Andreas et al. (Sept. 2010). "Bifurcation analysis of neural mass models: Impact of extrinsic inputs and dendritic time constants". In: *NeuroImage* 52.3, pp. 1041–1058. ISSN: 1053-8119. DOI: 10.1016/j.neuroimage.2009.12.081.

Sporns, Olaf (2007). "Brain connectivity". In: *Scholarpedia* 2.10, p. 4695. ISSN: 1941-6016. DOI: 10.4249/scholarpedia.4695.

– (June 2018). "Graph theory methods: applications in brain networks". In: *Dialogues in Clinical Neuroscience* 20.2, pp. 111–121. ISSN: 1958-5969. DOI: 10.31887/dcns.2018.20.2/osporns.

Sporns, Olaf, Giulio Tononi, and Rolf Kötter (2005). "The Human Connectome: A Structural Description of the Human Brain". In: *PLoS Computational Biology* 1.4, e42. ISSN: 1553-7358. DOI: 10.1371/journal.pcbi.0010042.

Stefanovski, Leon et al. (Aug. 2019). "Linking Molecular Pathways and Large-Scale Computational Modeling to Assess Candidate Disease Mechanisms and Pharmacodynamics in Alzheimer's Disease". In: *Frontiers in Computational Neuroscience* 13. ISSN: 1662-5188. DOI: 10.3389/fncom.2019.00054.

Strobbe, Gregor (Jan. 2015). "Advanced forward models for EEG source imaging". PhD thesis. Universiteit Gent.

Surbeck, Werner et al. (Apr. 2020). "Anatomical integrity within the inferior fronto-occipital fasciculus and semantic processing deficits in schizophrenia spectrum disorders". In: *Schizophrenia Research* 218, pp. 267–275. ISSN: 0920-9964. DOI: 10.1016/j.schres.2019.12.025.

Thilakavathi, B. et al. (July 2019). "EEG power spectrum analysis for schizophrenia during mental activity". In: *Australasian Physical & Engineering Sciences in Medicine* 42.3, pp. 887–897. ISSN: 1879-5447. DOI: 10.1007/s13246-019-00779-w.

Trappenberg, Thomas P. (2023). *Fundamentals of computational neuroscience*. Third edition. This edition also issued in print: 2023. - Previous edition: 2010. - Includes bibliographical references and index. - Description based on print version record. Oxford: Oxford University Press. 1396 pp. ISBN: 9780191965418.

Ublinskii, M. V. et al. (May 2015). "Characteristics of Diffusion in the Corticospinal Tract of Patients with Early Stage of Schizophrenia: Diffusion Tensor Magnetic Resonance Imaging". In: *Bulletin of Experimental Biology and Medicine* 159.1, pp. 29–31. ISSN: 1573-8221. DOI: 10.1007/s10517-015-2881-1.

Venables, N. C., E. M. Bernat, and S. R. Sponheim (Apr. 2008). "Genetic and Disorder-Specific Aspects of Resting State EEG Abnormalities in Schizophrenia". In: *Schizophrenia Bulletin* 35.4, pp. 826–839. ISSN: 1745-1701. DOI: 10.1093/schbul/sbn021.

Watts, Duncan J. and Steven H. Strogatz (June 1998). "Collective dynamics of 'small-world' networks". In: *Nature* 393.6684, pp. 440–442. ISSN: 1476-4687. DOI: 10.1038/30918.

Wheeler, Anne L. and Aristotle N. Voineskos (Aug. 2014). "A review of structural neuroimaging in schizophrenia: from connectivity to connectomics". In: *Frontiers in Human Neuroscience* 8. ISSN: 1662-5161. DOI: 10.3389/fnhum.2014.00653.

Whitford, Thomas J. et al. (2014). "Localized abnormalities in the cingulum bundle in patients with schizophrenia: A Diffusion Tensor tractography study". In: *NeuroImage: Clinical* 5, pp. 93–99. ISSN: 2213-1582. DOI: 10.1016/j.nicl.2014.06.003.

Whittington, Miles A et al. (Oct. 2011). "Circuits and brain rhythms in schizophrenia: a wealth of convergent targets". In: *Current Opinion in Pharmacology* 11.5, pp. 508–514. ISSN: 1471-4892. DOI: 10.1016/j.coph.2011.04.010.

Wikipedia contributors (2024). *Neuron — Wikipedia, The Free Encyclopedia*. [Online; accessed 2-July-2024]. URL: https://en.wikipedia.org/w/index.php?title=Neuron&oldid=1225016899.

Wilson, Robin J. (2009). *Introduction to graph theory*. 4. ed., [Nachdr.] Harlow: Prentice Hall. 171 pp. ISBN: 9780582249936.

Woodman, M. Marmaduke et al. (Apr. 2014). "Integrating neuroinformatics tools in TheVirtualBrain". In: *Frontiers in Neuroinformatics* 8. ISSN: 1662-5196. DOI: 10.3389/fninf.2014.00036.

Yuste, Rafael (July 2015). "From the neuron doctrine to neural networks". In: *Nature Reviews Neuroscience* 16.8, pp. 487–497. ISSN: 1471-0048. DOI: 10.1038/nrn3962.

Zhang, Jiawei (May 2019a). "Basic Neural Units of the Brain: Neurons, Synapses and Action Potential". In: *arXiv: Neurons and Cognition*. DOI: 10.48550/ARXIV.1906.01703. arXiv: 1906.01703 [q-bio.NC].

– (2019b). "Secrets of the Brain: An Introduction to the Brain Anatomical Structure and Biological Function". In: *ArXiv* abs/1906.03314. URL: https://api.semanticscholar.org/CorpusID:182952521.

Zhang, Yuanchao et al. (Nov. 2012). "Abnormal topological organization of structural brain networks in schizophrenia". In: *Schizophrenia Research* 141.2–3, pp. 109–118. ISSN: 0920-9964. DOI: 10.1016/j.schres.2012.08.021.

Zou, Li-qiu et al. (Mar. 2008). "Diffusion Tensor Imaging Study of the Anterior Limb of Internal Capsules in Neuroleptic-Naive Schizophrenia". In: *Academic Radiology* 15.3, pp. 285–289. ISSN: 1076-6332. DOI: 10.1016/j.acra.2007.09.026.